REPORT NO NCRE/R579

March 1972

THE THEORY OF EXPLOSION INDUCED SHIP WHIPPING MOTIONS

Naval Construction Research Establishment
St Leonard's Hill
Dunfermline
Fife

19

REPORT NO NCRE/R579

March, 1972

THE THEORY OF EXPLOSION INDUCED SHIP WHIPPING MOTIONS

ABSTRACT

The report presents a comprehensive account of the mechanics of, and methods for predicting, the interaction between the vertical vibration modes of a surface ship and a nearby underwater explosion. It summarises earlier work in the field and gives a full unified account of the author's recent work (reported piecemeal elsewhere).

Naval Construction Research Establishment
St Leonard's Hill
Dunfermline
Fife

Approved for Issue

Superintendent

ACKNOWLEDGEMENTS

The help and encouragement of Professor D C Pack of Strathclyde University, of Professor J L King of Edinburgh University and Mr S B Kendrick are gratefully acknowledged, both during the work, and for making it possible in the first place.

I should also like to acknowledge a great debt to my wife for her continual support and patience during many 'quiet' evenings.

SUMMARY

The principal aim of the thesis is to develop, and show how to solve, equations describing the flexural motions caused in a ship by the pulsations of the bubble of gaseous products from a nearby underwater explosion. Equations for this purpose were developed in the USA 15-20 years ago and the thesis presents an alternative, finite element formulation which is more general and which leads to equations in matrix form. In this form the equations are much more suitable for evaluation by computer. The method of solution of these equations of elastic motion, in terms of normal mode shapes, is described.

The approximations involved in the hydrodynamics of the bubble-ship interaction are examined in some detail and the limits of application of the theory are illustrated. The principal approximation in the hydrodynamics is the use of strip theory since this cannot allow for either the longitudinal flow which occurs when the bubble is close to the ship, or for the flow around the end of the ship when the bubble is in such a region. The accuracy of strip theory is examined in both these cases. An alternative to strip theory for describing the flow around a vibrating ship is presented. This approximates the full three-dimensional flow field around the ship by means of a set of line distributions of vertically oriented dipoles at the waterplane-ship centreline axis. The technique could also be of value for the determination of added water mass around a vibrating ship in more usual vibration problems.

The original American derivation of the equations assumed that the pulsating bubble was non-migrating. Suitable equations are developed to describe the upward migration of the bubble due to gravity and the effect of this migration on the motion of the ship.

For severe flexural motions of the ship some plastic yielding or even buckling could occur and a direct solution of the original finite element

equations, modified to include such effects, is presented. This shows the way in which they can change the motion of the ship.

The entire thesis is a theoretical exercise although the results for the non-migrating bubble case are compared with a few model test results published in connection with the original American work.

CONTENTS

A Introduction

When a fairly large explosive charge is detonated underwater close to a ship the shock wave it transmits to the water can do considerable damage to the ship. If close enough the hull plating may rupture and for charges further away there may still be considerable deformation of the structure nearest the charge. The shock wave also is partially transmitted into the structure and can cause further shock damage to internally mounted equipment. These effects follow close behind the detonation, typically within times of the order of 15 to 20 milliseconds, and are usually confined to the region of the ship closest to the explosion.

The explosion may however also excite a very different kind of response. Ships near underwater explosions often shake and bend overall in violent flexural vibrations. Such vibrations are usually confined largely to a vertical plane and, although very violent, are of much lower frequency (typically 1-5 Hz) than the shock motions accompanying the local damage. The amplitudes can be very large and can cause considerable structural damage to the ship. Unlike the direct shock damage, this damage can occur at parts of the ship quite remote from the site of the explosion. These bending motions are commonly termed 'whipping' motions. They also occur in severe storms if the bow of a ship emerges from the water and then slams back onto it. They constitute a superposition of the well known low frequency vertical bending vibration modes of the ship, excited to unusually large amplitudes. It is the aim of this thesis to investigate the nature of the interaction between the explosion and the ship which causes these whipping motions, and to develop suitable equations from which whipping motions can be calculated.

It is already known from earlier work principally by G Chertock (and described briefly in Section B) that such motions are connected closely to the motion of the water around the bubble of gaseous combustion products from the explosion. This bubble is well known to pulsate vigorously and the period of the pulsation is often very close to the low frequency vibration modes of ships. Chertock's work showed that the whipping is primarily due to the coupling between the vibration modes and the pulsating flow. This thesis extends the earlier work, investigates the hydrodynamic interaction between the explosion and the ship in more detail and, by using a different initial approach, provides a set of equations for calculating the ship response which show more clearly the nature of the forces acting on the ship and are also more readily solved by standard matrix methods on a computer.

The mechanics of the interaction involves several standard fields of study; the elastic nature of the ship, the hydrodynamics of vibration and the hydrodynamics of underwater explosions. The thesis attempts to tie together only the simplest ideas from each and to extend standard methods in each only where they appeared to be deficient from a whipping viewpoint: for example the strip theory of ship vibration and the equations for a pulsating migrating bubble. In consequence the bibliographies given in each field are rather basic; they are aimed simply at providing sufficient background information to apply adequately the methods developed. The first part of this thesis, sections A to K, is largely based on existing methods, although the methods have not previously been used for this particular application, and is concerned largely with establishing the equivalence of the present methods to the earlier work.

Section D extends strip theory to allow for the explosion induced motion of the surrounding water. Section G includes a simple approach to making an allowance for the effect of small bilge keels on the added water mass. Section I describes a large computer program written to evaluate the equations developed in sections C to H. Most of the new material in the thesis is contained in sections L to O and in R. Section L describes an alternative to the customary ship theory for the flow around the ship. Section M investigates the limits of application of the approximate analysis by comparing the forces predicted by the approximate method with exact solutions for very simple cases. Section N develops an approximate method for making an allowance for the effect of shock wave damage to the target. Section O investigates the effect of gravity on the explosion bubble and on the forces the bubble produces on the ship. Section R describes how the basic equations for the ship motion can be modified to allow for plastic yielding and buckling of the ship. Two further major programs were developed to evaluate the ship response (including allowances for gravity migration of the bubble and plastic deformation of the target) and are described in sections P and R. Several minor computer programs were developed to evaluate the exact solutions for comparison with the approximate analysis.

To make each section of the thesis as self-contained as possible the references and figures for each section are grouped at the end of the section.

B Background

Although a considerable amount of work has been carried out on the vibration and slamming aspects of ship whipping, very little work has been published on the explosion induced shipping motions. What work has been published is due entirely to a single author, G Chertock. His work is described in references [B1] to [B3] but, as it appears to be the sole predecessor of the work here it is worth describing it in some detail.

The ship target is assumed to be equivalent to an elastic free-free beam whose transverse displacements can therefore be represented by

$$y(x,t) = \sum_i q_i(t)\Psi_i(x) \qquad (B1)$$

where x is the longitudinal distance along the axis of the ship, y the vertical displacement of the cross-section at x (assumed rigid), $\Psi_i(x)$ the i^{th} normal mode shape for transverse vibration in vacuo and q_i is a generalised co-ordinate for the i^{th} mode (e.g. the amplitude at the bow or, alternatively, the root mean square displacement). The normal modes for such motions are orthogonal with the mass per unit length, m(x), as a weighting function.

$$\int_0^{\ell} m(x)\Psi_i(x)\Psi_j(x)dx = M_i\delta_{ij} \qquad (B2)$$

where M_i is the generalised mass associated with the i^{th} mode.

By using the orthogonality condition the equations of vertical transverse motion due to an arbitrary distribution of pressure over the surface of the ship can be written

$$M_i(\ddot{q}_i + \alpha_i^2 q_i) = Q_i = -\iint_S p(s,t)\Psi_i \cos\theta \, d\sigma \quad i = 0,1,2,\ldots \qquad (B3)$$

where α_i is the circular frequency for mode i, Q_i the generalised force and $d\sigma$ an element of area of the surface of the ship. The

angle β is the angle between the vertical and the normal to the surface and s refers to a point on the ship surface.

By neglecting the Bernoulli pressures, $\frac{1}{2}\rho u^2$, compared with the unsteady forces $\rho\frac{\partial\phi}{\partial t}$ in the usual Bernoulli pressure equation for incompressible flow, the fluid pressure on the ship can be expressed as a linear sum of the pressure due to the explosion induced fluid flow on the structure, assumed rigid, and the pressures due to the motion of the target in its various modes, so that

$$p(s,t) = p_{oo}(s,t) + \Sigma_i p_i(s,t) \tag{B4}$$

where p_{oo} is due to the explosion and p_i to the ith mode.

With this assumption of linearity, induced modal mass coefficient can be defined by

$$L_{ij} = -\left[\iint_s p_j(s,t)\Psi_i \cos\beta d\sigma\right]/\ddot{q}_i(t) \tag{B5}$$

and will be independent of time. Substituted into equation (B3) this gives

$$(M_i + L_{ii})(\ddot{q}_i + \omega_i^2 q_i) = -\iint p_{oo}\Psi_i \cos\beta d\sigma - \sum_{j\neq i} L_{ij}\ddot{q}_j;\quad i = 0,1,2,\ldots$$

$$\omega_i^2 = \frac{M_i a_i^2}{M_i + L_{ii}} \tag{B6}$$

In these equations the elastic modes are clearly coupled to each other by the entrained water around the ship through the coefficients L_{ij}, $i \neq j$. By a suitable transformation of the normal mode shapes Ψ_i and co-ordinates q_i it was shown that the equations can be uncoupled into

$$M_i'(\ddot{q}_i' + \omega_i'^2 q_i') = -\iint p_{oo}\Psi_i' \cos\beta d\sigma \tag{B7}$$

The procedure however is extremely difficult to carry out in practice due to the necessity to evaluate the cross-coupling coefficients. These can only be determined exactly by the solutions of a series of integral equations where the integrals are over the whole surface

of the ship hull. In practice, for physical reasons the L_{ij}'s are expected to be fairly small if the ship is long and slender or if there is sufficient fore-and-aft symmetry. Chertock avoided determination of the L_{ij} by assuming that ships are 'proportional bodies'

i.e. by his definition, $\oint p_i \cos\beta \, ds = a_i \rho m(x) \Psi_i(x)$

where the integral is a line integral taken round a ship cross-section, ρ is the density of water, and the relation applies at all ship cross-sections, i.e. for all i, a_i is assumed, for proportional bodies, to be a constant, independent of x. With this definition, by multiplying by Ψ_j and integrating over the length of the ship,

$$L_{ij} = \frac{1}{\ddot{q}_j} \iint p_j(s,t) \Psi_i \cos\beta \, d\sigma = -\frac{1}{\ddot{q}_j} \int_0^{\ell} \Psi_i \, dx \oint p_j \cos\beta \, ds = -\frac{a_j \rho}{\ddot{q}_j} \int_0^{\ell} m \Psi_j \Psi_i \, dx$$

i.e. $$L_{ij} = -\frac{a_j \rho}{\ddot{q}_j} M_i \delta_{ij}$$

so that the cross-coupling terms all vanish and the mode shapes in air and water are identical, although the frequencies will change due to the non-zero entrained water masses L_{ii}.

For the term p_{oo}, representing the pressure on the ship, if it were rigid, due to the flow around the explosion bubble, the well known result [B4] that the flow around a non-migrating bubble is equivalent to that of a simple source was used. Since the rate of change of the bubble volume is $\dot{V}(t)$, the strength of the source is $\dot{V}/4\pi$ and its potential is

$$\phi_o = \frac{\dot{V}}{4\pi r}$$

The pressure in the absence of the target is therefore

$$p_o = \rho \dot{\phi}_o = \frac{\ddot{V}}{4\pi r} \qquad \text{(B8)}$$

and the integral $-\iint p_{oo} \Psi_i \cos\beta \, d\sigma$ will be representable in the form

$$\mu \ddot{V}$$

where μ is a factor depending only on the charge position and the ship and mode shapes. For a charge sufficiently far from the ship the factor μ was shown to be given approximately by

$$\mu_i = \frac{\zeta}{4\pi} \int^{\ell} (\rho A + \frac{mL_{ii}}{M_i}) \frac{y_i}{r^3} dx \qquad (B9)$$

where ζ is the height of the axis of the ship above the charge centre and r is the standoff of the particular point on the ship axis from the charge centre. The final modal equation of motion is therefore

$$(M_i + L_{ii})(\ddot{q}_i + \omega^2{}_i q_i) = \mu \ddot{V}(t); \qquad (B10)$$

To determine the response of the ship then, equation (B10) is to be solved for each mode, using free-field values for the explosion bubble volume acceleration, $\ddot{V}$, and the modal components may then be summed to give the displacement function y(x,t). The principal assumptions made in the derivation are:

a. The charge is far enough from the ship for the explosion bubble motion not to be affected by the ship.

b. The ship motions remain completely elastic.

c. The ship is a 'proportional body', i.e. there is no fluid coupling between the 'in vacuo' elastic vibration modes when the ship is in the water.

d. The charge is at a distance from the ship large compared with the ship cross-section, so that the approximation (B9) applies.

e. There is no significant migration of the bubble during the motion.

f. Only incompressible water motions are of importance.

g. Structural and hydrodynamic damping are negligible.

To check the accuracy of his equations, Chertock carried out

two series of experiments on model targets. The first series used a 1.2 gm charge under a floating rectangular box 10 ft long by 9 ins wide by 6 ins deep. This target was slender, symmetric and nearly uniform and the mode shapes in air and water were indistinguishable so that the target certainly satisfied the requirement (c). The charge depth of 13 ins was carefully selected so that the normal repulsion from a free surface exactly balanced the upward buoyancy migration due to gravity so that requirement (e) was also satisfied. At the given depth the maximum bubble radius is about 6 ins so that (a) is satisfied and the geometry is clearly such that (d) is not really violated although it might be thought near the limits of acceptability since the cross-sectional dimensions are nearly comparable to the standoff. For the fundamental, 2-node whipping mode the predicted results agreed very well with the experimental (Reference B3) but for the 3-node mode the measured amplitudes were about 30 less than those predicted. For the 2-node mode the variation of whipping amplitude with the longitudinal location of the charge agreed very well with experiment.

The second series of tests used a submerged cylindrical model 8 ft long by 9 ins in diameter and two charge sizes, 1.2 gms and 8.2 gms were used. The charge and target were lowered to a series of depths and the variation in amplitude of the 2-node and 3-node modes were measured as the bubble period varied, due to depth, from in phase to out of phase with the modes. The effect of charge standoff was also investigated. For the 2-node mode agreement was again good everywhere but for the 3-node mode the experimental amplitudes were now greater than predicted. Prior to the tests vibration measurements were made both in air and water to determine the mode shapes and frequencies and to determine the values of L_{ii}

from the equation

$$\omega_i^2 = \frac{\lambda_i}{\lambda_i + L_{ii}} a_i^2 \qquad \text{(see equation (B6))}$$

Unlike the floating box model, the non-uniform mass distribution in the cylinder led to minor differences in the mode shapes for the two cases so that, for the cylinder, condition (c) was violated. To minimise the effect of violating condition (e) on these tests since gravity migration could not be balanced by surface repulsion, the axis of the cylinder was hung vertically. Gravity migration was consequently parallel to the axis and its effects minimised. In any case, for such tiny charges, particularly when fired at depth (between 12 ft and 900 ft in the tests), migration is very small.

From the experiments it is clear that, inside the restrictions of assumptions (a) to (e), and to some extent outside them, the analysis is quite accurate. The good agreement also indicates that, at least on small scale, the assumptions (f) and (g) are justified. Chertock in fact gives an argument, although not a completely convincing one, why the assumption (f) should be generally true even though initially, when the explosion emits the shock wave, the fluid motion is far from incompressible. The analysis however does not provide a fully reasonable method of computing the whipping of ships generally. Very few ships can be regarded as proportional bodies and in consequence the coupling coefficients L_{ij} must be found in some way. The approximate analysis only applies to distant charges where the distance from the charge to the ship is large compared with the ship cross section and there is no indication of how rapidly the approximation breaks down at closer ranges. For very small charges of the type used in the experiment and with the pressure still atmospheric or greater, explosion bubbles tend to migrate very little. On full

scale this is not true and bubbles migrate very vigorously. Such migration can lead to marked differences in the response of ships to charges vertically beneath them compared to charges at some distance to one side. In Chertock's analysis conditions change only slowly with stand-off from the ship's centreline. Lastly, being entirely dependent on elastic modes of vibration, it is very difficult to extend the analysis as it stands to the analysis of ship motions which are violent enough for plastic deformation to occur.

These points are all investigated in some detail in the thesis and a practical computation scheme is developed. Since methods of calculating the normal mode frequencies and shapes of ships have been well established over the last half century, their basis, strip theory for the hydrodynamics and an elastic free-free beam representation for the ship, is used here to re-formulate the whipping equations to apply to all ships, including those which are not proportional. The forcing action of the bubble pulsations on the ship can then be interpreted in terms of strip theory, which provides also a very simple means of including the effects of bubble migration. Use of the basic equations of an elastic beam also permits a relatively simple extension to cover plastic hinge formation in the ship. The equations used are developed in the subsequent sections.

To enable the powerful matrix manipulation subroutines readily available in most computers to be used in computing the ship response a finite element/lumped mass model has been used.

References:

B1 Chertock, G.; "The Flexural Response of a Submerged Solid to a Pulsating Gas Bubble", Jn. Applied Physics, Vol. 24, No. 2 (Feb. 1953).

B2 Chertock, G.; "Effects of Underwater Explosions on Elastic Structures", Fourth Symposium on Naval Hydrodynamics, ACR-92, Aug. 1962.

B3 Chertock, G.; "Excitation of Transient Vibrations of Idealised Ship Models by Underwater Explosions", 77th Meeting of the Acoustical Society of America, 8th April 1969.

B4 Cole, R. H. : "Underwater Explosions", Princeton Univ. Press. 1948.

C The Elastic Representation of the Ship

Since the latter part of the last century it has been customary to represent a ship as an elastic beam. Initially this was largely a necessary assumption to make strength calculations tractable but eventually, in 1905, a series of static bending moment experiments were carried out on a destroyer HMS WOLF (C1). These confirmed that the usual thin beam equations gave approximately the correct longitudinal stress distribution across each cross-section, although some deviations from a linear stress distribution were apparent near the deck. The results indicated the 'apparent' modulus of elasticity to be close to the usual 'tensile test' value for low bending moments but to fall in value for the higher moments. Calculated deflections, when compared with the measured deflections gave much lower apparent values for the modulus. The discrepancy in the deflections was later shown to be due to the neglect of shear deformations and in 1924 Taylor presented an excellent paper (C2) describing a modification to the straight-forward beam theory which made allowance for the effect of shear lag on the distribution of stress in beams of ship type cross-section. He showed that under typical conditions shear could make significant contributions to the total ship deflection.

Since that time, until very recently when three-dimensional finite element stress analysis computer programs became available to calculate stress distributions with some accuracy, the position has not changed greatly. A number of static bending experiments C3-C8 have been carried out on ships and all have confirmed that beam theory is quite satisfactory for computing both stresses and deflections even to the point of failure (C3 and C8) provided that long deck houses are not involved. Such deckhouses appear to behave in a variety of

ways depending on how they are supported. Instead of the stresses increasing away from the neutral axis, except in very long well supported deckhouses, the stresses decrease. If the deck on which they are supported is flexible enough, they may even have a curvature opposite to that of the main hull. However, in calculating the effect of deckhouses on longitudinal deflections it has become customary to treat the deckhouse as a normal part of the beam (if it is long enough) but to assign to it a reduced effectiveness factor depending on its size shape and support. Theories and methods for calculating such effectiveness factors are given in References C9-C12.

The application of beam theory to the vibration of ships has a history as long as its application to static calculations and Reference C13 gives an excellent review of the work. So long as shear deflections are included and an entrained mass of water allowed for, excellent results can be achieved in calculating the vibration frequencies of the first few lowest modes. However, shear deflections play an increasingly important part for the higher modes and the distortions of plane sections (assumed to remain plane in normal beam theory) become important. Also, higher modes begin to have frequencies similar to some of the transverse distortion modes and combined modes appear. Finally the usual strip theory method for allowing for the entrained water mass becomes increasingly inaccurate for the higher modes. In consequence, although high accuracy has been claimed (C14) for calculations of this type up to the 10 node mode, it is generally accepted that only the first few modes, with up to about 5-nodes, can be calculated with confidence. Fortunately in explosion induced whipping it is the lowest few modes which turn out to be the most significant.

To apply the lumped mass/weightless beam idealisation to a ship it may be assumed divided into a number of equal length sections. If, as is normally the case, the ship structure changes little in the length of any section, it can be assumed constant within each section with characteristics corresponding to those at the centre of the section. The forces and moments acting at the ends of any section are then readily determined in terms of the deflections and rotations there, all the ship weight, buoyancy and inertial forces being considered as lumped at the ends of sections. With the sign convention shown in Figure C1 , the standard beam equations are

$$\frac{dS}{dx} = 0$$

$$\frac{dM}{dx} = -S$$

$$M = EI\frac{d^2y}{dx^2}$$

If the angle of rotation at a cross-section is γ, then the slope of the deflection curve is

$$\frac{dy}{dx} = \gamma + \frac{S}{A_s G}$$

where A_s is the area of the cross-section effective in shear, and G the shear modulus. The integral of these equations may then be expressed in the form

$$\begin{bmatrix} y \\ \gamma \\ M \\ -S \end{bmatrix} = \begin{bmatrix} 1 & x & \frac{x^2}{2EI} & \left(\frac{x^3}{6EI} - \frac{x}{A_s G}\right) \\ 0 & 1 & \frac{x}{EI} & \frac{x^2}{2EI} \\ 0 & 0 & 1 & x \\ 0 & 0 & 0 & 1 \end{bmatrix} \begin{bmatrix} y_L \\ \gamma_L \\ M_L \\ -S_L \end{bmatrix} \qquad \text{(C1)}$$

where the suffix L refers to conditions at the left hand end of the beam section. If the conditions at the right hand end are substituted the equations may be inverted to give the forces and moments required

at each end of the beam to maintain there given displacements and rotations. These equations are

$$\begin{bmatrix} M_L \\ S_L \end{bmatrix} = \begin{bmatrix} 3\alpha\ell & -\alpha\ell(1-\epsilon) \\ 6\alpha & -3\alpha\ell \end{bmatrix} \begin{bmatrix} y_R \\ \gamma_R \end{bmatrix} - \begin{bmatrix} 3\alpha\ell & \alpha\ell^2(2+\epsilon) \\ 6\alpha & 3\alpha\ell \end{bmatrix} \begin{bmatrix} y_L \\ \gamma_L \end{bmatrix} \qquad (C2)$$

$$\begin{bmatrix} M_R \\ -S_R \end{bmatrix} = \begin{bmatrix} 1 & \ell \\ 0 & 1 \end{bmatrix} \begin{bmatrix} M_L \\ -S_L \end{bmatrix}$$

where

$$\epsilon = \frac{12(1+\nu)I}{\ell^2 A_s} \quad \text{and} \quad \alpha = \frac{2EI}{\ell^3(1+2\epsilon)} \qquad (C3)$$

If there are (n - 1) beam sections and the displacements $(y_1,\ldots,y_n)$ and rotations $(\gamma_1,\ldots,\gamma_n)$, are imposed at the n beam section ends, the forces $(S_1,\ldots,S_n)$ (considered positive upwards) and moments $(M_1,\ldots,M_n)$ (considered positive anticlockwise) necessary to maintain the imposed shape will be given by

$$\begin{bmatrix} \underset{\sim}{S} \\ \underset{\sim}{M} \end{bmatrix} = \begin{bmatrix} A & B \\ B^T & C \end{bmatrix} \begin{bmatrix} \underset{\sim}{y} \\ \underset{\sim}{\gamma} \end{bmatrix} \qquad (C4)$$

where the elements of the (nxn) matrices A, B and C are given by

$$a_{ii-1} = 6\alpha_{i-1} \;;\; b_{ii-1} = -3\alpha_{i-1}\ell_{i-1} \;;\; c_{ii-1} = \alpha_{i-1}\ell_{i-1}^2(1-\epsilon_{i-1})$$

$$a_{ii} = 6(\alpha_{i-1} + \alpha_i) \;;\; b_{ii} = -3\alpha_{i-1}\ell_{i-1} + 3\alpha_i\ell_i;$$

$$c_{ii} = \alpha_{i-1}\ell_{i-1}^2(2+\epsilon_{i-1}) + \alpha_i\ell_i^2(2+\epsilon_i)$$

$$a_{ii+1} = -6\alpha_i \;;\; b_{ii+1} = 3\alpha_i\ell_i \;;\; c_{ii+1} = \alpha_i\ell_i^2(1-\epsilon_i)$$

Here (ϵ_i, α_i) are the values given by (C3) for the i^{th} beam section and α_o and α_n are defined to be zero.

The stiffness matrix in equation (C4) may be readily shown to allow the two degrees of freedom in the vertical plane (translation and rotation) expected of a free-free beam, without giving rise to forces or moments. It is therefore of rank (n-2).

Under conditions where the applied moments are known to be very small it is not possible to specify the rotations. These will then be related to the displacements by the equation

$$\underset{\sim}{\gamma} = -C^{-1}B^{T}\underset{\sim}{y} \qquad (C5)$$

and the forces necessary to maintain the displacements $\underset{\sim}{y}$ are then

$$\underset{\sim}{S} = [A - BC^{-1}B^{T}]\underset{\sim}{y} \qquad (C6)$$

This form can be useful since for ship vibrations the rotary inertias are generally small enough to be neglected.

References:

1. Biles, J.H.; "The Strength of Ships with Special Reference to Experiments and Calculations Made upon HMS WOLF." Trans. I.N.A., Vol XLVII, 1905.

2. Taylor, J.L.; "The Theory of Longitudinal Bending of Ships." Trans. North East Coast Institution of Engineers and Shipbuilders, Vol. XLI, 1924-25.

3. Kell, C.O. ; "Investigation of Structural Characteristics of Destroyers PRESTON and BRUCE, Part 2 - Analysis of Data and Results." Trans. SNAME, Vol. 40, 1932.

4. Shepheard, R.B. and Turnbull, J. ; "Structural Investigation in Still Water on the Welded Tanker NEVERITA, Part II - The Tests and Their Results." Trans. I.N.A., Volume 88, 1946.

5. Shepheard, R. B. and Bull, F.B. ; "Structural Investigations in Still Water on the Tanker NEWCOMBIA." Trans. North East Coast Institute of Engineering and Shipbuilders, Vol. 63, 1947.

6. Vasta, J. ; "Structural Tests on the Liberty Ship S.S. PHILIP SCHUYLER." Trans. SNAME, Vol. 55, 1947.

7. Vasta, J. ; "Structural Tests on the Passenger Ship S.S. PRESIDENT WILSON - Interaction Between Superstructure and Main Hull Girder." Trans. SNAME, Vol. 57, 1949.

8. Lang, D. W. and Warren, W. G. ; "Structural Strength Investigations on Destroyer ALBUERA." Trans. I.N.A., Vol. 94, 1952.

9. Chapman, J. C. ; "The Interaction Between a Ship's Hull and a Long Superstructure." Trans. I.N.A., Vol. 99, No. 4, Oct. 1957.

10. Johnson, A. J. ; "Stresses in Deckhouses and Superstructures" Trans. I.N.A., Vol. 99, No. 4, Oct. 1957.

11. Caldwell, J. B. ; "The Effect of Superstructures on the Longitudinal Strength of Ships." Trans. I.N.A. Vol. 99, No. 4, Oct. 1957.

12. Schade, H. A. ; "Two Beam Deckhouses Theory with Shear Effects." Schiff und Hafen, Heft 5/1966, 18. Jahrgang.

13. Todd, F. H. ; "Ship Hull Vibration." Edward Arnold (Publishers) Ltd.

14. Anderson, G. and Normand, K. ; "A Method for the Calculation of Vertical Vibration with Several Nodes and some other Aspects of Ship Vibration." Trans. I.N.A., Vol. 111, No 3,367, July 1969.

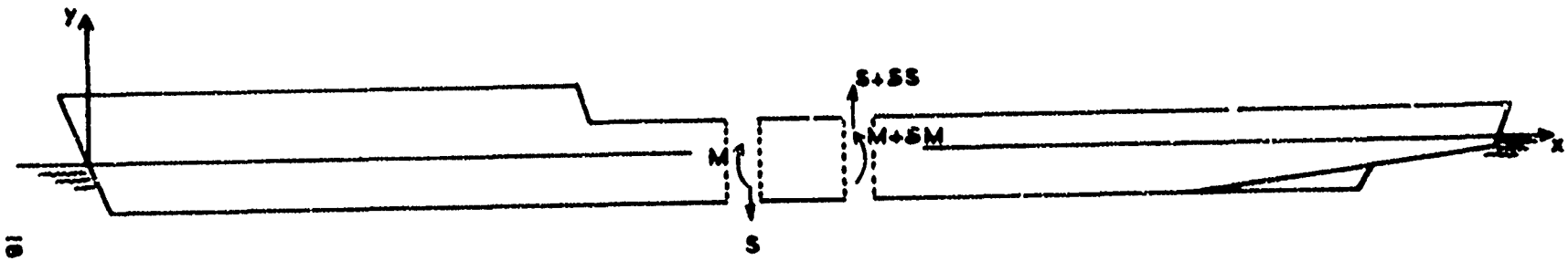

SIGN CONVENTION FOR BEAM REALISATION EQUATIONS

FIGURE C1

D The Hydrodynamic Forces on the Ship

Since 'strip' theory has over the last 50 years been the principal, in fact almost sole method of allowing for the entrained mass of water for vibration problems in still water, it has been used here in the initial formulation of the equations. An alternative, more accurate method is presented later. Strip theory was first introduced in 1929 by Lewis (D1) and has changed very little since that time. Lewis exploited the long slender nature of ships by assuming that close to the ship the hydrodynamic flow would be largely confined to planes perpendicular to the ship axis and so at each cross-section would approximate closely to the two-dimensional flow around a cylinder having the same cross-section as the ship hull at the point of interest. This should clearly give a good approximation to the local flow except near nodes, where the ship motion is largely a rotation about the node, or where the ship cross-section is changing fairly rapidly, for example near the bow and stern. Near these exceptional points there will be a significant flow along the ship axis. Ignoring these points, with their associated three-dimensional flow fields, the force per unit length on any cross-section of the hull will be identical to that of the corresponding two dimensional flow on the cylinder. Conformal transformations were used to extend the well-known flow around a two-dimensional circular cylinder into flows around appropriately shaped cylinders. Lewis use' the transformation

$$Z = s + \frac{a}{s} + \frac{b}{s^3}$$

to give the flow around the cross-sections shown in Figure D1. The added masses per unit length (μ) were related to the added mass of a circular cylinder of the same'beam'as the ship section by the formula

$$\mu = C \left[\frac{1}{2} \pi \rho \left(\frac{B}{2} \right)^2 \right]$$

The coefficients C are given for the cross-sections in Figure 1.

In order to allow, at least partially, for the three-dimensional flow effects, Lewis compared the strip theory flow around a prolate spheroid, vibrating in a certain 'mode' shape similar to a ship vibration mode, to the exact flow deduced by an expansion of the flow in terms of spheroidal harmonic functions. The kinetic energy of the approximate flow is naturally greater than that of the exact flow (Kelvin's minimum energy theorem) so that the deduced added mass will also be greater. Lewis suggested that the calculated added mass distribution for the ship shape should be reduced by a factor J, the ratio of the exact to the approximate kinetic energies for a spheroid with the same beam to length ratio as the ship.

The whole procedure gives very good results for the lower frequency vibration modes of ships and forms the basis of almost all current methods for calculating the effect of the water. It has two rather basic disadvantages however. Firstly, the reduction factor J for the 3-D flow effect depends on the shape of the mode to be calculated, which makes it difficult to formulate a single equation whose eigenvalues are the ship frequencies; a different equation has to be solved for each mode. Secondly there is no guarantee that an exact reduction factor would not vary along the length of the ship, and in general this is the case.

Although the method is still the basis for entrained mass calculations, numerous minor improvements have been made since Lewis' paper. Taylor (D2), arrived at the same approximate strip theory independently of Lewis and again calculated a reduction factor by comparison with the solution for a spheroid. However, Taylor's solution for the spherical vibration allowed a bending type of

motion, as well as the shearing motions, on which Lewis calculations were based, in the boundary condition on the spheroid. In consequence his reduction factors give smaller entrained masses than those of Lewis. Curves for both types of reduction coefficient are shown, for the 2-node vibration mode, in Figure D2. Taylor also gave a second set of reduction coefficients based on an exact solution for the three dimensional motion of an infinite cylinder vibrating transversely, its velocity distribution varying sinusoidally along its length. These reduction factors are also included in Figure D2. To calculate them the Taylor Form of ellipsoid motion was assumed. This has nodes at $\pm L(1-2B^2/L^2)^{\frac{1}{2}}/2\sqrt{5}$, measured from its centre. The distance between these nodes was assumed to be the half wavelength for the cylinder motion whence the appropriate reduction factor can be readily found. That they agree slightly better with Lewis' original results is not surprising since the boundary conditions used by the two methods coincide when the vibrating body has a constant cross-section. Only when appreciable changes in section occur, as close to ends of the spheroid, or, to a lesser extent, near the bow and stern of ships, do the boundary conditions and hence the calculated reduction factors differ.

Prohaska (D3), considerably generalised Lewis' two-dimensional cross-sections by considering the transformation

$$Z = s + a/s^m + b/s^n.$$

for the cases (m,n) = (1,5), (1,7) and (3,7). Lewis' sections of course are for (m, n) = (1, 3). From these results Prohaska found that for sections with some parts concave outwards, the added mass was very close to that for the same section with the concavity replaced by a tangent line. Making use of this device he then

found the coefficient C could be determined with good accuracy as a function simply of the section area coefficient β (the underwater area divided by beam x draft, BD) and the ratio beam/draft. He gave the functional form as the graph reproduced in Figure D3. This graph enables the added mass to be found to reasonable accuracy without the tedious comparison of the actual cross-section with those of Lewis to find the best fit.

The set of cross-sectional shapes for which the added mass is known has been further extended in recent years by Landweber and Macagno and co-workers D4, D5. These authors used a three parameter fit for the sections rather than the two parameter fits used by Lewis and Prohaska. Macagno also made use of 'close-fit' conformal mappings of sections, and other authors, e.g. Hoffman (D6) have demonstrated similar methods. These use an arbitrary number of coefficients in the series

$$Z = z + \frac{a_1}{z} + \frac{a_3}{z^3} + \frac{a_5}{z^5} + \ldots$$

to obtain as close a fit to the actual section as desired. Quite complicated computer programs have to be used however to obtain the coefficients for the best fit transformation.

Wendel (D7) has given the added mass for a square cross-section with 'bilge-keels'; plates projecting at 45^0 from each corner. These results are particularly interesting as they appear to be the only ones available on the effects of such keels. The method used to obtain them was an application of the Schwarz-Christoffel transformation. Unfortunately, the method is very tedious to apply and the results were not extended to general rectangles with bilge keels. The results for such shapes can however probably be estimated fairly well by Prohaska's method; simply using the added mass for the rectangle which circumscribes the ends of the bilge keels

(the dotted rectangle in Figure D4). For the square section Wendel quoted the results in the table for the % increase in the coefficient C for various values of d/b (the bilge keel width to half beam ratio). If the added mass of the circumscribed section is taken, the factor by which C is increased (relative to the original rectangle) is $(1 + \frac{d}{\sqrt{2}b})^2$. The % increases due to this factor have been included in the table.

d/b	C	% increase in C	% increase given by $(1 + d/\sqrt{2}b)^2$
0	1.512	0	0
0.0494	1.61	6.74	7.10
0.123	1.80	19.05	18.16
0.2278	2.11	39.5	34.8

Wendel's Bilge Keel Effect

The approximate result should be close enough for practical purposes. Wendel also commented on the constancy of the 3-D flow correction factor along the length of the ship and showed that in fact, even for such an unlikely case as a rigid sphere, the factor can be exactly constant, at least for rigid body motions.

This point was also considered by Kaplan (D8) who showed that for arbitrary 'slender' bodies the reduction factor is constant at least for rigid body motions. He also showed that the reduction factor is constant for both Lewis' and Taylor's assumed 2-node vibration modes of a spheroid. The proof for the Taylor mode shape however is not quite correct and in fact the local reduction factor does vary for this case. Kaplan's paper gives an excellent survey of the virtual mass problem as it stood in 1959. In it he discusses

the effects of viscosity, compressibility and surface waves and concludes that all should be very small (except possibly viscosity) for normal vibration frequencies.

The surface wave problem has been considered by a number of authors, e.g. Ursell(D9), Porter(D.0)and Choung Mook Lee,(D11). The results all show that for the pitching and heaving ship modes the effect of the surface waves changes the added mass appreciably and provides significant damping. However, for the vibration modes, which are of rather higher frequency, the effect of surface waves becomes negligible.

Hydrodynamic Forces in Moving water.

According to strip theory the hydrodynamic force on a ship cross-section which has an acceleration $\dot{v}$ is

$-\mu\dot{v}$ per unit length where $\mu = CJ\left[\tfrac{1}{2}\pi\rho\left(\frac{B}{2}\right)^2\right]$ (D1)

B is the ship beam, ρ the density of water, C a factor derived from a 2-dimensional flow problem and J is a correction factor for 3-D flow effects. To help determine the force when the surrounding water is also in motion it is helpful to show the dependence of C on the potential ϕ of the 2-D flow problem. With the geometry of Figure D5 the potential ϕ satisfies the following equations:-

$\nabla^2\phi = 0$ (incompressible flow)

$\phi = 0(\frac{1}{r})$, $r \to \infty$ (only a dipole field at large distances)

$\frac{\partial\phi}{\partial n} = -v\cos\theta'$ on Γ (the ship-shaped cylinder cross-section)

If the potential for the case $v = 1$ is denoted by $\bar{\phi}$, then $\phi = v\bar{\phi}$ and $\bar{\phi}$ satisfies $\nabla^2\bar{\phi} = 0$

$\bar{\phi} = 0(\frac{1}{r})$, $r \to \infty$

$$\frac{\partial \bar{\phi}}{\partial n} = -\cos\theta' \text{ on } \Gamma \qquad \text{(D2)}$$

The usual form of Bernouilli's equation gives the pressure in the fluid

$$p = p_o + \rho\frac{\partial}{\partial t}(v\bar{\phi}) - \tfrac{1}{2}\rho u^2 \qquad \text{(D3)}$$

where p_o is the hydrostatic pressure and u the local velocity. Neglecting ρu^2 compared to $\rho \frac{\partial \phi}{\partial t}$ gives $p = p_o + \rho\dot{v}\bar{\phi}$ and the force acting on the cylinder is simply

$$-\oint_\Gamma p\, dn = -\rho\dot{v}\oint_\Gamma \bar{\phi}\, dn \qquad \text{(D4)}$$

so that, comparing with (D1),

$$\mu = \tfrac{1}{2}\rho\oint_\Gamma \bar{\phi}\, dn \qquad \text{(D5)}$$

The factor $\frac{1}{2}$ allows for the upper half of the fluid not being present since y = o is the free surface.

When the surrounding fluid also has a velocity, U, at infinity, the potential ϕ' must satisfy the equations

$$\nabla^2\phi' = o$$

$$\phi' = -Uy + O(\tfrac{1}{r}),\ r \to \infty$$

$$\frac{\partial \phi'}{\partial n} = -v\cos\theta' \quad \text{on } \Gamma$$

Clearly this potential is given by $\phi' = -Uy - (U-v)\bar{\phi}$ for this satisfies the first two conditions and on Γ

$$\frac{\partial \phi'}{\partial n} = -U\frac{\partial y}{\partial n} - (U-v)\frac{\partial \bar{\phi}}{\partial r} = -U\cos\theta' - (U-v)(-\cos\theta') = -v\cos\theta'$$

as required.

The pressure in the water is now (again neglecting ρu^2 terms)

$$p = p_o + \rho\frac{\partial}{\partial t}[-Uy - (U-v)\bar{\phi}]$$

and the force on the cylinder is

$$-\oint_\Gamma p\, dn = \rho\dot{U}\oint_\Gamma y\, dn + \rho(\dot{U}-\dot{v})\oint_\Gamma \bar{\phi}\, dn$$

Now $\dot{\phi}\, ds\, dn$ is the area within the contour Γ, i.e. $2A$ where A is the underwater area of the cross-section, so that the force on the underwater section is

$$F = \rho A\dot{U} + \mu(\dot{U} - \dot{v}) \qquad (D6)$$

which reduces to the previous case when $\dot{U} = 0$. This equation is in fact rather obvious. The second term is the inertial force due to the relative acceleration of the cylinder and the fluid and the first is the 'buoyancy' force due to the pressure gradient required in the water to give it the acceleration $\dot{U}$. Under gravity the fluid effectively has an acceleration $\dot{U} = g$ and the first term becomes the weight of the displaced water, as is assumed in hydrostatic calculations.

This result is applied in the same way as normal strip theory. The vertical velocity of the water due to the explosion bubble motion can be calculated at each point of the ship axis, (the intersection of its centreplane with the waterline plane), as though the ship were not present. If the charge is far enough from the ship for this velocity distribution to vary only slowly along the length then at each cross-section the disturbance potential necessary to correct the local flow for the presence of the ship will, as above, be approximately $-(U-v)\bar{\phi}$ ($\bar{\phi}$ being appropriate to the section shape) and the force on the ship will be as given by (D6).

Since μ has been expressed in the form

$$\mu = C\left[\tfrac{1}{2}\pi\rho\left(\frac{B}{2}\right)^2\right]J$$

it is convenient to express $\Delta\rho$ similarly so that

$$\Delta\rho = \bar{\mu} = \bar{C}\left[\tfrac{1}{2}\pi\rho\left(\frac{\bar{B}}{2}\right)^2\right]$$

In this case however, since the 'buoyancy' force depends on a pressure gradient independent of the shape of the ship, no three-dimensional correction factor is required. The values of the coefficient $\bar{C}$ for Lewis' sections have been added to Figure D1. $\bar{C}$ is related to the usual section area coefficient, β, by

$$\bar{C} = \frac{3}{\pi} \frac{D}{B}\beta$$

References

1. Lewis, F M ; "The Inertia of the Water Surrounding a Vibrating Ship." Trans. SNAME, Vol 37, 1929.

2. Taylor, J L ; "Some Hydrodynamical Inertia Coefficients." Phil Mag S.7, Vol 9, No 55, Jan 1930.

3. Prohaska, C W; "The Vertical Vibration of Ships." The Shipbuilder and Marine Engine Builder, 1947.

4. Landweber, L and Macagno, M ; "Added Mass of a Three Parameter Family of Two-Dimensional Forms Oscillating in a Free Surface." Jn of Ship Research, Vol 2 No 4, 1959.

5. Macagno, M ; "A comparison of Three Methods for Computing the Added Masses of Ship Sections", Jn. of Ship Research, Vol 12, No 4, 1968.

6. Hoffman, D ; "Conformal Mapping Techniques in Ship Hydrodynamics." Webb Inst of Naval Architecture Report No 41-1, 1969.

7. Wendel, K ; "Hydrodynamic Masses and Moments of Inertia." Jahrbuch der Schiffbautechnische Gesellschaft, Vol 44, 1950; (also DTMB Translation 260, 1956).

8. Kaplan, P ; "A Study of the Virtual Mass Associated with the Vertical Vibration of Ships in Water." Stevens Inst. Tech., Davidson Lab. Report 734, 1959.

9. Ursell, F ; "On the Heaving Motion of a Circular Cylinder on the Surface of a Fluid." Quart. Jn. Mech. and Applied Maths, 2, 1949.

10. Porter, W R ; "The Pressure Distribution, Added Mass and Damping Coefficient for a Cylinder Oscillating in a Free Surface." Univ. Calif. Inst. Eng. Res. Series 82, Issue 16, 1960.

11. Choung Mook Lee ; "The Second Order Theory of Cylinders Oscillating in a Free Surface." Jn. Ship Research, Vol 12, No. 4, 1968.

CURVES REFER TO UNDERWATER CROSS SECTIONAL AREA

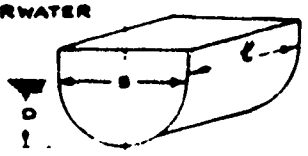

$$m_w = \tfrac{1}{2}\pi\rho\left(\frac{B}{2}\right)^2 \ell\, C\, J.$$

$$\bar{m}_w = \tfrac{1}{2}\pi\rho\left(\frac{B}{2}\right)^2 \ell\, \bar{C}.$$

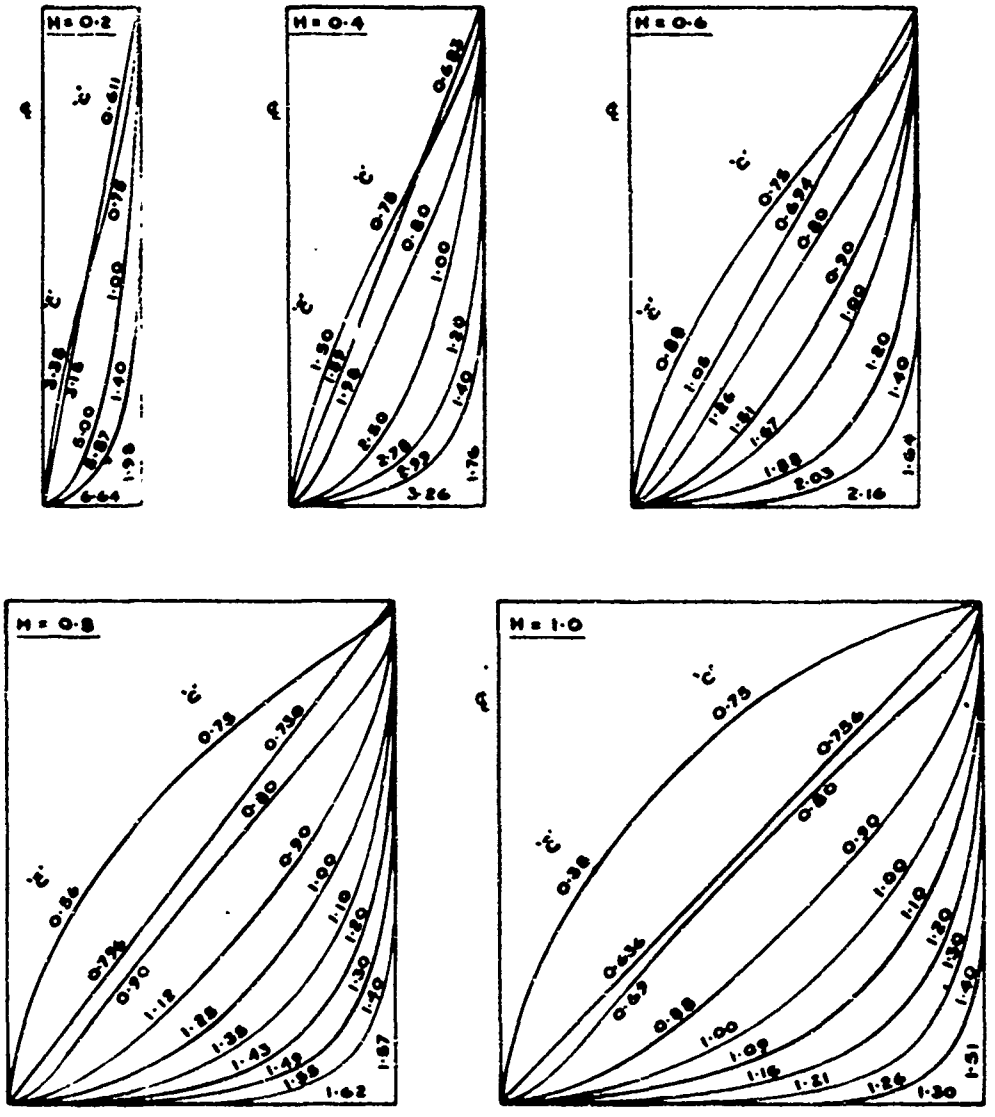

VALUE OF INERTIA COEFFICIENTS C AND $\bar{C}$

$$H = \frac{\text{HALF BEAM}}{\text{DRAFT}} = \frac{B}{2D}$$

FIGURE D1(a)

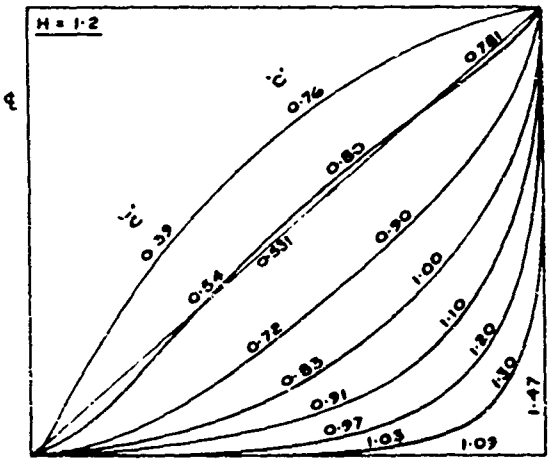

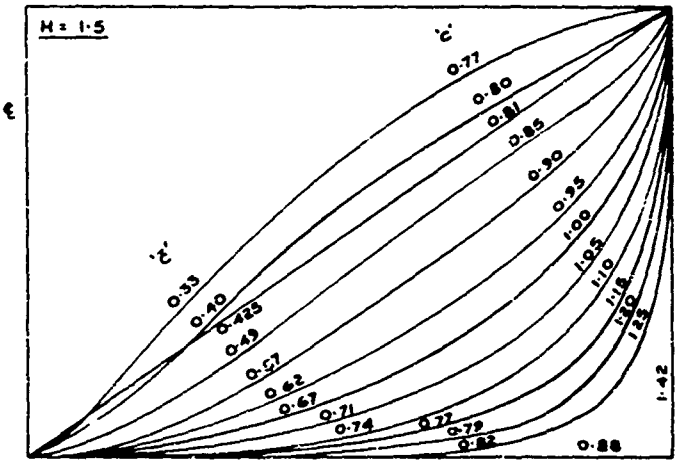

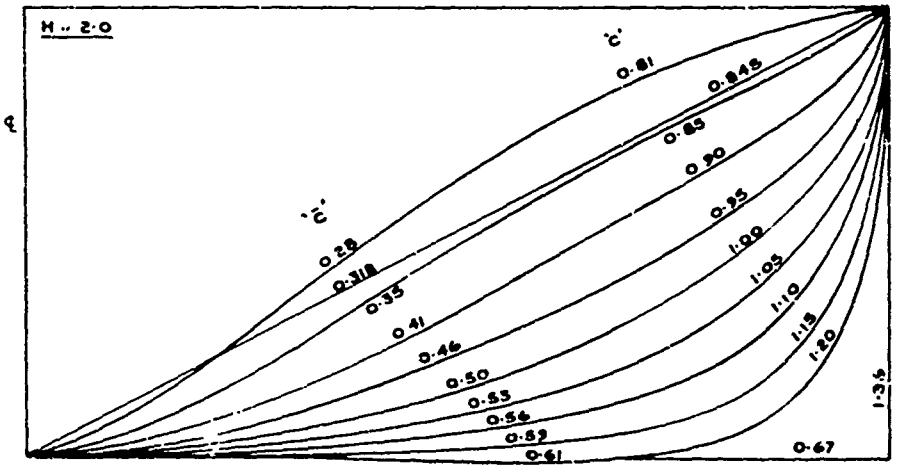

VALUE OF INERTIA COEFFICIENTS C AND $\bar{C}$

$$H = \frac{\text{HALF BEAM}}{\text{DRAFT}} = \frac{B}{2D}$$

FIGURE 5.1(a)

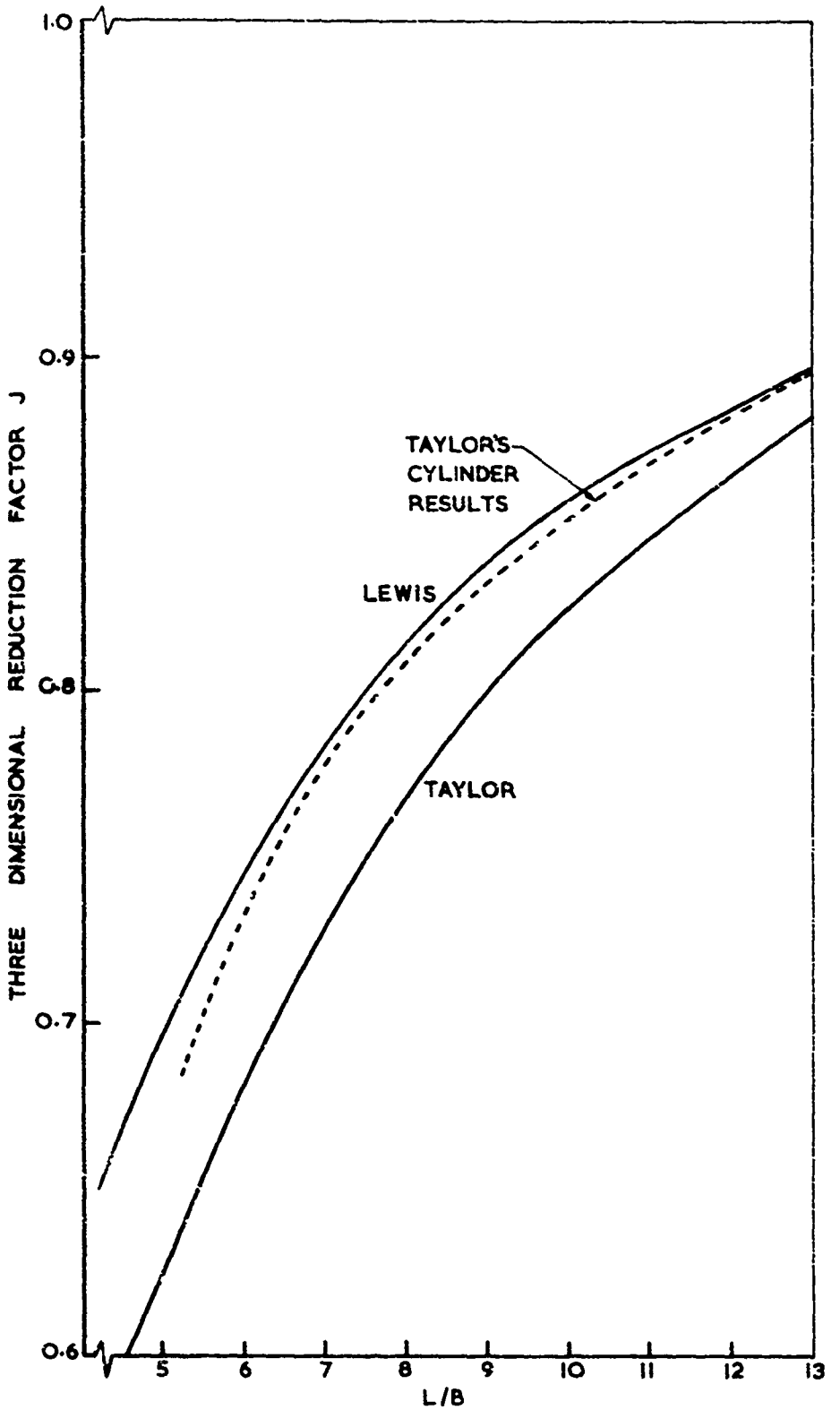

THREE - DIMENSIONAL REDUCTION COEFFICIENT

FIGURE D2

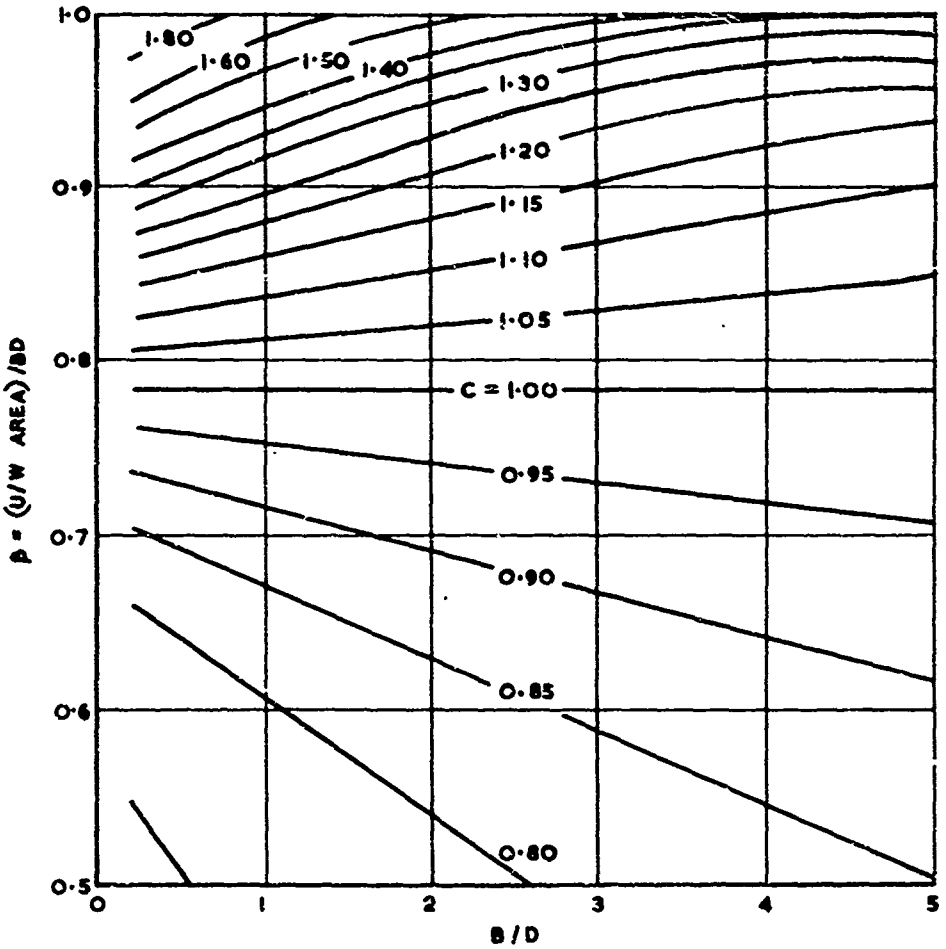

TWO - DIMENSIONAL SECTION VIRTUAL MASS COEFFICIENT

FIGURE D3

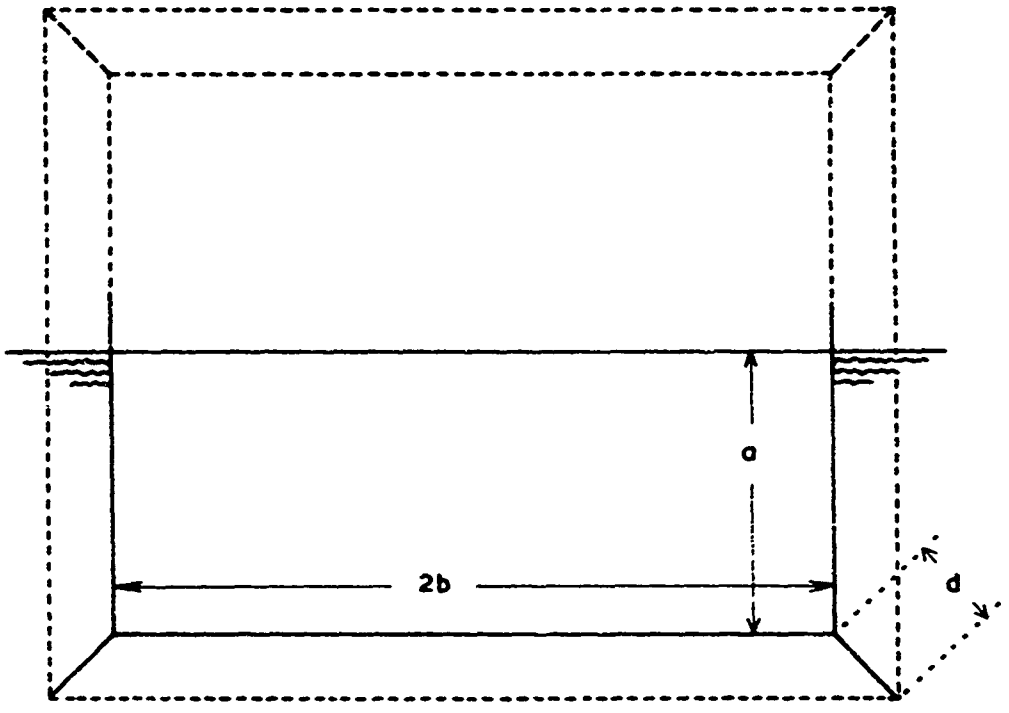

WENDEL'S RECTANGLE WITH BILGE KEELS

FIGURE D4

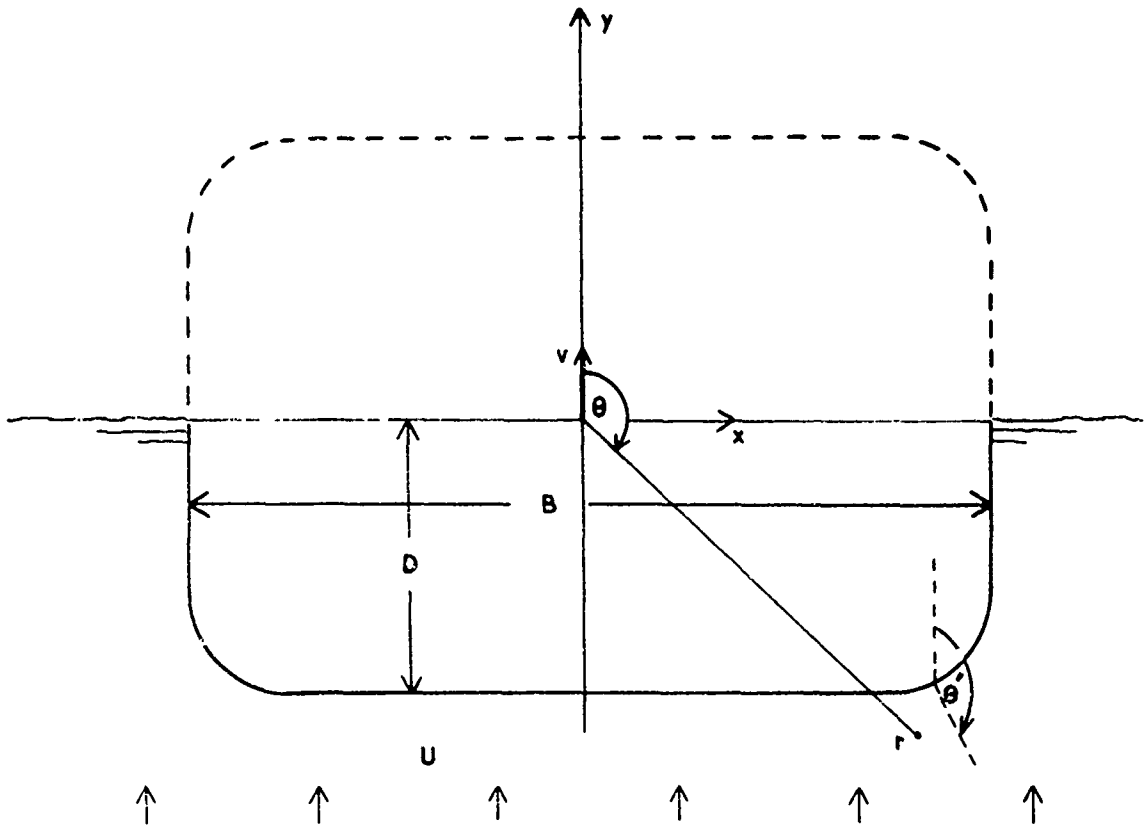

GEOMETRY FOR ACCELERATING FLOW

PAST A 2-D SHIP SECTION

FIGURE D5

E Equations of Motion

The only external forces acting on the ship are the hydrodynamic ones discussed in the previous section. These form a continuous distribution of force along the ship. In addition to these, the inertial forces due to the ship's own mass also act and again form a distribution along the entire length. The formulation of the elastic nature of the ship assumed only forces acting at the discrete 'nodes' between the beam sections. Current methods of finite element analysis generally use consistent-mass matrices derived from energy considerations. These divide the mass between the element nodes in the most effective manner. However, for the beam displacement shapes inherent in the elastic formulation the split is rather complicated and also much of the ship mass comes from material such as machinery, transverse bulkheads, etc., which is not continuously distributed. It is consequently convenient and reasonable to simply split the ship into n equal sections, lump the total mass and inertia of each section into a single mass and inertia at the centre of the section, and take the elastic beams to be the (n-1) equal lengths connecting these masses. The length ℓ of each elemental beam is L/n. If the variation in cross-sectional shape is fairly slow, the lumped hydrodynamic force and moment at the ith mass will be from (D6) (μ again being the added mass per unit length),

$$S_{hdi} = [\mu_i(\dot{u}_i - \ddot{y}_i) + \bar{\mu}_i \dot{u}_i]\ell$$

$$M_{hdi} = [\frac{d\mu_i}{dx}(\dot{u}_i - \ddot{y}_i) + \mu_i(\frac{d\dot{u}_i}{dx} - \frac{d\ddot{y}_i}{dx}) + \frac{d\bar{\mu}_i}{dx}\dot{u}_i + \bar{\mu}_i \frac{d\dot{u}_i}{dx}]\frac{\ell^3}{12} \qquad \text{(E1)}$$

where all terms of order $\frac{d^2}{dx^2}$ and $(\frac{d}{dx})^2$ have been neglected.

The corresponding hydrostatic terms (loss of buoyancy due to upward displacement will be

$$S_{hsi} = -B_i \ell\, y_i$$

$$M_{hsi} = -(\frac{dB_i}{dx} y_i + B_i \frac{dy_i}{dx})\frac{\ell^3}{12} \qquad \text{(E2)}$$

The normal inertial force and moment are

$$S_{Ii} = -m_i \ddot{y}_i \qquad (E3)$$

$$M_{Ii} = -r_i \frac{d\ddot{y}_i}{dx}$$

Combination of equations (E1) to (E3) gives

$$S_i = -(m_i+m_{wi})\ddot{y}_i - k_i y_i + (m_{wi}+\bar{m}_{wi})\dot{u}_i$$

$$M_i = -r'_{wi}\ddot{y}_i - k'_{ri} y_i + (r'_{wi}+\bar{r}'_{wi})\dot{u}_i - (r_i+r_{wi})\ddot{\gamma}_i - k_r\gamma_i +$$

$$(r_{wi}+\bar{r}_{wi})\frac{d\dot{u}_i}{dx} \qquad (E4)$$

where $m_{wi} = \mu_i \ell$, $\bar{m}_{wi} = \bar{\mu}_i \ell$, $r_{wi} = \frac{1}{12} m_{wi} \ell^2$, $\bar{r}_{wi} = \frac{1}{12} \bar{m}_{wi} \ell^2$

$$k_i = B_i \ell, \quad k_{ri} = \frac{1}{12} k_i \ell^2$$

$$r'_{wi} = \frac{1}{12}\left(\frac{d\mu}{dx}\right)_i \ell^3, \quad \bar{r}'_{wi} = \frac{1}{12}\left(\frac{d\bar{\mu}}{dx}\right)_i \ell^3$$

$$k'_{ri} = \frac{1}{12}\frac{dB_i}{dx}\ell^3$$

In matrix form these equations (E4) become

$$\begin{bmatrix} S \\ \sim \\ M \\ \sim \end{bmatrix} = -\begin{bmatrix} M + M_w & 0 \\ R'_w & R+R_w \end{bmatrix}\begin{bmatrix} \ddot{y} \\ \sim \\ \ddot{\gamma} \\ \sim \end{bmatrix} - \begin{bmatrix} K & 0 \\ K'_r & K_r \end{bmatrix}\begin{bmatrix} y \\ \sim \\ \gamma \\ \sim \end{bmatrix} + \begin{bmatrix} M_w+\bar{M}_w & 0 \\ R'_w+\bar{R}'_w & R_w+\bar{R}_w \end{bmatrix}\begin{bmatrix} \dot{u} \\ \sim \\ \dot{u}' \\ \sim \end{bmatrix} \qquad (E5)$$

where $u' = \frac{du}{dx}$ and the submatrices are all diagonal with the obvious elements. This equation is slightly inconvenient as it involves the off-diagonal submatrices R'_w, $\bar{R}'_w$ and K'_r. Over most of the length of a ship the cross-section is almost constant so that these terms will be very small except possibly near the ends. Strip theory already ignores longitudinal flow due to changing cross-section in these regions. It is therefore consistent with strip theory to neglect the terms and use the

equation

$$\begin{bmatrix} S \\ \sim \\ M \\ \sim \end{bmatrix} = - \begin{bmatrix} M+M_w & 0 \\ 0 & R+R_w \end{bmatrix} \begin{bmatrix} \ddot{y} \\ \sim \\ \ddot{\gamma} \\ \sim \end{bmatrix} - \begin{bmatrix} K & 0 \\ 0 & K_r \end{bmatrix} \begin{bmatrix} y \\ \sim \\ \gamma \\ \sim \end{bmatrix} + \begin{bmatrix} M_w+\bar{M}_w & 0 \\ 0 & R_w+\bar{R}_w \end{bmatrix} \begin{bmatrix} \dot{u} \\ \sim \\ u' \\ \sim \end{bmatrix} \quad \text{(E6)}$$

On applying D'Alembert's Principle, these are the forces and moments necessary to maintain the displacement shape $(\underset{\sim}{y}, \underset{\sim}{\gamma})$ in the elastic equations (C4). The equations of forced motion of the ship are therefore:-

$$\begin{bmatrix} M+M_w & 0 \\ 0 & R+R_w \end{bmatrix} \begin{bmatrix} \ddot{y} \\ \sim \\ \ddot{\gamma} \\ \sim \end{bmatrix} + \begin{bmatrix} A+K & B \\ B^T & C+K_r \end{bmatrix} \begin{bmatrix} y \\ \sim \\ \gamma \\ \sim \end{bmatrix} = \begin{bmatrix} M_w+\bar{M}_w & 0 \\ 0 & R_w+\bar{R}_w \end{bmatrix} \begin{bmatrix} \dot{u} \\ \sim \\ u' \\ \sim \end{bmatrix} \quad \text{(E7)}$$

and for the still-water vibration the right hand side may be dropped.

In general, for ship vibration, it has been found that rotary inertia effects are usually fairly small. On neglecting the appropriate terms and putting $R = R_w = K_r = \bar{R}_w = 0$,

$$\underset{\sim}{\gamma} = -C^{-1}B^T \underset{\sim}{y}$$

and

$$(M + M_w)\ddot{\underset{\sim}{y}} + (A+K - BC^{-1}B^T)\underset{\sim}{y} = (M_w+M_w)\dot{\underset{\sim}{u}} \quad \text{(E8)}$$

Neglect of rotary inertia in these lumped mass equations of motion differs from its neglect from the normal Timoshenko beam equations since here it has a slightly different meaning. In the Timoshenko beam equation rotary inertia refers to the inertia of an infinitesimally thin cross-sectional slice of the beam, and so is related purely to the depth of the beam and the amount of material away from the centre of rotation. Here the rotary inertia includes this term but also includes a term due to part of each lumped mass being a finite distance from the mass in the longitudinal direction. It therefore depends on the distance between the lumped masses and so is a

function of the beam representation rather than an intrinsic property of cross-sections of the beam. Only if the number of lumped masses representing the beam were allowed to tend to infinity would the two forms of rotary inertia coincide. In the equations used here, each fluid rotary inertia is entirely due to this lumping of longitudinal forces into a point load and so vanishes entirely in the limit of an infinite number of lumped masses.

It may be noticed that if the ship is in still water and is not vibrating then the equations (E7) or (E8) are satisfied by zero deflections everywhere. They therefore do not include any static bending moments and shear forces due to mismatches between the hydrostatic buoyancy and weight distributions. These static terms were omitted in equation (E4) for simplicity in the dynamic equations. Any stresses deduced from equations (E7) and (E8) during motion are to be superimposed on the existing static stress distribution in the ship.

The equations include the buoyancy terms K and K_r and so contain the heaving and pitching ship frequencies, at least for small displacements where the additional hydrostatic buoyancy forces are linear functions of the displacement.

F The Normal Mode Equations

The equations (E7) and (E8) are both linear and of the general form

$$M_1 \ddot{\underset{\sim}{y}} + S\underset{\sim}{y} = M_2 \dot{\underset{\sim}{u}} \qquad (F1)$$

where M_1 and M_2 are diagonal matrices and S is a symmetric positive definite, stiffness matrix. For these equations to predict the transverse ship motions with any accuracy, the ship has to be split into at least 20 lumped masses and the direct integration of the equations becomes rather tedious. This is especially so since the equations will then contain at least 20 normal mode frequencies the highest of which will be little less than that of the vibration of a single lumped mass on its two weightless beams, all the other masses being considered stationary. Clearly such a mode will have no physical meaning, but its frequency will be very high, and will become higher as the number of masses is increased. Direct numerical integration of equations (F1) requires a time increment no greater than about 1/6th of the period of this highest mode if numerical instabilities are to be avoided. In consequence the direct integration involves the integration of a large number of equations using a very small time increment.

A simple alternative is to split the equation into its normal modes and to reject at the outset the higher modes known to have no physical basis. Since M_1 is diagonal the simple transformation

$$\underset{\sim}{z} = M_1^{\frac{1}{2}} \underset{\sim}{y}$$

(where $M_1^{\frac{1}{2}}$ is diagonal with elements $m_i^{\frac{1}{2}}$) reduces (F1) to

$$\ddot{\underset{\sim}{z}} + E\underset{\sim}{z} = M_1^{-\frac{1}{2}} M_2 \dot{\underset{\sim}{u}}, \qquad (F2)$$

where $E = M_1^{-\frac{1}{2}} S M_1^{-\frac{1}{2}}$

Since S is symmetric and positive definite, E will have similar properties and its eigenvalues will be real and positive. The eigenvectors and eigenvalues of E can therefore be written in the form $\underset{\sim}{a}_i$, ω_i^2 and the vectors will form an orthogonal set,

$$\text{i.e.} \qquad \underset{\sim}{a}_i^T \underset{\sim}{a}_j = M_i \delta_{ij} \qquad \text{(F3)}$$

where M_i is a positive non-zero scalar. The vectors $\underset{\sim}{a}_i$ form a complete set so that the vectors $\underset{\sim}{a}$ and $M_1^{-\frac{1}{2}} M_2 \dot{\underset{\sim}{u}}$ may be expressed as

$$\underset{\sim}{a} = \sum_{i=1}^{N} \alpha_i(t) \underset{\sim}{a}_i \quad ; \quad M_1^{-\frac{1}{2}} M_2 \dot{\underset{\sim}{u}} = \sum_{i=1}^{N} \beta_i(t) \underset{\sim}{a}_i, \qquad \text{(F4)}$$

when E is of order (N x N).

Substitution of these expressions into equation (F2) and use of the orthogonality of the $\underset{\sim}{a}_i$ gives

$$\ddot{\alpha}_i + \omega_i^2 \alpha_i = \beta_i(t), \quad (i = 1, \ldots, N)$$

These equations are independent and only the few low frequency modes of interest need be solved.

The ship deflection shapes corresponding to the normal modes are given by

$$\underset{\sim}{y}_i = M_1^{-\frac{1}{2}} \underset{\sim}{a}_i$$

In terms of these displacement shapes the orthogonality relations (F2) become

$$\underset{\sim}{y}_i^T M_1 \underset{\sim}{y}_j = M_i \delta_{ij}$$

$$\text{ie} \qquad \sum_{k=1}^{N} m_k y_{ki} y_{kj} = M_i \delta_{ij} \qquad \text{(F5)}$$

Similarly, multiplying the second of equations (F4) by $\underset{\sim}{s}_j^T$ gives the forcing function $\beta_j(t)$ as

$$M_j \beta_j(t) = \underset{\sim}{s}_j^T M_1^{-\frac{1}{2}} M_2 \underset{\sim}{\ddot{\delta}} = \underset{\sim}{y}_j^T M_2 \underset{\sim}{\ddot{\delta}} = \sum_{k=1}^{N} m_{2k} y_{kj} \ddot{\delta}_k$$

$$\text{and} \quad \ddot{\alpha}_i(t) + \omega_i^2 \alpha_i(t) = \frac{1}{M_i} \sum_{k=1}^{N} m_{2k} y_{ki} \ddot{\delta}_k \quad , (i = 1, \ldots, N) \qquad \text{(F6)}$$

which gives the equations for the ith mode coefficients $\alpha_i(t)$ in terms of the hydrodynamic mass distributions, the displacement shape of the ith mode and the fluid accelerations at all the lumped mass positions.

If the coefficients $\alpha_i(t)$ are found by integration of equations (F6) the actual ship displacements, stresses etc. are easily determined from the equations:

$$\text{displacement} \qquad y(x,t) = \sum_{i=1}^{N} \alpha_i(t) y_i(x)$$

$$\text{velocity} \qquad \dot{y}(x,t) = \sum_{i=1}^{N} \dot{\alpha}_i(t) y_i(x)$$

$$\text{bending moment} \qquad M(x,t) = \sum_{i=1}^{N} \alpha_i(t) M_i(x) \qquad \text{(F7)}$$

$$\text{deck stress} \qquad \sigma(x,t) = \frac{\bar{y}(x)}{I(x)} M(x,t) \qquad (\ \bar{y} = \text{distance of the deck above the neutral axis}\ )$$

$$\text{shear force} \qquad S(x,t) = \sum_{i=1}^{N} \alpha_i(t) S_i(x)$$

where $y_i(x)$, $M_i(x)$ and $S_i(x)$ are the displacement, moment and shear force at the position x when the ship is in the ith mode (unit amplitude). With the normal mode shapes known (y_{ki}, γ_{ki} known at the kth mass) the displacement, moment and shear force for a point at a distance $\bar{x} = x - x_k$ from the left hand end are given by

$$\begin{bmatrix} y_i(x) \\ M_i(x) \\ S_i(x) \end{bmatrix} = \begin{bmatrix} 1 & \bar{x} & \frac{\bar{x}^2}{2EI_k} & -\frac{\bar{x}^3(1-\epsilon_k)}{6EI_k} \\ 0 & 0 & 1 & -\bar{x} \\ 0 & 0 & 0 & 1 \end{bmatrix} \begin{bmatrix} y_{ki} \\ M_L \\ S_L \end{bmatrix} \qquad \text{(F8)}$$

where M_L and S_L are given by equation (C2).

G Use of the Modal Equations for Free Vibration

To illustrate the use of the modal equations for free vibrations and to estimate their accuracy when used in ship calculations, three examples are considered:

a. A uniform solid beam in air and water

b. A hollow rectangular box-beam in air and water

c. A full scale ship

In some of the previous vibration calculations in the literature ships have been divided into up to 40 sections but 20 is the more usual number and has usually been found acceptable for the low modes. The examples are therefore based on 20 lumped masses. The calculations were carried out using the computer program I described later in section I.

a. Uniform Solid Beam

In 1928 in an early series of experiments on the effect of entrained water on the vibration of ships, Moullin and Browne (G1) used a series of uniform rectangular mild steel bars. The bars were 78 inches long, 2 inches deep and of varying thickness. The principal thickness was 1 inch. The cross-sectional moment of inertia for such a beam is $\frac{2}{3}BD^3$ (see Figure G1) i.e. 1/6 in^4. The shear area for a rectangular section is $2/3^{rds}$ of the cross-sectional area, i.e. $\frac{4}{3}in^2$. Then, for representing the beam by 20 equal lengths the equations of section C give:-

$\ell = 3.9"$; $I = .1667\ in^4$; $A_s = 1.333\ in^2$

$E = 30.10^6$ psi; $\nu = 0.3$

$$\epsilon = \frac{12(1+\nu)I}{\ell^2 A_s} = 0.1282 \quad ; \qquad \alpha = \frac{2EI}{\ell^3(1+2\epsilon)} = 0.1342.10^6 \text{ lb/in.}$$

The matrices A, B and C are then the (20 x 20) matrices

$$A = 10^6 \begin{bmatrix} .805 & -.805 & 0 & 0 & \cdots & 0 \\ -.805 & 1.610 & -.805 & 0 & \cdots & 0 \\ 0 & -.805 & 1.610 & -.805 & \cdots & 0 \\ \vdots & & & & & \vdots \\ & & & -.805 & 1.610 & -.805 \\ 0 & & & 0 & -.805 & .805 \end{bmatrix} \text{lb/in}$$

$$B = 10^6 \begin{bmatrix} 1.570 & 1.570 & 0 & 0 & \cdots & 0 \\ -1.570 & 0 & 1.570 & 0 & \cdots & 0 \\ 0 & -1.570 & 0 & 1.570 & \cdots & 0 \\ \vdots & & & & & \vdots \\ & & & -1.570 & 0 & 1.570 \\ 0 & & & 0 & -.1570 & -1.570 \end{bmatrix} \text{lb}$$

$$C = 10^6 \begin{bmatrix} 4.35 & 1.781 & 0 & 0 & \cdots & 0 \\ 1.781 & 8.70 & 1.781 & 0 & \cdots & 0 \\ 0 & 1.781 & 8.70 & 1.781 & \cdots & 0 \\ \vdots & & & & & \vdots \\ & & & 1.781 & 8.70 & 1.781 \\ 0 & & & 0 & 1.781 & 4.35 \end{bmatrix} \text{lb-in}$$

and these define the shear forces S_i(lb) and bending moments M_i(lb.in) for a given displacement shape y_i (in), γ_i (radians)

according to

$$\begin{bmatrix} \underset{\sim}{S} \\ \underset{\sim}{M} \end{bmatrix} = \begin{bmatrix} A & B \\ B^T & C \end{bmatrix} \begin{bmatrix} \underset{\sim}{y} \\ \underset{\sim}{Y} \end{bmatrix}$$

Since the density of steel is .284 lb/in^3, the mass of each 'lumped mass' is 2.216 lb. For the rectangular cross section one of the curves in Lewis' paper (G2) gives C = 1.361. The uncorrected added mass for each section is therefore

$$\pi\rho\left(\frac{B}{2}\right)^2 \ell C = 0.601 \text{ lb}$$

(the usual factor ½ has been dropped since for a fully submerged bar no surface correction factor is necessary). For a beam with L/B = 39, the 3-D reduction factor is 0.983 so that 3-D flow affects the bar very little. The buoyancy term is not actually needed for the free-vibration calculation but for this example it is $\rho A\ell = 2\rho BDC = .2815$ lb. The immersion force k_i is of course zero for a submerged bar. The rotary inertia of each section about its centre $\frac{\rho_s}{6} BD\ell(\ell^2+4D^2) = 2.99$ lb.in^2. The rotary inertia of the surrounding water is $1/12 m_w \ell^2$ and of the buoyancy it is $1/12 \bar{m}_w \ell^2$ so that

$m_i = 2.216$ lb; $m_{wi} = .591$ lb; $\bar{m}_{wi} = .282$ lb

$r_i = 2.99$ lb.in.^{2}; $r_{wi} = .749$ lb.in.^{2}; $\bar{r}_{wi} = .358$ lb.in.^{2}

Using these values, the normal mode analysis described in section F is readily carried out using standard computer matrix manipulation

subroutines. For the beam vibrating in air alone ($m_{wi} = r_{wi} = 0$), and with shear deflections suppressed, (A_s made very large) the calculated frequencies are compared with the exact frequencies for a free-free uniform beam in the following table. The exact frequencies are given by

$$f_i = \frac{x_i^2}{2\pi}\sqrt{\frac{EI}{\mu L^4}}$$

where x_i has the values

4.730, 7.853, 10.995, 14.137, 17.278, 20.420, 23.561, 26.703, 29.845, 32.986, ... (the roots of cos x cosh x = 1)

and these frequencies do not include the effect of shear deflections.

COMPARISON OF EXACT AND LUMPED MASS FREQUENCIES FOR A UNIFORM BEAM VIBRATING IN AIR

Number of nodes	2	3	4	5	6
Exact frequency	34.13	94.1	184.4	304.9	455.5
Calculated frequency	34.08	93.6	182.4	299.0	442.2
% error	0.15	0.53	1.08	1.94	2.92

Number of nodes	7	8	9	10
Exact frequency	636.2	846.9	1088	1359
Calculated frequency	610.1	801.3	1013	1243
% error	4.10	5.39	6.90	8.54

The agreement to within 0.15% for the basic two node frequency is quite reasonable and confirms the general accuracy of the lumped-mass formulation and the computer routines used. For the higher

modes the accuracy naturally falls off but that it should be only 8½% in error for the ten node frequency is surprising considering that only a 20 lumped mass system was used so that there are only two lumped masses per half wavelength.

To show the effects of rotary inertia, shear deflections and immersion in water on this beam a series of calculations were run to produce the results in the table. The 'exact' results again contain no correction for shear effects.

FREQUENCIES FOR A UNIFORM BEAM IN AIR AND WATER

Case \ Number of nodes	2	3	4	5	6
1A	34.1	94.1	184	305	456
2A	34.3	94.7	186	308	462
3A	34.1	93.6	182	299	442
4A	34.3	94.6	186	307	458
5A	34.1	93.5	182	298	439
6A	33.5	-	-	-	-
1W	30.3	83.6	164	271	405
2W	30.4	84.1	165	274	410
3W	30.3	83.2	162	266	393
4W	30.4	84.1	165	273	407
5W	30.3	83.1	162	265	391
6W	30.2	≈82	-	-	-

Cases: 1 ; 'Exact' uniform beam frequencies (without shear)

2 ; Calculated excluding shear and rotary inertia

3 ; Calculated excluding shear but including rotary inertia

4 ; Calculated including shear but excluding rotary inertia

5 ; Calculated including both shear and rotary inertia

6 ; Measured value

Clearly neither rotary inertia nor shear affects the frequencies greatly for this beam. Shear in fact has almost no effect but inclusion of rotary inertias drops the 6-node frequency by about 4%. The agreement with the measured frequencies is within the experimental error.

The main conclusion from this example is that for a normal beam, with well defined physical properties, the method is capable of giving good results and quite high accuracy can be obtained for the first few modes by using a 20-lumped-mass model.

b. Hollow Rectangular Box-Beam

In his experiments on the whipping induced by underwater explosions, Chertock (G3) used a thin-walled, stiffened, rectangular box-beam. The dimensions are shown in Figure G1. In this case the structure cannot be defined quite so exactly as for the solid beam. The top of the box had a 4" wide opening along its entire length, and during tests a cover was bolted on to close the opening. The degree of fixity of the cover, and its strength, will affect the cross-sectional inertia considerably. It is assumed that the bolts were really tight and that the cover was simply equivalent to the missing material. Ignoring the stiffeners, the elastic data is

$$E = 29.10^6 \text{ psi}, \nu = 0.3, \ell = 6 \text{ inches}$$

$$I = 9.51 \text{ in}^4, A_s = .529 \text{ in}^2.$$

The total ballasted weight was 105 lb so that the draft was 2.70 in. Then $H = \frac{B}{2D} = 1.668$ and the added mass coefficient $C = 1.40$ (again from Lewis' paper (G2)). The length/breadth ratio $L/B = 13.33$ so that $J = 0.903$ and this time the effect of the 3-D flow correction is quite significant.

In the calculation of the added masses the factor $\frac{1}{2}$ is included to allow for the free surface effect. The lumped mass data is:-

$m_i = 5.25$ lb; $m_{wi} = 8.69$ lb; $\bar{m}_{wi} = 5.25$ lb; $k_i = 1.947$ lb/in

$r_i = 50$ lb.in^2; $r_{wi} = 26.0$ lb.in^2; $\bar{r}_{wi} = 15.8$ lb.in^2;

$k_{ri} = 5.85$ lb.in

Here the structure lumped inertia is a rough estimate since the exact figure would vary from mass to mass (the stiffeners being discrete and several transverse bulkheads being present).

A table of results for the same cases as for the uniform beam is readily constructed:-

Cases: 1; 'Exact' uniform beam frequencies (without shear)

2; Calculated excluding shear and rotary inertia

3; Calculated excluding shear but including rotary inertia

4; Calculated including shear but excluding rotary inertia

5; Calculated including both shear and rotary inertia using the Taylor formulation of shear area.

5a; Calculated including both shear and rotary inertia using the Taylor formulation of shear area.

6; Measured frequencies

FREQUENCIES FOR CHERTOCK'S BOX BEAM MODEL

Case \ Number of nodes	0	1	2	3	4	5
1A	0	0	86	238	466	771
2A	0	0	88	244	479	794
3A	0	0	87	235	451	726
4A	0	0	86	227	414	628
5A	0	0	85	221	399	602
5(a)A	0	0	85	217	389	580
6A	0	0	81	191-197	-	-
1W	-	-	53	146	286	473
2W	1.07	1.26	54	150	294	487
3W	0.96	1.34	54	146	284	462
4W	1.16	1.17	53	139	254	385
5W	1.11	1.22	53	137	249	376
5(a)W	1.11	1.22	52	135	242	362
6W	1.15-1.35	1.15-1.35	49-51	98-108	-	-

The agreement this time is much less satisfactory. The 'exact' uniform beam results still agree well with the appropriate case 3, and the remaining calculated results are all quite consistent. Unfortunately there is a considerable difference between the calculated results and those measured on the model. For the fundamental modes in air and water the calculated frequencies are higher than those measured by 4.7% and 4% respectively, and for the three node modes the corresponding figures are 12% and 31%. Since the lumped mass model has been shown to be accurate for such low modes, and still agrees with the 'exact' uniform beam solution, the difference must be due either to non-beam-like behaviour of the model or to incorrect assignment to parameter values (masses, sectional inertias, shear areas etc.).

In addition to the natural frequencies, the mode shapes and longitudinal strain distributions were also measured in Chertock's experiments and the strains deduced from the curvatures in the normal modes were found to be rather greater than the measured strains suggesting that either large shear deflections were occurring or the sectional inertias were lower than expected. The above calculated results, in appropriate cases, contain the effect of shear but it was thought that perhaps the simple beam theory shear area formula

$$A_s = \frac{It}{m}$$

(where I is the cross-sectional inertia, t the thickness of material on the neutral axis and m is the moment of the area on one side of the neutral axis) might not be very accurate for the thin-walled box beam. By using an alternative formula, due to Taylor (G4), for the shear area of thin walled girder, a smaller value for the shear area was obtained and this gave the results for case 5(a) above. A common practice in ship calculations is to assume the shear area is simply equal to the area of vertical plating. The three types of shear area for the box beam model are:-

	actual cross-sectional area	$= 1.44 \text{ in}^2$
shear areas	area of vertical plate	$= 0.576 \text{ in}^2$
	beam type shear area	$= 0.529 \text{ in}^2$
	Taylor shear area	$= 0.429 \text{ in}^2$

It is clear from the results however that the differences in shear area do not account for the discrepancy in frequencies. An alternative partial explanation could be that the cross-sectional inertia, I was too large. As noted earlier, the model in fact had a 4 inch wide gap in the centre of the top plating, which was

closed off during the tests by a bolted-on lid. Assuming that the lid was totally ineffective, the moment of inertia and shear area become

$$I = 7.51 \text{ in}^4, \quad A_s = 0.513 \text{ in}^2$$

instead of $I = 9.51, \quad A_s = 0.529 \text{ in}^2$ as with the lid.

The change in inertia will reduce the calculated frequencies by the factor

$$\left[\frac{7.51}{9.51}\right]^{\frac{1}{2}}$$

so that the new frequencies in air and water will be approximately

No. of nodes	2	3	4	5
frequency in air	76	193	346	515
frequency in water	46	120	215	322

The fundamental mode frequency is now too low but that of the 3 node mode is about right. It is possible that any relative motion between the lid and the main box could affect the modes rather differently and this seems a plausible reason for the differences in frequencies.

This beam shows up the usual features of ship structures: the added water mass is very large, 1.6 times the structure mass, the three dimension fluid flow correction is appreciable; 10% of the added mass, and shear deflections are very important, particularly for the higher modes. The shear correction for the 5-node mode frequency is 26%. The data for this model however are not adequate to differentiate between the 3-D flow corrections of Taylor and Lewis or between the normal beam-type shear area and Taylor's shear area.

c. Full Scale Ship

The data for a destroyer were recently calculated as part of a vibration test and are given in the following table. As for the uniform beams, the ship was divided into 20 equal length sections and the mass and rotary inertia of each section was lumped at its centre. The lumped masses are then connected by 19 equal length weightless beams whose elastic characteristics correspond to cross-sections mid-way between the masses. If $x = o$ corresponds to the bow and L is the length of the ship, the lumped masses are at the positions

$$x_i = (i - \tfrac{1}{2})L/20 \quad ; \quad i = 1, \ldots, 20$$

and the cross-sections characterising the weightless beams are at

$$x_i = iL/20 \quad ; \quad i = 1, \ldots, 19$$

The data require some explanation. The ship mass and buoyancy are fairly easily obtained from the ship's design drawings. The added mass was obtained from Lewis' formula by calculating the parameters a and b of the Lewis transformation with the correct beam/draft ratio and passing through a selected point of the cross-section. Several other points on the cross-section were then computed to verify the acceptability of the fit. The appropriate values of C and $\bar{C}$ were computed and comparison of the buoyancy calculated from $\bar{C}$ with the ship design value gave further general confirmation of the fit.

Mass Number	Distance from bow feet	Ship Mass tons	Added mass tons	Buoyancy tons	Immersion force tons/foot	Rotary inertia tons/ft	Section area in	Shear area in	Section inertia ft.in	Distance NA to keel feet
1	8.8	34	3	14	2.50	3050	333	111	37200	17.7
2	26.4	41	18	42	5.71	2120	422	109	44000	16.5
3	44.0	62	47	68	8.97	2900	510	107	52400	15.7
4	61.6	64	77	94	11.29	3660	603	106	61500	15.1
5	79.2	120	113	117	13.50	4410	693	108	71300	15.0
6	96.8	225	149	138	15.25	4700	818	122	86000	15.2
7	114.4	241	184	156	16.78	4750	1077	162	110100	14.2
8	132.0	103	218	172	18.04	7990	845	136	69200	10.2
9	149.6	155	239	184	18.65	5050	860	136	71600	10.3
10	167.2	136	248	193	18.83	6060	875	137	73200	10.5
11	184.8	158	254	185	18.92	3300	875	138	72800	10.6
12	202.4	191	252	185	18.90	4710	863	138	71600	10.7
13	220.0	127	237	181	18.69	3920	841	136	68400	10.7
14	237.6	137	221	173	18.38	2980	783	129	62000	11.1
15	255.2	139	203	162	18.00	2300	727	120	52800	11.6
16	272.8	238	176	145	17.25	4550	654	108	42600	12.3
17	290.4	177	151	120	16.71	3650	544	98	28800	12.0
18	308.0	60	137	92	15.40	1330	478	82	19900	10.0
19	325.6	56	86	63	12.00	2920	420	67	12000	6.2
20	343.2	54	60	35	9.90	1240				
	Total	2518	3073	2519						

The method is considerably more complex than applying Prohaska's curves but ensures a good representation of the section and, once programmed for a computer, is straightforward. Choosing the collocation point either at 1/3rd of the draft above the keel, or at the point of attachment of the bilge keel gave the most reasonable results. The existence of a bilge keel in the midship region is itself a complication. To allow for its effect references C13 and G5 both recommend the use of Wendel's correction factor (D7). Applying Wendel's figures for the square gives an increase of 19% (since the beam is 19 feet and the keel width 2 feet). Applying the approximation of section D (the draft was only 12 feet) gives the value 14%. Since both of these values appeared to be rather large an alternative approach was tried. The radius of curvature at the turn of bilge was rather larger than the width of the bilge keel so it was assumed that the flow near the keel would be fairly similar to the flow along a flat wall with a plate projecting out at right angles. The latter flow is simply one half of the two-dimensional flow normal to an isolated flat plate. This flow is well known. The velocity of the flow past the plate can be related to the vertical velocity of the ship section by computing the velocity which would exist at the root of the bilge keel according to Lewis' transformation, if the keel were not present. Suitable resolution of the resulting force on the keel then gives an appropriate added mass. The method is described fully in Appendix 1. The correction for the bilge keel is found by this method to be between 3% and 4% and this is the value which is included in the table. In fact the keel is not particularly important in whipping calculations since using the full Wendel value instead of the value used here would reduce the basic 2-node

vibration frequency by about 2½ only. For vibration purposes this difference might be more significant.

To correct the added mass for the three-dimensional flow effects, the Taylor correction factor for the 2-node mode of vibration was used. For this ship, with a length/beam ratio of 9.3 the factor is 0.807 and so is again quite significant; without it the added mass would be 750 tons greater and the basic frequency would be dropped by around 6½%. Lewis' reduction factor for this case is 0.847 which would increase the added mass by about 150 tons and so reduce the frequency by a little over 1%.

Calculation of the rotary inertias is extremely time consuming and was not carried out for this ship. It had however been carried out earlier for a fairly similar ship and the values for that ship have been scaled to apply to the present one.

The cross-sectional moments of inertia for the beam sections were calculated in the usual way with all continuous longitudinal material up to and including the main deck being considered effective. The forecastle deck was also included entirely right back to the break of fo'c'sle. The deck houses however were so short that no correction was necessary. One common method of estimating the shear area is to take the area of all vertical plating. This was tried but led to frequencies which were too high. The shear areas calculated by beam theory, i.e.

$$A_s = \frac{It}{m}$$

are about half the values given by the vertical plating method and lead to much better frequencies. Even this method however is questionable since it depends heavily on b, the thickness of the side plating at the neutral axis. For a few cross-sections the neutral axis occurs within inches of the waterline, where, for armour

reasons, there is an abrupt change in plating thickness. Applying the above equation rigorously could lead to the shear area changing by a factor 2 if the neutral axis moved a few inches. Clearly some kind of average is required. Taylor's method for the shear areas of thin walled box girders applies well in this case and several of the inertias calculated by the normal beam formula were recalculated in this way. The results confirmed the beam formula exceptionally well.

The normal mode frequencies given by the computer program for the four cases:-

1. Shear deflections suppressed, rotary inertia suppressed
2. Shear deflections suppressed, rotary inertia included
3. Shear deflection included, rotary inertia suppressed
4. Shear deflection included, rotary inertia included

are shown in the table, together with the actual frequency where this was known.

CALCULATED DESTROYER FREQUENCIES

Number of Nodes	Frequency (Hz)				Measured
	Calculated				
	1	2	3	4	
0 Heave	0.21	0.21	0.21	0.21	-
1 Pitch	0.23	0.23	0.23	0.23	-
2)	1.68	1.66	1.54	1.53	1.59
3)	3.98	3.93	3.13	3.11	3.20
4) Vibration modes	6.90	6.75	4.67	4.64	4.77
5)	11.02	10.64	6.41	6.37	6.29
6)	16.04	15.59	8.09	8.05	-
7)	22.54	21.13	9.61	9.56	-

The agreement is quite satisfactory for the four vibration modes for which an experimental frequency is known, except for the basic mode. Even this mode is quite adequate for whipping calculations where only a few cycles are of interest. Once again rotary inertia is a very minor effect whereas shear is very important, reducing even the basic mode by 9% and for the higher, 6 and 7 modes, the frequency is more than halved. The calculated and measured mode shapes are compared in Figure 2. The agreement is again very good except for the basic mode. This shape however could not be compared directly as the vibration generator was incapable of providing a sinusoidal input at such a low frequency and an estimated 9% contamination of the first mode by the second has been removed from the plotted experimental values. Part of the frequency discrepancy may be due to errors in the assumed mass distribution. A sister ship in a similar displacement condition was found to have a frequency of 1.51 Hz.

References

1. Moullin E B and Browne A D; "On the Periods of a Free-Free bar Immersed in Water." Proc. Phil. Soc., Vol. 24, Pt III (1928).

2. Lewis F M; "The Inertia of the Water Surrounding a Vibrating Ship." Trans. SNAME Vol. 37, 1929.

3. Chertock G; "Transient Flexural Vibrations of Ship-like Structures Structures Exposed to Underwater Explosions": Jn Acoustical Soc of America, Vol 48, No 1 (Part 2), July, 1970.

4. Taylor J L; "The Theory of Longitudinal Bending of Ships." North East Coast Eng & Shipbuilders Inst. Vol. XLI 1924-25.

5. Leibowitz RC and Kennard E H; "Theory of Freely Vibrating Non-Uniform Beams, Including Methods of Solution and Application to Ships." DTMB Rep. 1317, 1961.

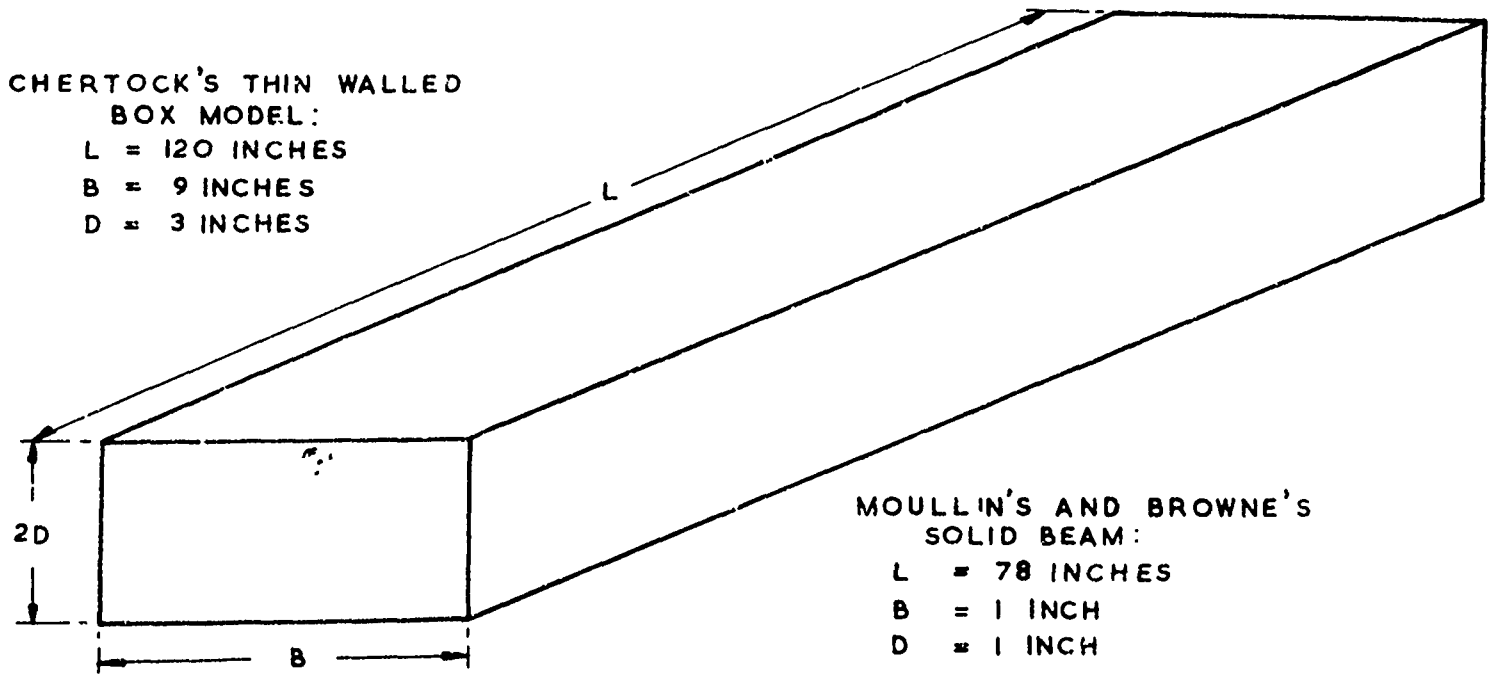

NOMENCLATURE AND DIMENSIONS FOR THE BEAM MODELS

FIGURE 61

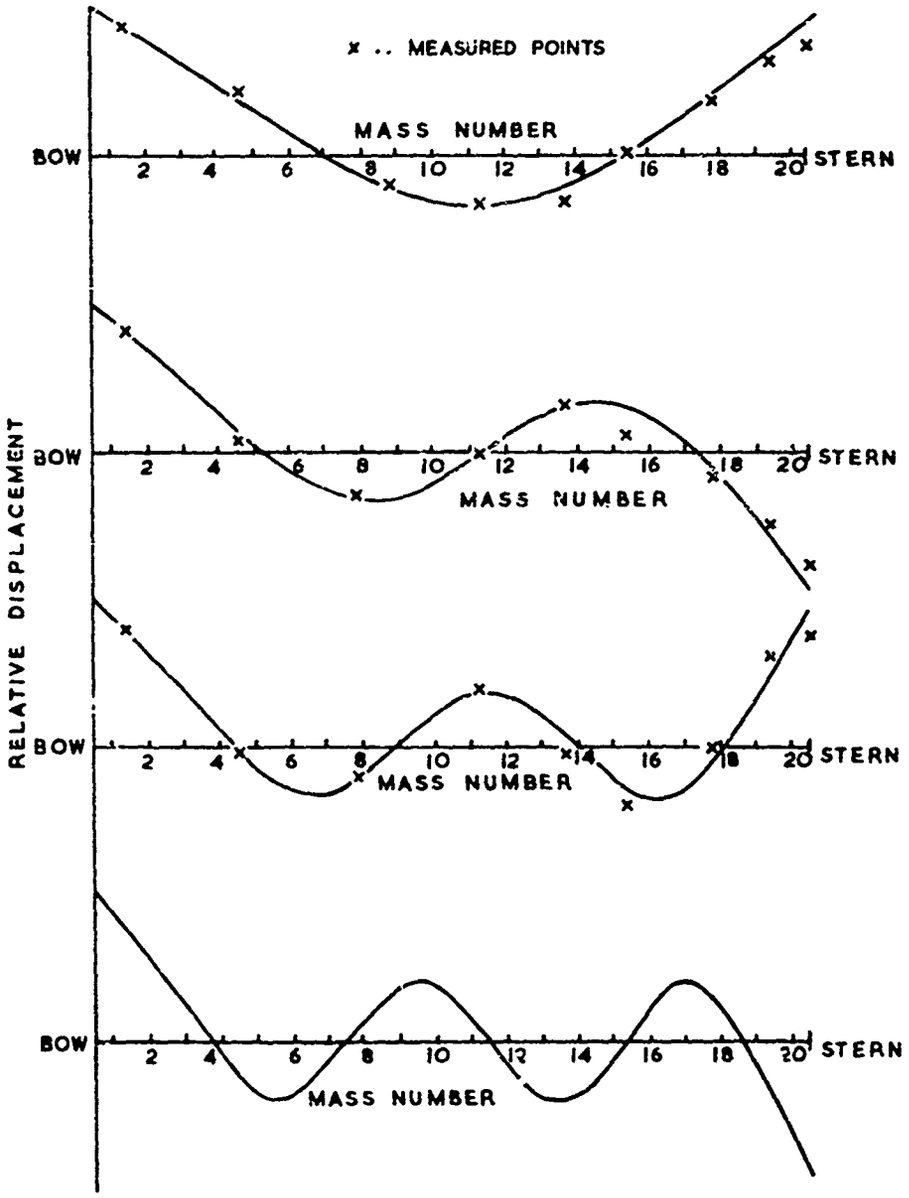

CALCULATED AND MEASURED MODE SHAPES FOR A DESTROYER

FIGURE G2

H Explosion Induced Forcing Function

Following Chertock's original analysis, which was found satisfactory for the models, the compressible phase of the explosion pressure wave, and the migration of the bubble of explosion products, are both neglected here. They will be discussed later. Under these assumptions the flow, in the absence of the ship and any boundary surfaces (eg the free surface or the bottom) will be spherically symmetric and if the volume of the bubble is V(t) the velocity at a distance r from the bubble centre will be given by

$$u = \dot{V}/4\pi r^2 \qquad \text{(H1)}$$

The acceleration of the water will therefore be

$$\dot{u} = \frac{\dddot{V}}{4\pi r^2} - \frac{2\dot{V}}{4\pi r^3}\frac{dr}{dt} = \frac{\ddot{V}}{4\pi r^2} - \frac{\dot{V}^2}{8\pi^2 r^5}$$

The second term clearly decays much more rapidly than the first away from the bubble and, in any case, it is consistent with the earlier development of the forces via strip theory to neglect forces of the type $\frac{1}{2}\rho u^2$, so the second term is neglected here. The possible magnitude of this and similar terms is investigated later. The water acceleration is therefore, in the present approximation,

$$\dot{u} = \frac{\ddot{V}}{4\pi r^2} \qquad \text{(H2)}$$

Referring to the geometry shown in Figure H1, this acceleration, when resolved vertically at the ship axis gives

$$\dot{u}_i \cos\psi_i = \frac{\ddot{V}}{4\pi R_i^2}\frac{D}{R_i} = \frac{\ddot{V}D}{4\pi R_i^3} \; ; \quad R_i^2 = D^2 + H^2 + (x_i - x_w)^2$$

To allow for the presence of a free surface at the ship axis, an image bubble of opposite sign to the real one must be added at the reflection position above the free surface. At the free surface the image will have the effect of doubling the vertical accelerations and cancelling out any horizontal ones, so that the final vertical acceleration is

$$\frac{\ddot{V}D}{2\pi R_i^3} \qquad \text{(H3)}$$

Substituting this into equation (F6) gives the modal equation

$$\ddot{\alpha}_i + \omega_i^2 \alpha_i = \lambda_i \ddot{V} \; ; \quad \lambda_i = \frac{D}{2\pi} \frac{\sum_{k=1}^{n} (m_{wk} + \rho A_k \ell) y_{ki} / R_k^3}{\sum_{k=1}^{n} (m_k + m_{wk}) y_{ki}^2} \qquad \text{(H4)}$$

for the case where rotary inertias are neglected. The same equation applies, but with an obvious modification to λ_i, when rotary inertias are included. The similarity of equation (H4) to equation (B10), given by Chertock's analysis, is clear. The factor 2 between the expressions is due to including the effect of the free surface in equation (4). Equation (H4) is slightly less accurate than (B10), due to the 'lumping' procedure, but is more general since it is not restricted to 'proportional bodies'. It is however still restricted to slender bodies where strip theory is applicable.

The equations (H4) require only initial conditions and specification of the bubble volume history for their solution. The equations governing the pulsations of a non-migrating bubble are well known except very late in the bubble collapse phase where mathematical instabilities in the equations reflect an observed physical instability. An excellent account of the equations and their derivation is given by Cole (H1), but a brief outline is

included here as it provides a useful lead-in to the modifications for migration effects.

The velocity in the water is given by equation (H1), i.e.

$$u = \frac{\dot{V}}{4\pi r^2} = \frac{a^2\dot{a}}{r^2}$$

where a is the bubble radius. The kinetic energy is therefore

$$KE = \int_a^\infty \tfrac{1}{2}\rho u^2 . 4\pi r^2 . dr = 2\pi\rho a^3 \dot{a}^2$$

The potential energy of the bubble is a combination of the internal energy of the gas products and the potential energy of the hole in the water, so that

$$PE = \frac{4}{3}\frac{\pi a^3 p}{\gamma - 1} + \frac{4}{3}\pi a^3 p_\infty$$

where p is the gas pressure, and p_∞ the ambient pressure at the bubble centre. Since the pulsations are very rapid the adiabatic equation of state is appropriate, i.e.

$$p = k_1 \rho_g^\gamma = \frac{k_1 W^\gamma}{(\frac{4}{3}\pi a^3)^\gamma}$$

where W is the charge weight. If E_o is the total energy tied up in the bubble motion and Z_o is the hydrostatic head of water at the bubble $(\frac{p_\infty}{\rho g})$, the equation of energy conservation is

$$E_o = KE + PE = 2\pi\rho a^3\dot{a}^2 + \frac{4}{3}\pi\rho a^3 g Z_o + \frac{k_1}{(\gamma-1)(\frac{4\pi}{3})^{\gamma-1}} \frac{W^\gamma}{a^{3(\gamma-1)}}$$

This may be written more simply in terms of the non-dimensional variables $x = a/L$, $\tau = t/T$;

$$L = \left[\frac{3E_o}{4\pi\rho g Z_o}\right]^{1/3} ; \quad T = \left[\frac{3}{2gZ_o}\right]^{1/2} L \ , \qquad (H5)$$

as

$$x^3\ddot{x}^2 + x^3 + k/x^{3(\gamma-1)} = 1 \ , \qquad (H6)$$

k being the constant

$$k = \frac{(\rho g Z_o)^{\gamma-1}}{\gamma-1} \cdot k_1 \left(\frac{W}{E_o}\right)^{\gamma}$$

Equation (H6) is the differential equation satisfied by the bubble radius and applies so long as the bubble is spherical and remote from all surfaces. In practice small bubbles fairly deep remain spherical throughout their motion except for very short periods centred about the bubble minimum. At these times the bubble surface is unstable and greatly distorts. The bubble minimum and maximum radii are given by (H6) when $\dot{x} = o$, i.e.

$$x^3 + \frac{k}{x^{3(\gamma-1)}} = 1 \qquad (H7)$$

and for small k are approximately

$$x_o \sim k^{\frac{1}{3(\gamma-1)}} \left[1 + k^{\frac{1}{\gamma-1}}/3(\gamma-1)\right]; \text{ minimum} \qquad (H8)$$

$$x_m \sim 1 - \frac{k}{3}\left[1 + (\gamma - \frac{2}{3})k\right] ; \text{ maximum}$$

The various constants in these equations have been determined empirically by Arons [H2]. He found that, for TNT, the correct variation of bubble period (from explosion to minimum) with depth could only be reproduced by equation (H6) if

$$\gamma \sim 5/4$$

and then the actual value of the period is correct if

$$E_o = \epsilon W$$

where ϵ, the energy per unit mass of charge is approximately 490 cal/gm. Comparing further the experimental peak bubble pressure with the predicted value gives

$$k \sim .0552\, Z_o^{1/4} \qquad \text{(H9)}$$

Together with the theoretical expression for k given after equation (H6) this provides the gas equation of state

$$p = 8.15\rho_g^{5/4}$$

where p is in kbars and ρ_g in gms/cc. Jones (H3) had some time earlier predicted theoretically that this equation should be

$$p = 7.8\rho_g^{1.25}$$

for the low pressures involved during most of the bubble period.

With Aron's values, the scale constants L and T and the bubble maximum radius a_m and period T_p are given approximately by

$$\begin{aligned} L &= 13.6\, W^{1/3}/Z_o^{1/3} \quad \text{ft} \\ T &= 2.94\, W^{1/3}/Z_o^{5/6} \quad \text{seconds} \\ a_m &= 12.6\, W^{1/3}/Z_o^{1/3} \quad \text{ft} \\ T_p &= 4.36\, W^{1/3}/Z_o^{5/6} \quad \text{seconds} \end{aligned} \qquad \text{(H10)}$$

where W is the weight of the charge in lbs of TNT and Z_o is the hydrostatic head in feet of water. The bubble volume acceleration

is then given by

$$\ddot{V}(t) = \frac{4\pi}{3}\frac{L^3}{T^2}(\dddot{x}^3) = 1220\, W^{1/3} Z_o^{2/3} (\dddot{x}^3) \text{ ft}^3/\text{sec}^2 \qquad \text{(H11)}$$

where $\dddot{x}^3$, by differentiating (6), is given by

$$\dddot{x}^3 = 3x^2 \ddot{x} + 6x\dot{x}^2 = \frac{3x}{2}\left[1/x^3 - 4 + (3\gamma-4)k/x^{3\gamma}\right] \qquad \text{(H12)}$$

The pressures in the water around the bubble are also proportional to $\dddot{x}^3$ for, except close to the bubble where $\frac{1}{2}\rho u^2$ terms are important, the pressure is simply

$$p = \rho\dot{\phi}$$

Here ϕ is the velocity potential for the flow around the bubble i.e.

$$\phi = \frac{\dot{V}}{4\pi r}$$

so that

$$p = \frac{\rho\ddot{V}}{4\pi r} \qquad \text{(H13)}$$

and with the same units as before

$$pr = \frac{\rho}{4\pi}\ddot{V} = 1.341\, W^{1/3} Z_o^{2/3} (\dddot{x}^3) \text{ psi-ft.} \qquad \text{(H14)}$$

The equations (H10) for the period and amplitude of the bubble motion apply strictly only to TNT. To produce bubble details for close comparison with Chertock's experiments the basic bubble equations can be used. The detonator which produced Chertock's bubble was fired 13 inches below the model, i.e. at a depth of 16 inches below the surface so that $Z_o = 33 + 1.33 = 34.33$.

The observed radius was 5.4 inches and the period 23.5 msecs. This period will have been reduced somewhat from the free-water period given by equation (H16) due to the proximity of the water surface. The empirical correction factor for this effect is

(see reference H4) $(1 - 0.2 \frac{a_{in}}{a})$ i.e. 0.932 for this bubble.

The equivalent free-water period is consequently 23.5/.932 = 25.2 msecs. Now

$$\frac{T_p}{a_m} = \frac{T}{L} \frac{\tau_m}{x_m} = \left(\frac{3}{2gZ_o}\right)^{1/2} \frac{\tau_m}{x_m} \qquad \text{(H15)}$$

so that the ratio of period to amplitude is independent of the energy release and depends only on Z_o and on k (through τ_m, x_m). From reference H3, the solutions of equation (H6) for $\gamma = 1.25$ give

k	x_m	x_o	τ_m	τ_m/x_m
0	1.0000	0.0000	1.492	1.492
0.1	0.9645	0.0464	1.4821	1.537
0.2	0.9235	0.1172	1.4804	1.603
0.3	0.8742	0.2031	1.4918	1.706
0.4	0.8100	0.3064	1.5120	1.867

From equation (H15), for Chertock's detonator,

$$\frac{\tau_m}{x_m} = \left(\frac{2gZ_o}{3}\right)^{1/2} \frac{T_p}{a_m} = 1.520$$

so that k =0.066 (for TNT at the same depth the value would have been 0.134) and $x_m = 0.978$, $\tau_m = 1.483$. Then, to give the correct radius,

L = 5.52 inches and so T = 16.95 msecs.

With these values,

$$pr = \frac{\rho}{4\pi} \ddot{V} = \frac{4\pi}{3} \frac{\rho L^3}{4\pi T^2} \ddot{x^3} = \frac{2}{9} \rho L g Z_o \ddot{x^3} = 18.71 \ddot{x^3} \text{ psi-inches}$$

These results apply only up to the first bubble minimum since near the minimum energy is lost from the pulsation both by acoustic radiation and by cooling from water spray projected into the bubble

as its surface becomes unstable. By a similar process to the above, again making allowance for the surface effect, the observed values 17.6 msecs, 3.9 inches and 15.2 msecs, 3.2 inches for the period and radius for the second and third pulses lead to the values:

k = 0.120, T = 13.1 msecs, L = 4.25 inches (second pulsation)

k = 0.217, T = 10.7 msecs, L = 3.48 inches (third pulsation)

These give results for the first three bubble pulsation which are compared with the measured values of pr in Figure 2. Chertock's theoretical values for pr were very similar to these but were obtained for a constant k = 0.134 (corresponding to TNT) and neglecting the surface effect. His length and time scales were arbitrarily chosen to give the observed values. The steady increase in k found here for the later pulsations is to be expected since, from equation (H6), k is proportional to $(E_o)^{-\gamma}$ and for successive pulses E_o becomes steadily smaller.

To produce pressure or particle velocity histories similar to those in Figure 2 the differential equation (H6) has to be integrated and then (H12) gives the necessary values of $\tilde{x}$. The integration is most conveniently carried out using the technique described in reference (H6). This technique uses Tschebyscheff polynomials to evaluate the definite integral which equation (H6) gives for the time taken to expand from minimum radius to maximum radius. The technique may be readily extended to give the indefinite integral for $\tau(x)$. The method gives high accuracy with very few terms.

References

H1. Cole R H; "Underwater Explosions". Princeton Univ. Press 1948

H2. Arons A B; "Secondary Pressure Pulses Due to Gas Globe Oscillation in Underwater Explosions. II Selection of Adiabatic Parameters in the Theory of Oscillation." Und. Exp. Res. Vol. II - The Gas Globe, ONR.

H3. Jones, H and; Miller, A R — "The Detonation of Solid Explosive. The Equilibrium Conditions in the Detonation Wave Front and the Adiabatic Expansion of the Products of Detonation". Proc Roy Soc Series A Vol 194, No 1039 (Nov 1948).

H4. Kennard, E H; — "Migration of Underwater Gas Globes due to Gravity and Neighbouring Surfaces". Underwater Exp Res Vol II - The Gas Globe, ONR.

H5. Swift, E and Decius, J C; — "Measurement of Bubble Pulse Phenomena, III Radius and Period Studies". Und Exp Res Vol II - The Gas Globe, ONR.

H6. Shiffman, M and Friedman, B; — "Studies on the Gas Bubble Resulting from Underwater Explosions: On the Best Location of a Mine Near the Seabed'. Und Exp Res Vol II - The Gas Globe, ONR.

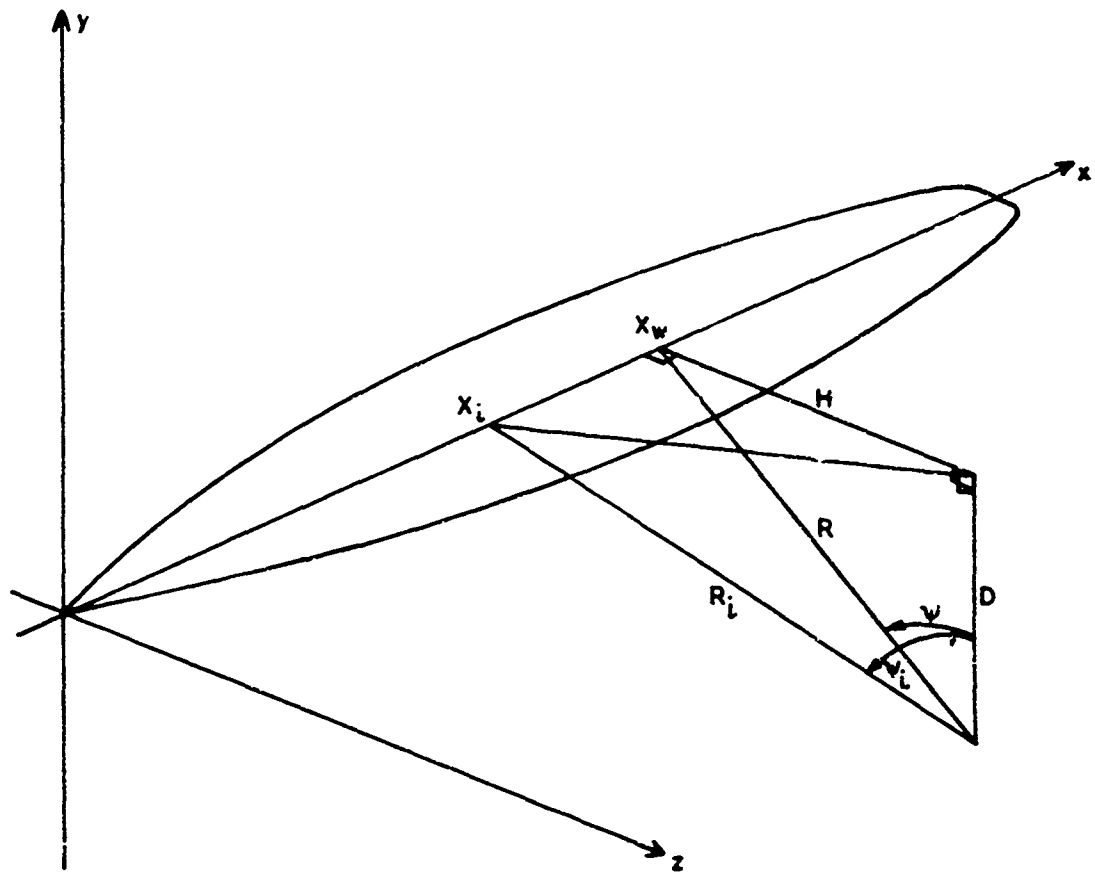

SHIP / EXPLOSION GEOMETRY

FIGURE H1

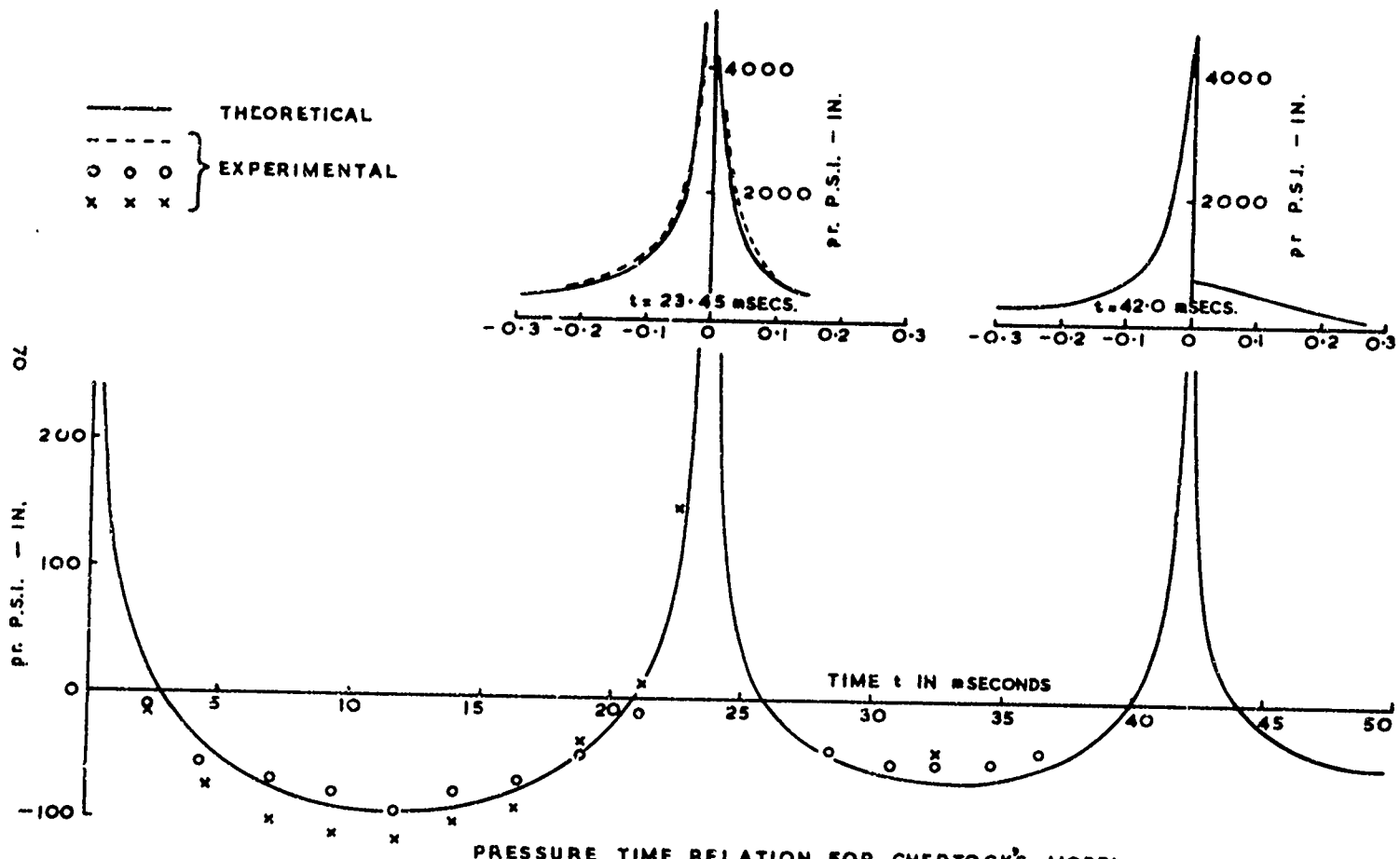

PRESSURE TIME RELATION FOR CHERTOCK'S MODEL

FIGURE H2

I. Description of Computer Program I

To simplify the application of the preceeding equations to actual cases a computer program was written in FORTRAN and implemented on Atlas, KDF-9 and IBM 7090 computers. Copies of the program are held at the Naval Construction Research Establishment and a detailed specification for the program structure, the data format and units and types of output which can be produced are given in Reference [I1]. A brief description of the program is given here. It is possible that the normal mode part of the program could have application to ship vertical vibration problems. The program produced all the results described in Section G.

The elastic nature of the ship structure is specified by giving the number n of lumped masses to be used in the representation (up to 40 on Atlas), the cross-sectional inertias and shear areas of the (n-1) beams connecting the masses and the elastic constants (Young's Modulus and Poisson's Ratio) of the hull material. The ship inertial properties are specified by giving a ship mass to be associated with each lumped mass together with an added water mass and the mass of water displaced by the section of ship associated with the lumped mass. If rotary inertia is thought to be significant the rotary inertia to be associated with each lumped mass, due to the ship mass must also be given. Added water rotary inertias are assigned by the program. Normal pitch and heave motions are included and at each lumped mass an immersion force per unit submergence may be given.

From the elastic structure data the computer builds up the stiffness matrices in equation (C4) and, if rotary inertia is not required, eliminates the rotations as in equation (C6). The inertia mass data are then used to build up the mass matrices in equation (E9). The transformation described in section F is

used to produce a symmetric matrix whose eigenvalues and vectors are found by an HGW type of eigenvalue subroutine.

If a series of positions (up to 20 on Atlas) are specified along the ship the program then calculates the coefficients $y_i(x)$, $M_i(x)$ and $S_i(x)$ from equation (F8) for use in equations (F7). The program then integrates the modal coefficient equation (H4) and recombines the equations as in (F7) to produce histories of the relevant quantities at each of the specified positions along the ship. It is necessary to give the position of the charge relative to the ship in the data so that the program can form the forcing function coefficients λ_i in equations (H4). The bubble volume history is specified by a subroutine. A table of values of $(\tau, x^3(\tau))$ is used for interpolation.

Normally the program carries out the integration assuming that initially the α_i and their time derivatives $\dot{\alpha}_i$ are all zero but, if a particular initial velocity distribution is specified in the data, the program resolves it into an equivalent set of non-zero $\dot{\alpha}_i$'s to start the integration.

In order to integrate the differential equations by step-by-step methods a time increment is required. For the linear oscillator equations the Runge-Kutta integration routine is stable if this increment is less than about 1/6th of the period of the highest frequency mode present. The data needed for the program includes the number of steps to be used in each such period. Ten steps seems to give quite accurate results judged by comparing with a similar integration using 20 steps per period. Although this increment ensures stability of the differential equations

it is far too large to give an adequate representation of the bubble forcing function near the positive pressure 'spikes'. In these regions the program automatically reduces the step length to ensure the representation is reasonable.

References

[1]. Hicks A N ; "The Elastic Theory of Explosion Induced Whipping Computer Program Specification." NCRE Report R550, September 1968.

J Complete Example

For the box model described in section G, together with the bubble forcing function derived in section H, the computer program was used to predict the motion of the model in Chertock's experimental tests. Figure J1 compares the measured and predicted result for the two-node mode coefficient for a charge fired at 16 inches beneath the free surface, directly under the centre of the model. The agreement for the early motion is quite good but in the later motion the experimental amplitudes become slightly less than predicted and also the two curves gradually swing out of phase. The differences in phase are possibly due to a reduction in the model frequency due to the amplitude of the motion. The difference first shows significantly at around 27 mseconds, at which time the strains in the model are about 3/4 of yield. Prior to this time, the difference between the two curves is very small and explainable by the 2Hz spread in the measured frequency. The reduced experimental amplitudes could well be due either to damping, which is neglected in the theoretical model, or to minor inaccuracies in the bubble forcing function, which is not known at all accurately in the later stages.

FigureJ1 also shows the lowest frequency rigid body mode and it is clear that the vertical displacement of the model largely follows the changes in the bubble volume. The mode shape shown is not actually either a pure heaving or pure pitching mode. The frequencies of the two motions were so close that, to the accuracy specified in the eigenvalue routine in the computer program, they were identical and, although the routine always produces orthogonal vectors for multiple eigenvalues, the first is arbitrarily chosen in the corresponding eigenvector space. For this geometry the

two rigid body modes, when taken together, produce a pure heaving motion.

Figures J2, J3 and J4 show the relative effect of variations in the charge position: longitudinally, athwartship and in depth, for the first three whipping modes. For the 2-node mode the experimental results given by Chertock have been added to the figures and the agreement is excellent. The effect of mode shape on the longitudinal variation is evident. For the transverse and depth variations no curves have been given for the second (3-node) whipping mode since at all points in the transverse plane through the model centre (where these results apply) the amplitude induced for this mode is zero, the centre being a node. From the curves it may be seen that the amplitude of the third mode decays slightly more rapidly than that for the basic mode, both transversely and with depth. To produce such comparisons it is not necessary to carry out complete integrations. Since the equations are linear and, except for very minor variations in the bubble period with depth, the bubble volume acceleration is the same for all charge locations, the modal amplitudes are proportional to the forcing function coefficients (λ_i in section H). It is these coefficients which are compared in Figures J2, J3 and J4.

The results of this example show that the lumped mass/weightless beam idealisation of the ship, together with the strip theory approximation for fluid effects, can represent the whipping motions of a small scale model quite accurately. Comparison with Chertock's original work shows that the present theoretical model is as accurate as his original formulation, while being slightly more general in that it applies also to non-proportional bodies. It is also more adaptable and can readily be extended to include other

effects such as gravity migration and plastic deformation of the target. The use here of strip theory shows up particularly clearly the nature of the forces acting on the ship and their distribution alon[illegible].

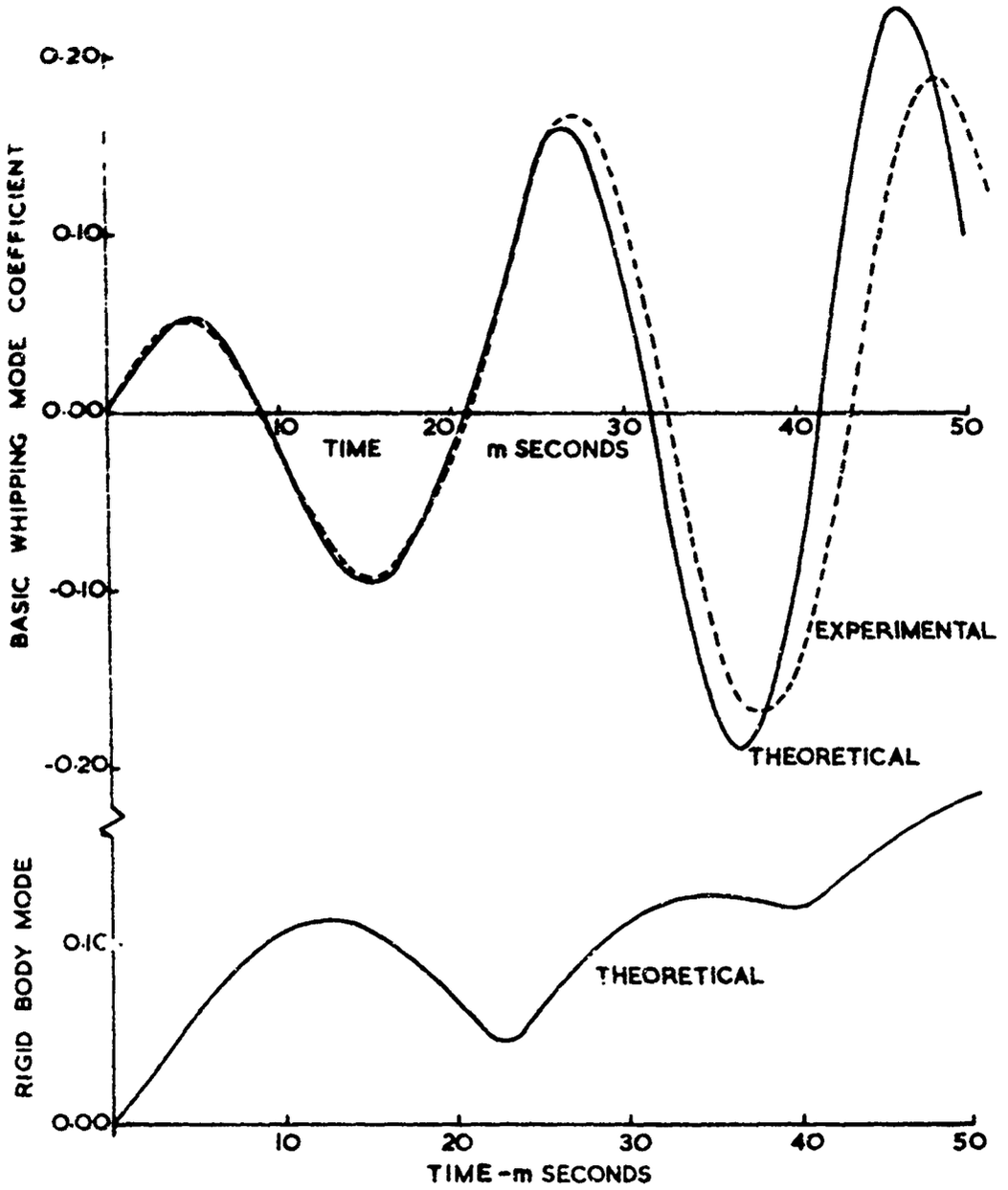

PREDICTED AND MEASURED RESPONSES

FOR CHERTOCK'S MODEL

FIGURE J1

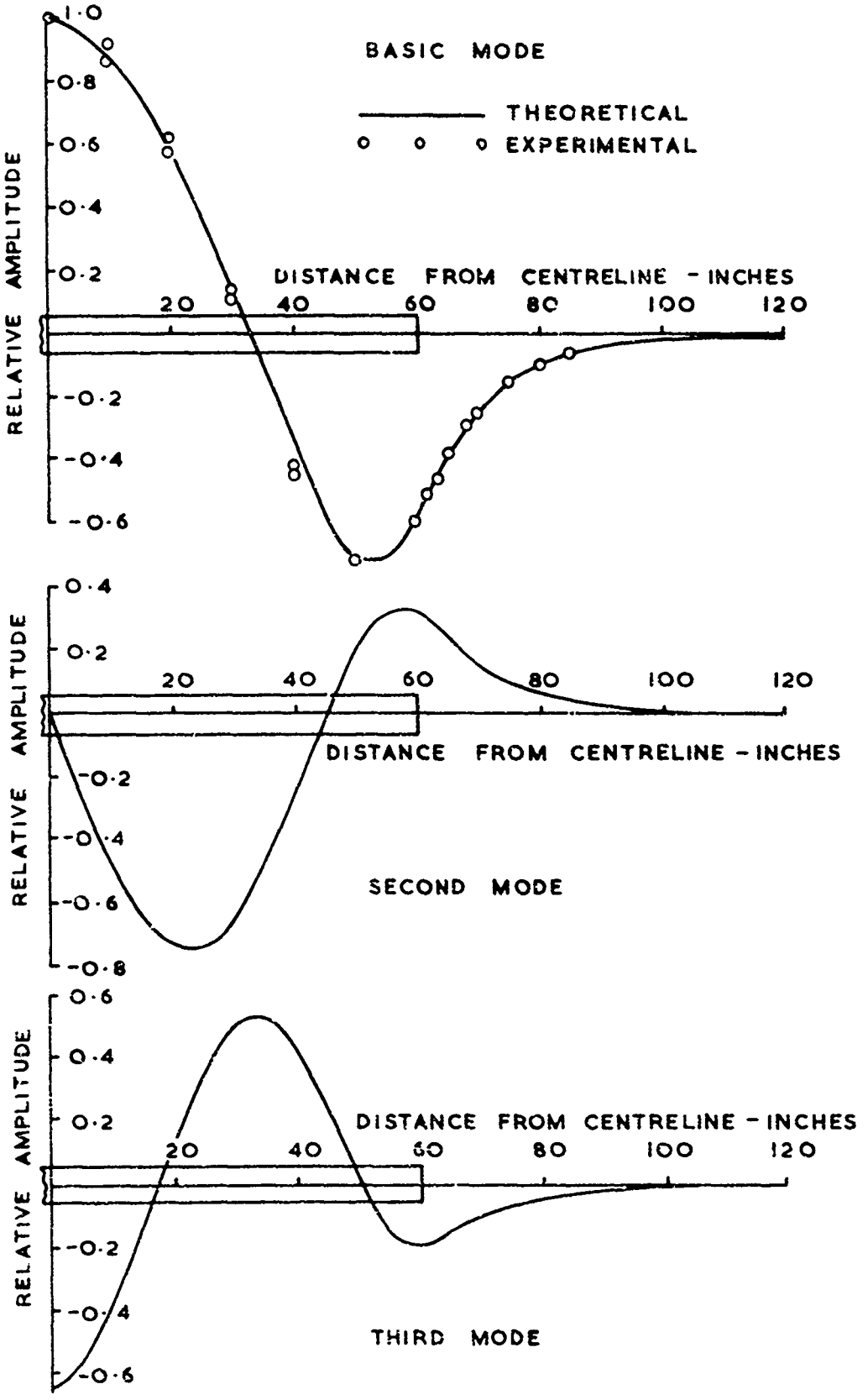

RELATIVE VARIATION OF WHIPPING MODE AMPLITUDES WITH LONGITUDINAL CHARGE POSITION

FIGURE 32

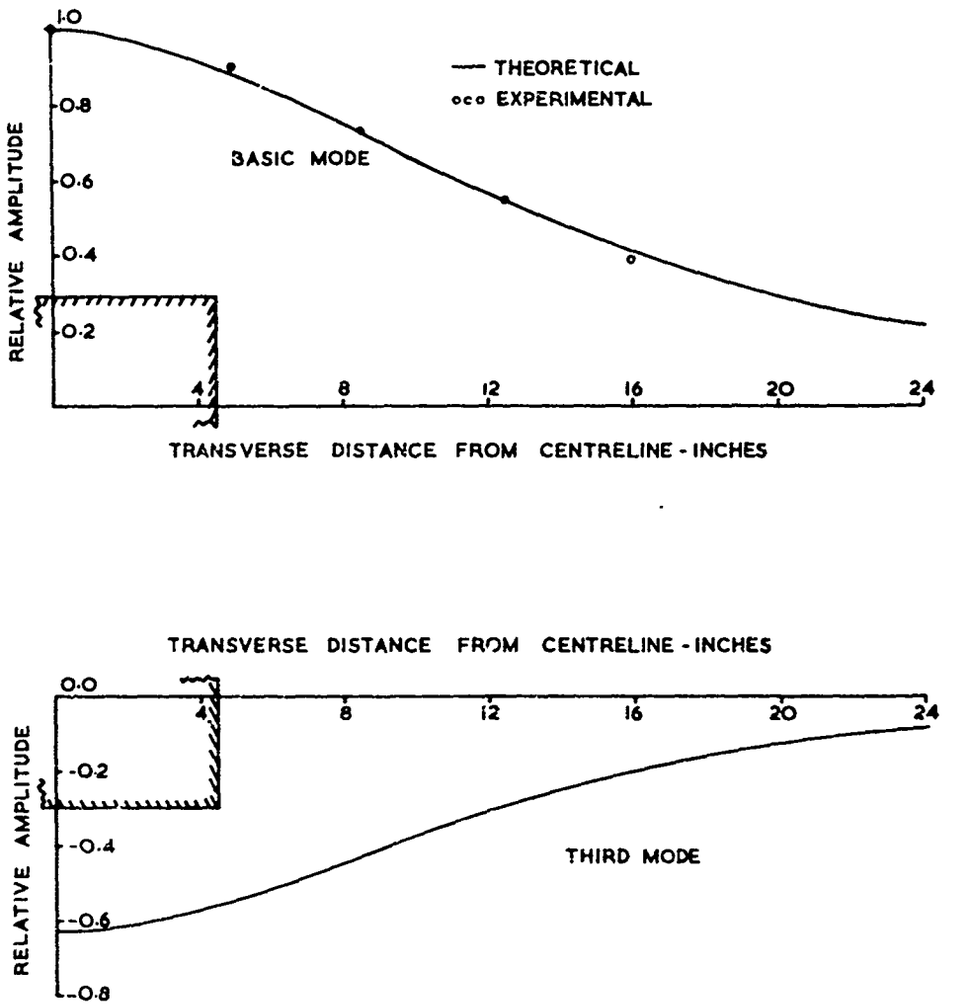

RELATIVE VARIATION OF WHIPPING MODE AMPLITUDES WITH TRANSVERSE CHARGE POSITION

FIGURE J3

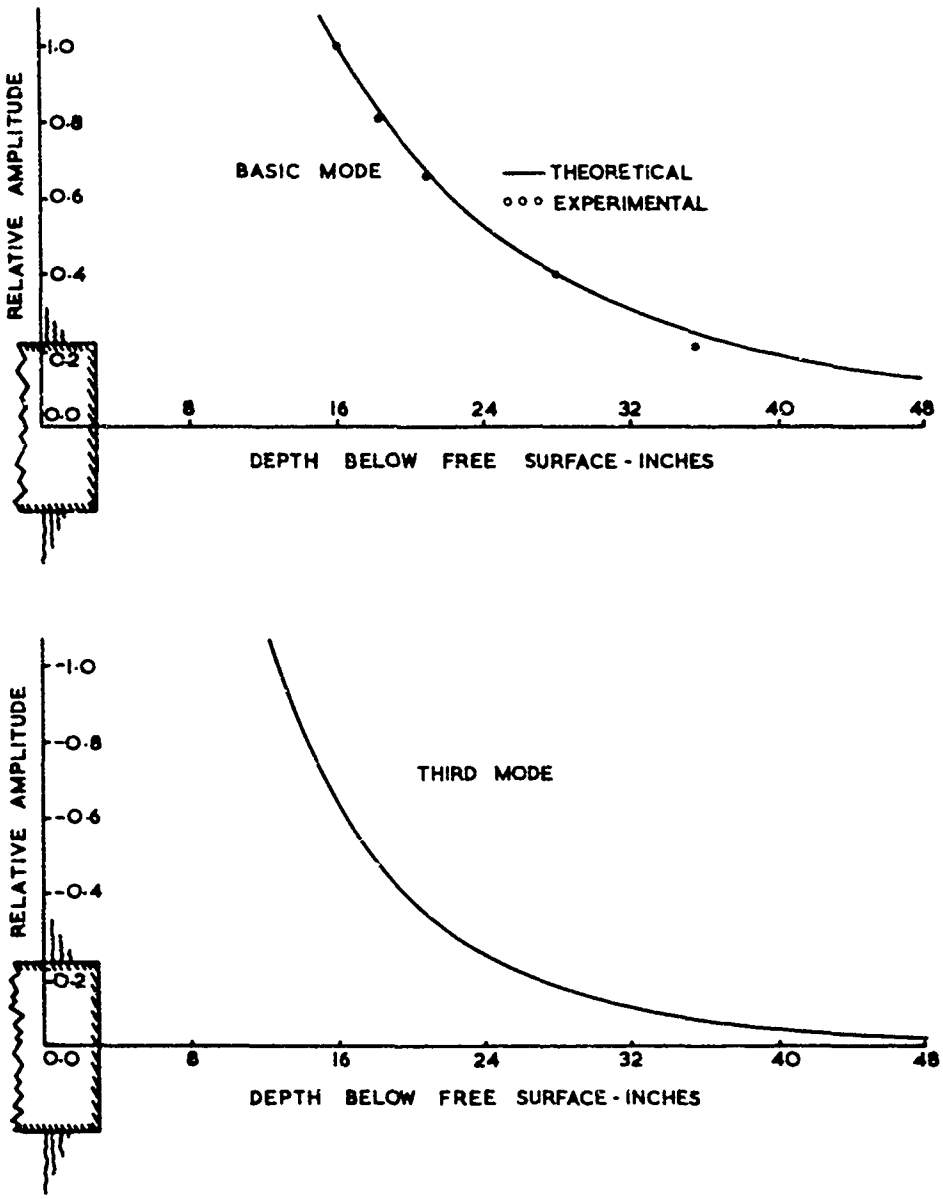

RELATIVE VARIATION OF WHIPPING MODE AMPLITUDE WITH CHARGE DEPTH

FIGURE J4

K The Early Compressible Phase

In the development of the theory as presented in sections E, F and H, it has been assumed that the motion of the ship is independent of the initial shock wave, that in fact the ship behaves as though initially a highly compressed bubble of gas were suddenly released from rest to accelerate and expand outward and then pulsate. In fact the bubble at no stage can be considered to be at rest and the water surrounding it does not accelerate to high velocities in the way this model suggests. What actually happens is that when the detonation wave in the explosive reaches the water it transmits a shock wave into the water and almost instantaneously raised the bubble surface to a very high velocity. Similarly in the surrounding water the shock wave raises the velocity to a high value and all these initial high velocities gradually decay until they fall to the incompressible velocities, after which normal incompressible bubble motion takes place. Even the initial bubble size assumed in section H is fictitious, being usually considerably larger than the original charge size. It is merely the size of bubble which, if the water were really incompressible, would pulsate with the period and maximum radius which are observed in experiments.

Chertock's original work (B1) gave a qualitative argument, based on an application of Green's theorem to the flow potentials, assuming them to be solutions of the wave equation, why it should be expected that the acoustic shock wave phase would not produce significant motion. In fact his arguments do not rigorously apply to the type of discontinuous function involved in the early interaction and, in addition, did not really include all the interaction waves (reflected, diffracted, etc.). In addition, for surface ships at least, non-linear effects are certainly present during the initial phases as cavitation effects are well established

(K1) during the shock wave hull plating interaction phase of the motion. Cavitation has the effect of largely preventing any reflection of incident momentum, so ensuring that the momentum in the shock wave is fully absorbed by the ship.

In consequence the neglect of the shock wave, or at least its replacement by a zero velocity, high pressure bubble, must be considered to be justified principally by the experimental evidence. On small scale the agreement between the observed and predicted model motions certainly fully justifies the assumed artificial bubble. However, the scaling laws of underwater explosions are such that it is generally true that shock wave effects are relatively much smaller than bubble effects on small scale. The assumption cannot therefore be considered established for a larger scale by the small scale experiment.

There are however other heuristic reasons for expecting that it should still be valid at least for some conditions. For a target deep enough for cavitation not to be significant Murray, (K2), showed by an exact solution that when a spherical acoustic wave interacts with an infinite neutrally buoyant, circular cylinder (considered to be rigid in cross-section but infinitely flexible in shear along its length), the transverse velocity of the cylinder asymptotically tends to the nearby water particle velocity of the incident wave. He found in fact that initially the cylinder jumped to a considerably higher velocity which then decayed to the incompressible value after a period equivalent to several transit times of the cylinder diameter by the acoustic wave. For non-neutrally buoyant circular cylinders, the associated two-dimensional problem of a plane wave incident on a circular cylinder of elastic cross-section has been considered by Haywood

(K3) who found that in this case the cylinder, after again reaching a fairly high initial velocity, slowed down to the asymptotic velocity

$$\frac{2u}{1 + \mu/\pi a^2 \rho} \qquad (K1)$$

where u is the undisturbed water particle velocity at the cylinder centre, due to the passage of the shockwave. In this equation a is the cylinder radius and μ is the mass of the cylinder per unit length. The previous incompressible assumption gives the same result, as the fluid impulse which produces a velocity u in the water imparts a momentum $(\mu_w + \bar{\mu}_w)u$ per unit length of the cylinder. This momentum is given to the cylinder and its added water mass so that, if the resulting cylinder velocity is v,

$$v(\mu + \mu_w) = (\mu_w + \bar{\mu}_w)u. \qquad (K2)$$

For a circular cylinder the added mass per unit length, μ_w, is $\pi\rho a^2$ as also is the buoyancy per unit length, $\bar{\mu}_w$. Whence (K2) gives the same value for v as (K1).

These results suggest that, at least when cavitation is not important, the incompressible assumption at the start will lead to quite good results in the later motion. Where cavitation leads to most of the momentum in the shock wave being absorbed by the target again the deviation from the incompressible theory should be small because the total momentum in the initial positive phase is generally at least 80% due to the 'incompressible' pressures which follow behind the very short duration compressible shock wave head of the positive phase. The subsequent motion of the ship and its entrained water will therefore again be largely as though the incompressible motion only were present at the start.

References

K1. Taylor G I ; "The Pressure and Impulse of Submarine Explosion Waves on Plates", Underwater Explosion Research Vol. 1 - The Shock Wave, Off. Naval Research (1950).

K2. Murray W W; "Interaction of a Spherical Acoustic Wave with a Beam of Circular Cross Section", UERD Report 1-55 (1958).

K3. Haywood J H; "Response of an Elastic Cylindrical Shell to a Pressure Pulse", Quart. Jn. of Mech. & App. Math., Vol XI, Part 2, 1958.

An alternative to the Strip Flow Method for the Added Water Mass

The usual theory for calculating the hydrodynamic forces on a ship, applied as described in Section D, is clearly an extremely simple, and, for the 2-node mode at least, very accurate method of determining such forces. For the higher whipping modes the experimental evidence is very limited. The strip theory does however have one possible drawback in the present application. In the development of the normal mode form of the equations described in section F, all the mode frequencies and shapes were found simultaneously through the eigen values of a single matrix. This matrix naturally involves the strip theory added water masses and, through them, the correction factor J which compensates for three dimension flow effects. In consequence, in the development used here the same value for J is applied to all the modes. This conflicts with the customary use of the factor , where a different value for J is used for each mode shape (including the pitch and heave modes). To use the customary method here would mean developing a separate matrix (using the appropriate value for J) for each mode, and extracting just the appropriate eigen root and vector from each matrix. In the examples given earlier the simpler alternative was adopted of applying the 2-node mode correction factor to the added masses (since that is the mode contributing most to flexural stresses) and ignoring the fact that all the other modes, pitch and heave included, will be somewhat in error.

The type of correction factor which should be used in vibration calculations has been the subject of a great deal of discussion ever since strip theory was first used. The two independent originators of the theory, Lewis (L1) and Taylor (L2) both presented reduction factors but, due to assuming slightly different boundary conditions

they arrived at different reduction factors. Which factor to use, Lewis' or Taylor's, is still discussed today. A further difficulty, which has been raised in numerous papers ((L3) contains a useful discussion) is that it has never been rigorously established that the correction factor should be constant over the length of the ship, as is implicitly assumed in normal useage. In fact, in at least one recent paper (L4) a correction factor has been presented which does vary along the length, although in this particular case no basis for the given variation was presented.

Because of these basic difficulties in the customary strip theory, particularly as applied to the whipping problem, the alternative approach described here has been developed. The fundamental weakness of strip theory is that the force it predicts on each cross-section is related only to the motion of that cross-section and not to the probably slightly different motions of neighbouring cross-sections. In the notations used in section E, the vertical hydrodynamic force S_{wi} on the ith mass is, according to strip theory, $S_{wi} = - m_{wi}\ddot{y}_i$ and the total vector of hydrodynamic forces is

$$\underset{\sim}{S}_w = - M_w \underset{\sim}{\ddot{y}} \qquad (L1)$$

where M_w is a diagonal added mass matrix. This standard form of strip theory equation clearly cannot be valid for general motions. If one section of the ship is accelerating upward it will certainly experience a downward hydrodynamic force so a diagonal term is certainly expected. However, its upward acceleration will induce a downward fluid acceleration around it as fluid moves to fill the space vacated beneath it. Part of this flow will be around neighbouring cross-sections and so will induce a downward forces on these sections too. For the above equation to be generally true then it is necessary for M_w to contain also off-diagonal

elements. In fact all elements of M_w should be nonzero but, since each section will affect principally its nearest neighbours, the magnitude of the off diagonal elements will decay rapidly away from the main diagonal. The problem is to approximate the elements of M_w in a simple, readily calculable manner. Since the general ship problem is much more complex, attention is directed first to the case of an exisymmetric ship. A method for applying the axi-symmetric results to a normal ship is described later.

Mathematical Model for an Axi-Symmetric Ship

For such a ship it is possible to satisfy fairly well the fluid boundary condition of equality of hull and fluid velocities along the normals to the hull by means of a vertical dipole distribution along the axis of the ship. This distribution should normally be continuous but, if the ship is considered to be divided into a number of sections and the number is large enough, then it should be reasonable to assume that the line distribution in each section, i, has a constant strength μ_i.

Since the velocity potential at the point (r,θ,x) due to a dipole at the point (o,o,s) (referred to the cylindrical polar coordinates of Figure 1) is given by

$$\phi = \frac{\mu r \cos\theta}{[r^2+(x-s)^2]^{3/2}} \text{ , where } u = -\nabla\phi,$$

the potential due to a line distribution of dipoles of strength μ_i per unit length and extending from $x_{i-1/2}$ to $x_{i+1/2}$ is

$$\phi_i(r,\theta,x) = \mu_i r\cos\theta \int_{x_{i-1/2}}^{x_{i+1/2}} \frac{ds}{[r^2+(x-s)^2]^{3/2}}$$

whence $$\phi_i = \frac{\mu_i \cos\theta}{r} \left\{ \frac{x-x_{i-1/2}}{[r^2+(x-x_{i-1/2})^2]^{1/2}} - \frac{x-x_{i+1/2}}{[r^2+(x-x_{i+1/2})^2]^{1/2}} \right\} \qquad (L2)$$

The radial velocity u_r produced by the distribution is given by

$$u_{ri}(x) = -\frac{\partial\phi_i}{\partial r} = \frac{\mu_i \cos\theta}{r^2} \left\{ \frac{x-x_{i-1/2}}{[r^2+(x-x_{i-1/2})^2]^{1/2}} - \frac{x-x_{i+1/2}}{[r^2+(x-x_{i+1/2})^2]^{1/2}} + \frac{r^2(x-x_{i-1/2})}{[r^2+(x-x_{i-1/2})^2]^{3/2}} - \frac{r^2(x-x_{i+1/2})}{[r^2+(x-x_{i+1/2})^2]^{3/2}} \right\} \qquad (L3)$$

$$u_{xi}(x) = -\frac{\partial\phi_i}{\partial x} = \mu_i r\cos\theta \left\{ \frac{1}{[r^2+(x-x_{i+1/2})^2]^{3/2}} - \frac{1}{[r^2+(x-x_{i-1/2})^2]^{3/2}} \right\} \qquad (L4)$$

The total velocities produced by all the distributions are therefore

$$u_r(x) = \sum_{j=1}^{n} u_{rj}(x) \quad \text{and} \quad u_x(x) = \sum_{j=1}^{n} u_{xj}(x)$$

The boundary condition at the hull is that the velocities of the fluid and the hull, resolved in the direction of the normal to the hull, should be equal. For the axi-symmetric shape considered, the angle λ between the normal to the hull and the radial direction is given by $\lambda = -\tan^{-1} b'$ where $b(x)$ is the radius of the ship, and

$b' = db/dx$. The boundary condition is therefore,

$$v\cos\lambda - v'b\sin\lambda = u_r\cos\lambda + u_x\sin\lambda \qquad (L5)$$

where $v(x)$ is the distribution of vertical velocity along the length. This condition allows for both shearing and flexing of the ship. For the more interesting, lower frequency, modes of vibration, $v'b$ will be small compared to v since the wavelength will be much greater than the half beam. λ will also normally be small except possibly in the immediate neighbourhood of the stern. The term $v'b\sin\lambda$ will therefore be very small. u_x, the flow along the ship, is produced partly by the variation in v along the ship (i.e. by v') and partly by the changing shape of the ship (b'). It too will therefore, normally be small when v' and b' are small. It is generally possible then to simplify the boundary condition (L5) to

$$v = u_r \qquad (L6)$$

except when rapid changes occur in either the ship underwater cross-sectional area or in the velocity distribution along its length (e.g. for high modes). This simplification in the boundary condition reduces slightly the amount of data needed to specify the ship and its motion. It is roughly equivalent to neglecting rotary inertia in the dynamic equations of the ship itself.

Neither of the boundary conditions (L5) or (L6) can be satisfied everywhere by the assumed velocity potential. However, either can be satisfied at up to n 'collocation' points along the ship and if these points are suitably chosen the boundary condition will not be seriously violated anywhere. The most convenient choice for the collocation points is at the mid-points, x_i, of the ship sections and satisfying equation (L6) at these points gives

$$(\dot{\underset{\sim}{y}} - \underset{\sim}{u}) = \frac{1}{b^2} A\underset{\sim}{\mu} \tag{L7}$$

where b is the maximum value of b(x), $\dot{y}(x)$ the vertical velocity of the ship, u(x) the vertical velocity at the ship due to the explosion and the matrix $A = (\alpha_{ij})$ where

$$\alpha_{ij} = \frac{b^2}{b_i^2}\left\{ \frac{x_i - x_j + \ell/2}{[b_i^2 + (x_i - x_j + \ell/2)^2]^{1/2}} - \frac{x_i - x_j - \ell/2}{[b^2_i + (x_i - x_j - \ell/2)^2]^{1/2}} + \right.$$

$$\left. \frac{b_i^2 (x_i - x_j + \ell/2)}{[b_i^2 + (x_i - x_j + \ell/2)^2]^{3/2}} - \frac{b^2_i (x_i - x_j - \ell/2)}{[b^2_i + (x_i - x_j - \ell/2)^2]^{3/2}} \right\} \tag{L8}$$

Equation (L7) may then be inverted to determine the strengths $\underset{\sim}{\mu}$ of the line distributions necessary to satisfy the boundary condition (L6) for the given velocity distribution $\dot{\underset{\sim}{y}}$. This gives

$$\underset{\sim}{\mu} = b^2 A^{-1} (\dot{\underset{\sim}{y}} - \underset{\sim}{u})$$

The upward vertical force per unit length on the section at the point x_i is given by

$$f_i = -2\int_o^\pi p \cos\theta \, b_i d\theta$$

where $p = \rho\dot{\phi}$ is the fluid pressure.

Here the potential $\phi = \phi_o + \sum_{j=1}^{n} \phi_j$ since the fluid motion due to the explosion (and having the potential ϕ_o) is included. Thus

$$f_i = -2\rho\int_o^\pi b_i \phi \cos\theta d\theta = 2\rho \dot{u}_i b_i^2 \int_o^\pi \cos^2\theta d\theta - 2\rho\left\{ \frac{b}{\ell} \sum_{j=1}^{n} \beta_{ij}\dot{\mu}_j \int_o^\pi \cos^2\theta d\theta \right\}$$

$$= \pi\rho b_i^2 \dot{u}_i - \frac{\pi\rho b}{\ell} \sum_{j=1}^{n} \beta_{ij}\dot{\mu}_j \tag{L9}$$

where $\beta_{ij} = \frac{\ell}{b} \left\{ \frac{x_i - x_j + \ell/2}{[b_i^2 + (x_i - x_j + \ell/2)^2]^{1/2}} - \right.$

$$\left. \frac{x_i - x_j - \ell/2}{[b_i^2 + (x_i - x_j + \ell/2)^2]^{1/2}} \right\}$$

In the vicinity of the ship, ϕ_o has been approximated by $\phi_o \simeq -u_y = -ub_i \cos\theta$ on the ship surface. The velocity u is the explosion induced velocity at the ship axis.

Since in any actual motion conditions along the ship will be continuous, the upward force/unit length at the centre of the section will approximate the average force/unit length over the whole section and the total upward force S_i, on the section will be approximately

$$S_i = \ell f_i = \pi\rho b_i^2 \ell \dot{u}_i - \pi\rho b \sum_{j=1}^{n} \beta_{ij}\mu_i$$

$$\text{i.e.} \quad \underset{\sim}{S} = \bar{M}_w \underset{\sim}{\dot{u}} - \pi\rho b B \underset{\sim}{\dot{\mu}} = \bar{M}_w \underset{\sim}{\dot{u}} - \pi\rho b^3 BA^{-1} (\underset{\sim}{\ddot{y}} - \underset{\sim}{\dot{u}}) \qquad \text{(L10)}$$

where B is the matrix (β_{ij}) and $\bar{M}_w$ is the diagonal matrix with elements $\bar{m}_{wi} = \pi\rho b_i^2 \ell$. The matrix $\bar{M}_w$ is exactly the same 'buoyancy' matrix as found before in section E.

The required inertial water mass matrix M_w is therefore given by

$$M_w = \pi b^3 \rho BA^{-1} \qquad \text{(L11)}$$

This matrix depends only on the shape of the ship and is completely independent of the type of motion (or vibration mode). With M_w known the force distribution for any vertical acceleration distribution $\underset{\sim}{\ddot{y}}$ is readily found. A short computer routine has been written to compute the non-dimensional matrix BA^{-1} and the force distributions

deduced from it, by equation (L10), for given distributions of vertical acceleration.

Comparison of Results with known Exact Force Distributions

There are two forms of fluid flow, suitable for comparison, for which exact solutions are known: - the flows around a vibrating prolate spheroid and around an infinite circular cylinder whose transverse velocity varies sinusoidally along its length. The exact results for both cases have been compared with the results from the foregoing analysis.

a. Vibrating Prolate Spheroid

The methods involved in the solution of the flow about a prolate spheroid are discussed in some detail by Lamb (L5). Lewis (L1) gave the first solution in connection with transverse shear vibrations and Taylor (L2) gave a second solution using a different, more realistic boundary condition involving flexure as well as shear. A more general solution by Macagno and Landweber (L6) contains both the earlier solutions as special cases.

The coordinate system used in these solutions is the ellipsoidal set (ζ,μ,ω) illustrated in Figure L1. The curves of constant ζ and μ represent confocal systems of ellipsoids and hyperboloids of two sheets respectively. In terms of the cylindrical coordinates (r,θ,x)

$$r = k(\zeta^2-1)^{1/2}\,(1-\mu^2)^{1/2}$$

$$x = k\zeta\mu$$

If $\zeta = \zeta_o$ represents the given ellipsoid, assumed to be of length 2a and diameter 2b, then k and ζ_o are given by

$$k = (a^2-b^2)^{1/2} = a(1-\beta^2)^{1/2}$$

$$\zeta_o = (1 - \rho^2)^{-1/2} \quad \text{where } \beta = b/a$$

If the vertical velocity distribution along the axis of the ellipsoid is $v(x/a)$

then the boundary condition on the surface of the ellipsoid will be

$$u_n = -\frac{\partial \phi}{\partial n}_{\zeta=\zeta_o} = (v \cos\lambda - \frac{dv}{dx} b \sin\lambda) \cos\theta$$

which is the type of condition used by Taylor, allowing for flexure as well as shear. If $v(x/a)$ is a polynomial of degree N, then the solution for the potential can be written

$$\phi = \sum_{n=1}^{N+1} a_n Q_n^1(\zeta) P_n^1(\mu) \cos\theta$$

where $P_n^1(\mu)$, $Q_n^1(\zeta)$ are associated Legendre functions of the first and second kinds respectively. Substituting this expression for ϕ into the boundary condition gives

$$\frac{k}{\beta} v(\mu) - \beta k \mu \frac{dv(\mu)}{d\mu} = -\sum_{n=1}^{N+1} a_n \frac{dQ_n^1}{d\zeta}_{\zeta=\zeta_o} \cdot \frac{dP_n}{d\mu} ; \quad -1 < \mu < 1$$

(since $x = a\mu$ on the ellipsoid $\zeta=\zeta_o$). By assumption $v(x/a)$ is a polynomial so that

$$v = \sum_{n=1}^{N+1} v_n \left(\frac{x}{a}\right)^{n-1}$$

and the boundary equation becomes

$$\sum_{n=1}^{N+1} \frac{dP_n}{d\mu} \left[-\frac{\beta}{k} \frac{dQ_n^1}{d\zeta}\right]_{\zeta=\zeta_o} \cdot a_n = \sum_{n=1}^{N+1} [1-(n-1)\beta^2] v_n \mu^{n-1} ; \quad -1<\mu<1$$

which determines the coefficients a_n of the potential in terms of the

coefficients v_n of the velocity distribution. This equation is most easily solved by first integrating with respect to μ, giving

$$\sum_{n=1}^{N+1} \lambda_n [P_n(\mu) - P_n(o)] = \sum_{n=1}^{N+1} \frac{1-(n-1)\beta^2}{n} v_n \mu^n$$

where λ_n represents $-a_{nk} \beta \frac{dQ_n^1}{d\zeta} \Big|_{\zeta=\zeta_o}$. Multiplying by $P_m(\mu)$ and integrating from -1 to +1 gives, using the orthogonality relation for Legendre Polynomials

$$\lambda_m = (m+\tfrac{1}{2}) \sum_{n=1}^{N+1} \frac{1-(n-1)\beta^2}{n} v_n I_{mn} \quad , \quad (m=1,\ldots,N+1)$$

where $I_{mn} = \int_{-1}^{+1} \mu^n P_m(\mu) d\mu = o$, $n < m$ or $(n-m)$ odd

$$= 2 \cdot \frac{n(n-1)\ldots(n-m+2)}{(n+m+1)(n+m-1)\ldots(n-m+3)} \quad , \quad (n-m) \text{ even}$$

From these equations, given v_n, λ_m is easily found and so then, from its definition, is a_m.

With the coefficients a_n known in the expression for the velocity potential, the force distribution on the ellipsoid is readily found from

$$f(x) = -2 \int_o^\pi b(x) p \cos\theta d\theta \quad \text{where } p = \rho\dot{\phi}$$

i.e.

$$f(x) = -\pi\rho b(x) \sum_{n=1}^{N+1} a_n Q_n^{1\prime}(\zeta_o) P_n^{1\prime}(x/a) \qquad \text{(L12)}$$

A short computer routine has been written to compute the values of $f(x)/\pi\rho b^2$ given b/a and values for the coefficients $\dot{v}_1,\ldots,\dot{v}_5$. It is limited to velocity distributions which can be represented by quartic equations but this is sufficient for the lowest few modes.

Figures L2 and L3 compare the exact force distributions given by the above equation with the results given by the approximate 3-D flow method, for two ellipsoids with b/a ratios of 1/5th and 1/10th. The values given by normal strip theory, i.e.

$$\frac{f(x)}{\pi\rho b^2} = (1-x^2/a^2)\sum_{n=1}^{N+1} \dot{v}_n \left(\frac{x}{a}\right)^{n-1} \qquad \text{(L13)}$$

have also been added to the figures. The Lewis correction factors have been used for the strip theory results since these are known for four of the five nodes. The values used for the coefficients $\dot{v}_1,\ldots,\dot{v}_5$ for these cases were

coefficient / Mode	$\dot{v}_1$	$\dot{v}_2$	$\dot{v}_3$	$\dot{v}_4$	$\dot{v}_5$
Heave	1	0	0	0	0
Pitch	0	1	0	0	0
2-node vertical	-0.2	0	1	0	0
3-node vertical	0	-0.429	0	1	0
4-node vertical	0.0274	0	-0.534	0	1

the first four of these distributions being those used by Lewis. The fifth distribution has nodes at 0.155L, 0.38L, 0.62L, 0.845L, L being the total length. These nodes are in about the correct position for a 4-node ship vibration mode but the relative amplitudes are not good since the distribution gives too much prominence to the ends and too little to the central section.

For the b/a = 1/10th ellipsoid (for a ship with a length to beam ratio of 10) the results of the 3-D approximation and strip theory both agree well with the exact analysis and there is little to choose between them. Near the centre of the ellipsoid, where changes in the radius are smallest, the 3-D approximation is slightly better but at the ends, where the radius is changing rapidly, strip theory is the better. For the b/a = 1/5th (L/B = 5) ellipsoid the results are similar but the divergence of both approximations from the exact solution is quite serious near the ends, even for modes as low as the second vibration mode. Again there is little to choose between the approximate 3-D flow and strip theory. However, in each case the strip theory uses a different correction factor for each mode whereas the 3-D approximation deduces all the forces from a single matrix equation.

One point which should be borne in mind in these comparisons is that the boundary conditions are not quite the same for the three methods. Strip theory necessarily uses a shear type boundary condition since it can only relate the force on a section to the vertical velocity there. The 3-D approximate analysis too, based on equation (L9), also includes only shearing motions. The definition of matrix A (equation L8) is based on the approximate form of the boundary condition equation (L6), which is equivalent to including shear only. The exact solution includes flexure as well as shear. The necessary modifications to the 3-D approximation in order to satisfy the more exact boundary equation (L5), and the results it gives, are described later.

b. Infinite Circular Cylinder

Taylor (L2) was the first to consider this example in a ship vibration context. The infinitely long cylinder is assumed to have a transverse velocity distribution

$$v(x) = v_o \cos kx$$

The velocity potential for this distribution Taylor found to be

$$\phi = \frac{v_o K_1(kr)}{kK_1'(kb)} \cos\theta \cos kx$$

where b is the cylinder radius and K_1 is a modified Bessel function of the second kind. The force distribution may be found as before and is

$$f(x) = -2\int_o^\pi p \cos\theta b d\theta = -2\rho b\int_o^\pi \dot{\phi}\cos\theta d\theta = -\pi\rho b^2 \frac{\dot{v}_o K_1(kb)}{kbK_1'(kb)} \cos kx \qquad (L14)$$

The wavelength of this distribution is of course $\lambda = 2\pi/k$.

The example is not ideal for comparing with the 3-D approximation since the latter is firmly tied to a body of finite length (although it could obviously be modified to deal with a periodic distribution of infinite length). To compare results the approximate analysis was applied to a finite length of cylinder, 3 full wavelengths being the selected length in the hope that the central wavelength would be free of end effects. Since the computer program for the 3-D approximation is restricted to only 20 sections this gives only 6 different dipole distribution regions per wavelength. The results are compared with the exact values from the above equation in the table. In this case, because the cylinder is of uniform diameter there is no difference in the two forms of boundary condition.

λ/b \ x/λ	π/b	$\pi/2$	$5\pi/b$	$7\pi/b$	$3\pi/b$	$11\pi/b$	$13\pi/b$	$5\pi/2$	$17\pi/b$
5 exact	-.448	0	.448	.448	0	-.448	-.448	0	.448
3-D	-.445	-.00	.445	-.0014	-.0014	-.449	-.452	-.0140	.383
10 exact	-.631	0	.631	.631	0	-.631	-.631	0	.691
3-D	-.609	-.0003	.609	.609	-.0013	-.611	-.616	-.0189	.511
15 exact	-.762	0	.762	.762	0	-.762	-.762	0	.762
3-D	-.741	-.0001	.741	.741	-.0004	-.744	-.745	-.0096	.674
20 exact	-.826	0	.826	.826	0	-.826	-.826	0	.826
3-D	-.839	-.0007	.839	.839	.0007	-.839	-.840	-0015	.823

Values or $F(x)/\pi\rho b^2 v_o$ for an Infinite Cylinder

For all values of λ/b, the forces are clearly very accurate near the centre being within 4% of the exact value in all cases. The points given were the only ones used, indicating the coarseness of the representation; equivalent in a ship representation to using twenty points to represent the fifth vibration mode (6 nodes). Since the values from the 3-D approximation are constant to at least $x/\lambda = 7\pi/b$, the differences from the exact result are due to the coarse mesh rather than the finite length. For the $\lambda/b = 5$ case the lengths of the sections are nearly equal to their radii, whereas for the $\lambda/b = 20$ case the sections are each nearly 9 radii long.

Application of the Technique to non-axisymmetric Ships

Clearly it would be possible in principle to extend the 3-D approximation by adding distributions of higher multipoles along the ship axis, and determining their strength by satisfying a boundary condition around the circumference of the ship as well as along it. Alternatively (and more accurately) surface distributions of sources could be used over the surface of the ship. Either technique would, however, require very large amounts

of data to represent the ship shape and would require the inversion of a very large matrix. The success of the strip method using Lewis sections for the cross-sectional shapes points to simpler approaches.

In the solution of the two dimensional flows about ship-type cross-sections, although the velocity potential may in fact consist of a super-position of 2-D multipoles of all orders, the added mass of each section depends only on the dipole term, the shape of the section determining its strength. In the 3-D case it should, therefore, be approximately correct to account for the shape of the section via the strengths of the dipole distributions.

Since Lewis' original work, it has been customary to represent the added mass per unit length of the 2-D cross-sections in the form

$$\frac{\pi}{2} \rho b^2 C$$

where b is the half beam of the section and C is a constant depending on the section shape. Values for C have been computed for a great variety of shapes (References L1, L2, L7, L8, L9, L10 and L11). The above value for the added mass is also that due to a circular cylinder of radius

$$b_{equiv} = b \sqrt{C} \qquad \text{(L15)}$$

For a non-axisymmetric ship then, each cross-section may be compared with the known shapes, C determined, and then (15) gives the appropriate radius for an axisymmetric approximation to the actual shape. There are no reasonably simple non-axisymmetric 3-D flows with exact solutions which can be used for comparison but the procedure should give reasonable results. Certainly in the 2-node vibration mode, in the central section of the ship where the added

mass is most important, the technique will give very good answers since in this region the flow is very nearly 2-D and in the 2-D case the method is exact.

Use of the Full Boundary Condition

The results given so far for the 3-D approximation have all been based on the approximate equation (L6) for the boundary equation at the ship surface instead of the correct equation (L5). If the full equation is to be used, then the bending rotations γ_i of the ship must be included. If the expressions (L3) and (L4) for $u_r(x)$ and $u_x(x)$ are substituted into the boundary condition (L5) the result is

$$\dot{y}_i - u_{oi} + b_i b_i'(\gamma_i - u_{oi}') = \sum_{j=1}^{n} [u_{rj}(x_i) - b_i' u_{xj}(x_i)] = \frac{1}{b^2} \sum_{j=1}^{n} \bar{\alpha}_{ij} \mu_j$$

where

$$\bar{\alpha}_{ij} = \alpha_{ij} + b^2 b_i b_i' \{[b_i^2 + (x_i - x_j + \ell/2)^2]^{-3/2} -$$

$$[b_i^2 + (x_i - x_j - \ell/2)^2]^{-3/2}\}$$

This may be written in the matrix form

$$(\dot{\underset{\sim}{y}} - \underset{\sim}{u}) + \bar{B}\,(\dot{\underset{\sim}{\gamma}} - \underset{\sim}{u}') = \frac{1}{b^2}\,\bar{A}\underset{\sim}{\mu} \qquad \text{(L16)}$$

where $\bar{B}$ is a diagonal matrix with elements $b_i b_i'$. $\underset{\sim}{u}$ is again the water motion at the ship axis due to the explosion (calculated

as though the ship were not present), and $\underset{\sim}{u}'$ is its derivative with respect to x.

Inverting the equation gives

$$\underset{\sim}{\mu} = b^2\bar{A}^{-1}(\underset{\sim}{\dot{y}}-\underset{\sim}{u}) + b^2\bar{A}^{-1}\bar{B}(\underset{\sim}{\dot{\gamma}}-\underset{\sim}{u}') \tag{L17}$$

and the force distribution f(x) follows as before. Since changes in the cross-section are now included it is appropriate in this case to deduce from f(x) both the force and moment at each lumped mass by means of the integrals

$$S_i = \int_{x_{i-1/2}}^{x_{i+1/2}} f(x)dx; \quad M_i = \int_{x_{i-1/2}}^{x_{i+1/2}} (x-x_i)f(x)dx$$

whence

$$\underset{\sim}{S} = \bar{M}_w\underset{\sim}{\dot{u}} - \pi\rho\bar{C}\underset{\sim}{\dot{\mu}}$$

$$\underset{\sim}{M} = \bar{R}_w\underset{\sim}{\dot{u}}' - \pi\rho\bar{D}\underset{\sim}{\dot{\mu}} \tag{L18}$$

where the elements of the matrices $\bar{C}$ and $\bar{D}$ are given by

$$\bar{c}_{ij}/\ell = (1+b_i'^2)^{-\frac{1}{2}}(r_{1+} - r_{1-} - r_{2+} + r_{2-})$$

$$+ \frac{x_1-\alpha_1}{(1+b_i'^2)^{\frac{1}{2}}}\log\left(\frac{\alpha_1+\frac{1}{2}+r_{1+}}{\alpha_1-\frac{1}{2}+r_{1-}}\right) - \frac{x_2-\alpha_2}{(1+b_i'^2)^{\frac{1}{2}}}\log\left(\frac{\alpha_2+\frac{1}{2}+r_{2+}}{\alpha_2-\frac{1}{2}+r_{2-}}\right)$$

where $x_1 = \dfrac{x_i-x_j+\ell/2}{\ell}$; $x_2 = \dfrac{x_i-x_j-\ell/2}{\ell}$; $\alpha_1 = \dfrac{b_ib_i'/\ell + 1}{1+b_i'^2}$;

$$\beta_1 = \frac{b_i/\ell - x_1b_i'}{1+b_i'^2}$$

$$r_{1+} = [(\alpha_1+\tfrac{1}{2})^2+\beta_1^2]^{\frac{1}{2}}; \quad r_{1-} = [(\alpha_1-\tfrac{1}{2})^2+\beta_1^2]^{\frac{1}{2}}, \text{ with}$$

similar expressions for α_2, β_2, r_{2+} and r_{2-},

$$\bar{d}_{ij}/\ell^2 = \tfrac{1}{2}(1+b_i'^2)^{\frac{1}{2}}\left[(\alpha_1+\tfrac{1}{2})r_{1+} - (\alpha_1-\tfrac{1}{2})r_{1-} - (\alpha_2+\tfrac{1}{2})r_{2+} + (\alpha_2-\tfrac{1}{2})r_{2-}\right]$$

$$+ \frac{\beta_1^2}{2(1+b_i'^2)^{\frac{1}{2}}}\log\left(\frac{\alpha_1+\frac{1}{2}+r_{1+}}{\alpha_1-\frac{1}{2}+r_{1-}}\right) - \frac{\beta_2^2}{2(1+b_i'^2)^{\frac{1}{2}}}\log\left(\frac{\alpha_2+\frac{1}{2}+r_{2+}}{\alpha_2-\frac{1}{2}+r_{2-}}\right)$$

$$+ \frac{x_1-2\alpha_1}{(1+b_i'^2)^{\frac{1}{2}}}(r_{1+}-r_{1-}) - \frac{x_2-2\alpha_2}{(1+b_i'^2)^{\frac{1}{2}}}(r_{2+}-r_{2-})$$

$$- \frac{2\alpha_1+\frac{\alpha_1^2+\beta_1^2}{x_1-2\alpha_1}}{(1+b_1'^2)^{\frac{1}{2}}}\log\left(\frac{\alpha_1+\frac{1}{2}+r_{1+}}{\alpha_1-\frac{1}{2}+r_{1-}}\right) + \frac{2\alpha_2+\frac{\alpha_2^2+\beta_2^2}{x_2-2\alpha_2}}{(1+b_i'^2)^{\frac{1}{2}}}\log\left(\frac{\alpha_2+\frac{1}{2}+r_{2+}}{\alpha_2-\frac{1}{2}+r_{2-}}\right) \qquad \text{(L19)}$$

Thus

$$\begin{bmatrix} \underset{\sim}{S} \\ \underset{\sim}{M} \end{bmatrix} = \begin{bmatrix} \bar{M}_w & 0 \\ 0 & \bar{R}_w \end{bmatrix}\begin{bmatrix} \underset{\sim}{\dot{u}} \\ \underset{\sim}{\dot{u}'} \end{bmatrix} - \pi\rho b^2 \begin{bmatrix} \bar{C}\bar{A}^{-1} & \bar{C}\bar{A}^{-1}\bar{B} \\ \bar{D}\bar{A}^{-1} & \bar{D}\bar{A}^{-1}\bar{B} \end{bmatrix}\begin{bmatrix} \underset{\sim}{\ddot{y}} - \underset{\sim}{\dot{u}} \\ \underset{\sim}{\ddot{Y}} - \underset{\sim}{\dot{u}'} \end{bmatrix}$$

i.e.

$$\begin{bmatrix} \underset{\sim}{S} \\ \underset{\sim}{M} \end{bmatrix} = \begin{bmatrix} \bar{M}_w + M_{w1} & M_{w2} \\ M_{w3} & \bar{R}_w + M_{w4} \end{bmatrix}\begin{bmatrix} \underset{\sim}{\dot{u}} \\ \underset{\sim}{\dot{u}'} \end{bmatrix} - \begin{bmatrix} M_{w1} & M_{w2} \\ M_{w3} & M_{w4} \end{bmatrix}\begin{bmatrix} \underset{\sim}{\ddot{y}} \\ \underset{\sim}{\ddot{Y}} \end{bmatrix} \qquad \text{(L20)}$$

which gives the hydrodynamic force and moment at each lumped mass. Use of this equation instead of equation E(1) in the derivation of the equations of motion gives, in place of equation E(8), the equation

$$\begin{bmatrix} M + M_{w1} & M_{w2} \\ M_{w3} & R+M_{w4} \end{bmatrix} \begin{bmatrix} \ddot{y} \\ \ddot{\gamma} \end{bmatrix} + \begin{bmatrix} A+K & B \\ B^T & C+K_r \end{bmatrix} \begin{bmatrix} y \\ \gamma \end{bmatrix} = \begin{bmatrix} M_{w1}+\bar{M}_w & M_{w2} \\ M_{w3} & M_{w4}+\bar{R}_4 \end{bmatrix} \begin{bmatrix} \mathring{u} \\ \mathring{u}' \end{bmatrix} \tag{L21}$$

As in section E, since rotary inertia effects appear to be minor they can be neglected and

$$\underset{\sim}{\gamma} \sim - C^{-1}B^T \underset{\sim}{y}$$

so that the reduced equation of motion is

$$[M + M_{w1} - M_{w2}C^{-1}B^T]\ddot{\underset{\sim}{y}} + [(A+K)-BC^{-1}B^T]\underset{\sim}{y} = (M_{w1} + \bar{M}_w)\mathring{\underset{\sim}{u}} + M_{w2}\mathring{\underset{\sim}{u}}' \tag{L22}$$

Here not all rotary inertia terms have been neglected. The terms affecting the displacement equation (the M_{w2} terms) are retained since these are the terms which differentiate between the 'shear' and 'shear plus flexure' boundary conditions. Even when normal rotary inertia is suppressed these terms can have some effect on the hydrodynamic forces.

The force distributions given by equation (L18) (with $\mathring{\underset{\sim}{u}} = o$) have been added to Figures L2 and L3 where they differ appreciably from the simpler 3-D approach used earlier. The significant improvement in the accuracy of the results for the higher modes, particularly for the smaller length/beam ratio ellipsoid, is evident. The results using equation (L18) (based on the full boundary condition (L5)) are everywhere almost identical to the exact values.

In computing the results from equation (L18), in order to ensure that no more data should be used than is normally necessary in ship

vibration calculations, the slopes b'of the ellipsoids were estimated numerically from the given radius b_i at the collocation points. The method appears to be adequate for the rather extreme slopes involved in ellipsoids and so should be quite satisfactory for ship forms where shape changes are less severe.

Modification of the Normal Mode Equations

Because the matrix M_1 in the new equations of motion

$$M_1 \ddot{y} + Sy = M_2 \hat{u} + M_3 \hat{u}' \qquad \text{(L23)}$$

is now no longer a diagonal matrix, the transformation

$$z = M_1^{\frac{1}{2}} y \qquad \text{(L24)}$$

used in section F can no longer be applied. In fact M_1 is no longer a symmetric matrix and the transformation technique should not really be applied at all. An alternative, once asymmetry is accepted would be to re-write the equation as

$$\ddot{y} + M_1^{-1} Sy = M_1^{-1} M_2 \hat{u} + M_1^{-1} M_3 \hat{u}'$$

and solve the homogenous part

$$\ddot{y} + M_1^{-1} Sy = 0$$

directly. This unfortunately would considerably restrict the available computer routines since most of the really efficient routines deal only with symmetric matrices. However, in all cases so far considered, the matrix M_1 has been found to be almost symmetric, except for elements corresponding to the end lumped masses, and there the actual values of the elements tend to be small. To avoid having to use general matrix methods the matrix M_1 was arbitrarily made symmetric by replacing all the elements m_{1ij} by $(m_{1ij} + m_{1ji})/2$.

The forces resulting from this amended matrix were compared with those produced by the correct matrix for the two ellipsoid cases and the two sets of forces were found to differ by no more than 3% anywhere. Over most of the length of the ellipsoid the forces were identical. Since the vibration frequencies depend approximately, on the square root of these forces, even this small difference will be further reduced in the effect on the eigenvalues and use of the modified matrix seems justified.

With M_1 symmetric, a standard Choleski decomposition routine (L14) may be used to generate a matrix L such that

$$LL^T = (M + M_w) \tag{L25}$$

and the transformation (L24) is replaced by

$$\underset{\sim}{z} = L^T \underset{\sim}{y}$$

giving

$$\ddot{\underset{\sim}{z}} + E_1 \underset{\sim}{z} = L^{-1} M_2 \dot{\underset{\sim}{u}} + L^{-1} M_3 \underset{\sim}{u},$$

where $E_1 = L^{-1} S L^{-T}$, a symmetric matrix. The eigenvalues and vectors of E_1 can be found just as before and the normal mode technique can then be applied exactly as in section F.

Application to a Ship Vibration Calculation

For the destroyer considered in section G the same basic data were used, with a modified version of the computer program, to predict the normal mode vibration frequencies. The results obtained are compared in the table with the straightforward strip theory technique. The calculated results are for the cases

1. Normal strip theory with the Taylor correction for the 2-node mode

2. 3-D approximation based on equation (L11) (the approximate boundary condition)

3. 3-D approximation based on equation (L22) (the full boundary condition).

In each of these cases the effect of shear deflection is included but that of rotary inertia has been suppressed.

Number of Nodes		Frequency (H_z)			Measured
		Calculated			
		1	2	3	
0	Heave	0.21	0.20	0.20	-
1	Pitch	0.23	0.22	0.22	-
2	Vibration Modes	1.54	1.51	1.52	1.59 (1.50)
3		3.13	3.14	3.17	3.20 (3.09)
4		4.67	4.77	4.81	4.77
5		6.41	6.72	6.78	6.29
6		8.09	8.68	8.79	-
7		9.61	10.45	10.61	-

It is clear that the method changes the results little, which is to be expected since the length to beam ratio of the destroyer is close to that of the more slender of the two ellipsoids, where the exact, strip theory and 3-D approximation force distributions were found to be all very similar. The large difference between the calculated results and the measured values reflects mainly the inaccuracy of the ship data since measurements on a sister ship in a similar displacement condition, gave the values shown in brackets. Unfortunately the higher mode frequencies were not measured for the second ship.

For a different class of destroyer similar results were obtained and are shown in the following table.

Number of Nodes		Frequency (H_z)			Measured
		Calculated			
		1	2	3	
0	Heave	0.20	0.20	0.20	-
1	Pitch	0.22	0.23	0.23	-
2)		1.64	1.64	1.66	1.68
3)	Vibration	3.16	3.20	3.22	3.35
4)	Modes	4.92	4.96	5.00	4.97
5)		6.90	6.96	7.03	6.63

In each of these cases the calculated mode shapes were virtually independent of the hydrodynamic approximation used.

Conclusions Regarding the Hydrodynamic Flow

The results for the force distribution on ellipsoids show that in general the 3-D flow approximation, using the full boundary condition, should provide more accurate results than normal strip theory. However, the difference is only marked for small values (≈5) of the ratio (length/beam). For a value of this ratio of 10 the 3-D flow approximation was still very accurate but strip theory also gave good results even close to the ends.

The considerable difference between the inertial mass matrices given by strip theory and by the 3-D approximation, and the close agreement of the results they give, suggests that, so far as vibration of the ship as a beam of rigid cross-section is concerned, little improvement from more exact ideal fluid theories is possible. Any remaining discrepancies between measured and predicted hydrodynamic forces are probably largely due to non-ideal flow, free surface effects, non-linear Bernoulli forces or the distortion of cross-sections.

References

L1 Lewis F M ; "The Inertia of the Water Surrounding a Vibrating Ship." Trans. SNAME, Vol. 37, 1929.

L2 Taylor J L; "Some Hydrodynamical Inertia Coefficients." Phil. Mag. S.7 Vol 9, No. 55 Jan 1930.

L3 Kaplan P ; "A Study of the Virtual Mass Associated with the Vertical Vibration of Ships in Water." Stevens Inst. Tech., Davidson Lab. Report 734, 1959.

L4 Anderson G; & Norrand K "A Method for the Calculation of Vertical Vibration with Several Nodes and Some Other Aspects of Ship Vibration." Paper read to the INA Dec. 15 1968.

L5 Lamb, H ; "Hydrodynamics" 6 Edition, Cambridge Univ. Press, 1932.

L6 Macagno E O & Landweber L ; "Inrotational Motion of the Liquid Surrounding a Vibrating Ellipsoid of Revolution." Jn. Ship Research, Vol. 2, No. 1, 1958.

L7 Prohaska C W ; "The Vertical Vibration of Ships." The Shipbuilder and Marine Engine Builder, 1947.

L8 Wendel K ; "Hydrodynamic Masses and Moments of Inertia" Jahrobuch der Schiffbautcehnische Gesellschaft Vol 44, 1950.

L9 Landweber L; & Macagno M "Added Mass of Two-Dimensional Forms Oscillating in a Free Surface." Jn. Ship Research, Vol 1, 1957.

L10 Landweber L; & Macagno M "Added Masses of a Three-Parameter Family of Two-Dimensional Forms Oscillating in a Free Surface." Jn. Ship Research, Vol 2, No 4 (1959).

L11 Macagno M ; "A comparison of Three Methods for Computing the Added Masses of Ship Sections." Jn Ship Research Vol 12, No 4, 1968.

L13 Hoffman D ; "Conformal Mapping Techniques in Ship Hydrodynamics." Webb Inst. of Naval Architecture Report No 41-1, 1969.

L14 Martin R S ; & Wilkinson J H Reduction of the Symmetric Eigenproblem $Ax = \lambda\beta x$ and Related Problems to Standard Form." Numerische Mathematik, 11, 99-110, 1963.

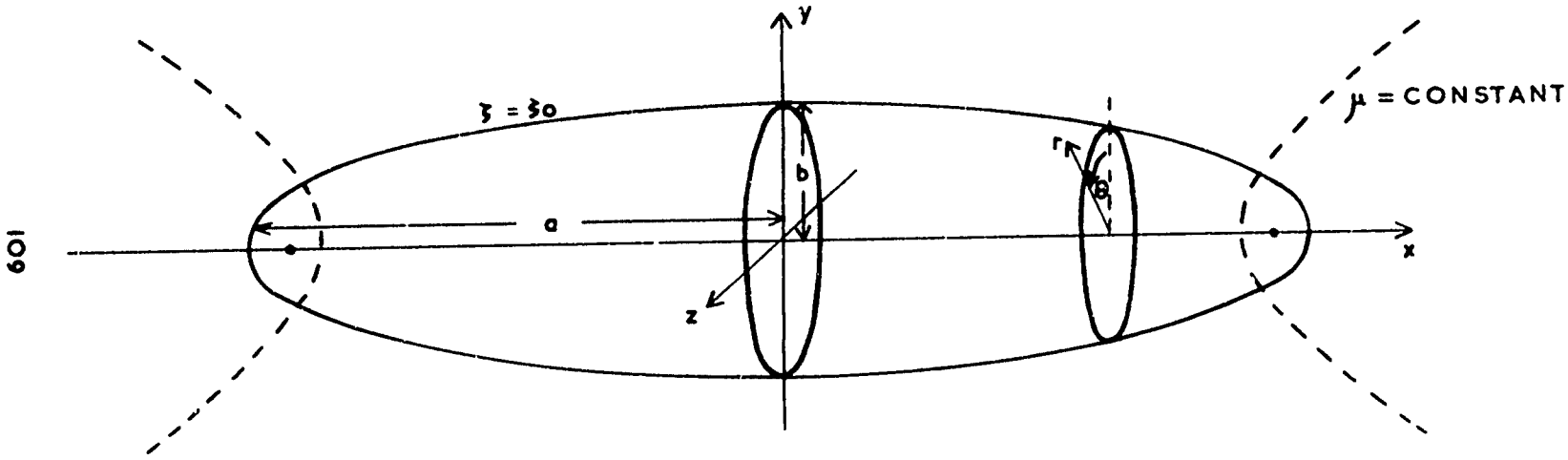

601

CYLINDRICAL AND ELLIPSOIDAL COORDINATE SYSTEM
FOR VIRTUAL MASS APPROXIMATION

FIGURE L1

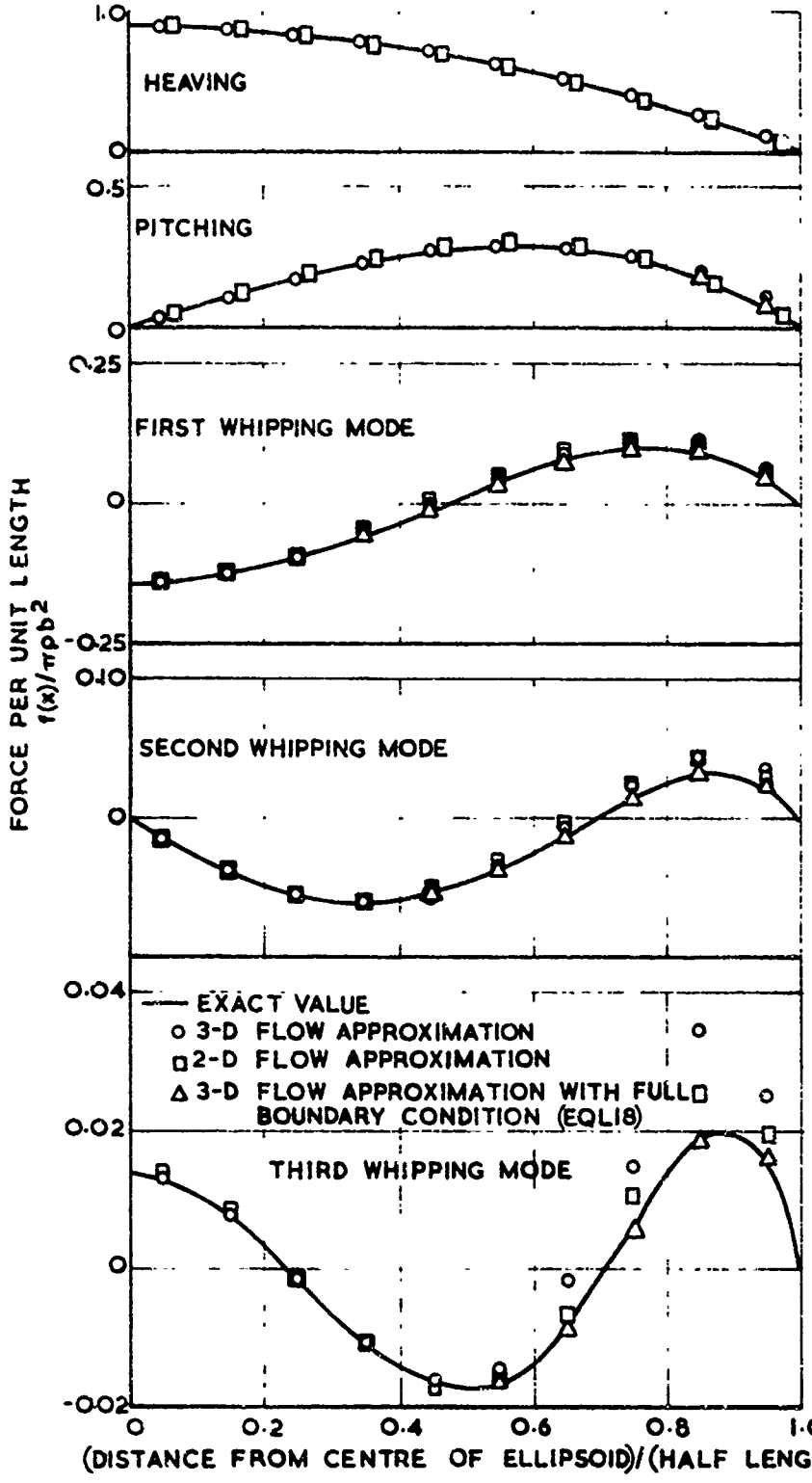

COMPARISON OF THREE- AND TWO-DIMENSIONAL FLOW APPROXIMATIONS WITH THE EXACT SOLUTION FOR A VIBRATING ELLIPSOID (B/L = 1/5)

FIGURE L2

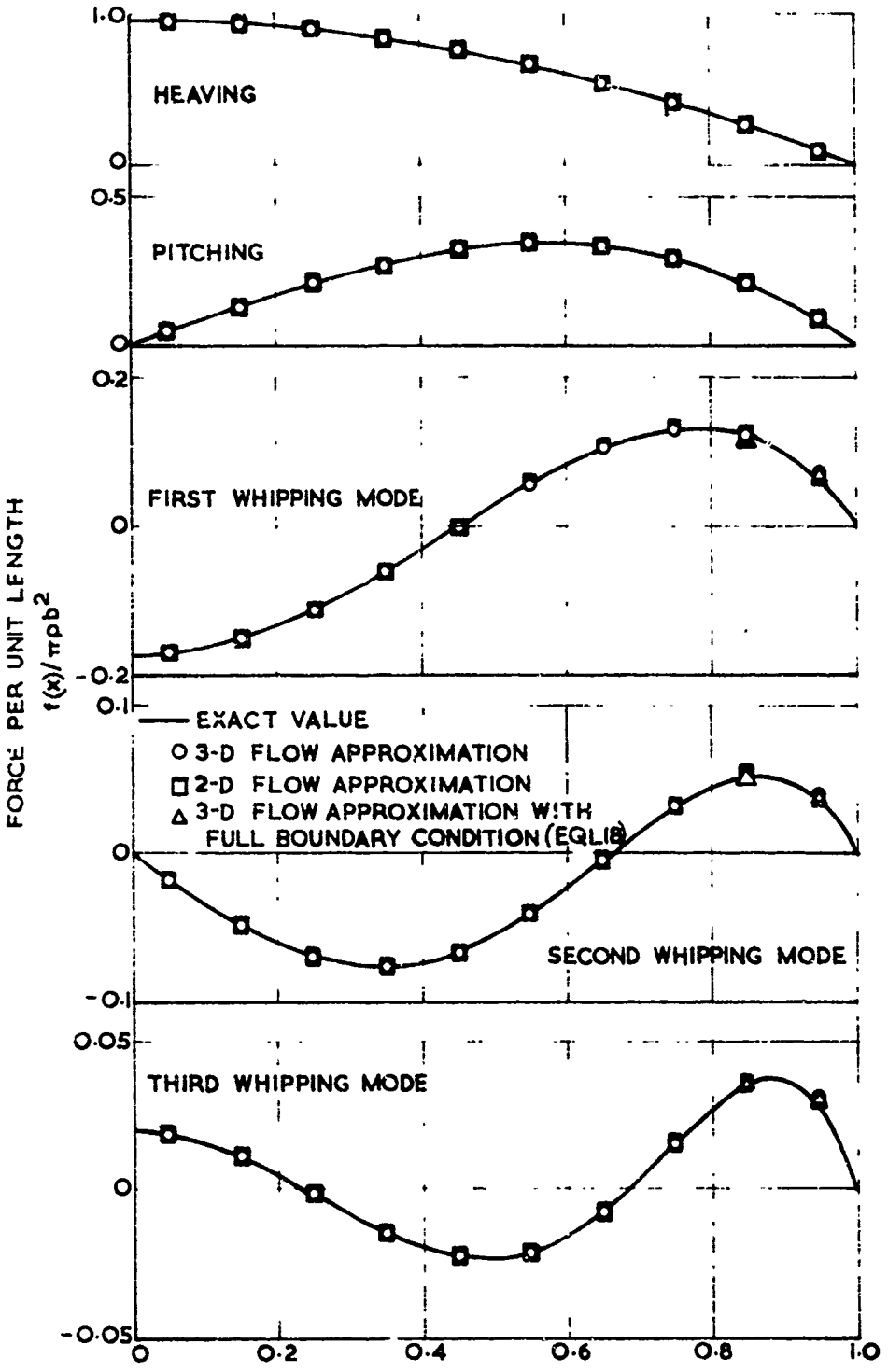

COMPARISON OF THREE- AND TWO-DIMENSIONAL FLOW APPROXIMATIONS WITH THE EXACT SOLUTION FOR A VIBRATING ELLIPSOID (B/L= 1/10)

FIGURE L3

M Limits of Applicability of the Theory

The theory as so far presented has been shown to give very good agreement with the limited experimental results available but involves a number of assumptions, some of them quite drastic. In this section some of these assumptions are discussed in more detail to show more clearly the limitations of the theory.

Most of the approximations are those normally encountered in ship vibrations and in consequence they have been investigated extensively already. The limitations of beam theory for the elastic representation of the ship are beginning to be appreciated and alternative approaches, e.g. (M1) have been proposed. In general though, particularly for slender ships, beam theory has been found quite adequate. In the hydrodynamics of ship vibrations it is customary to neglect the 'Bernoulli', $\frac{1}{2}\rho u^2$ pressure terms, and, for the free surface condition even the linear gravity terms are neglected. Both these points have been considered by several authors, e.g. (M2) and (M3) and have been found small for the vibration modes although they can be significant in the pitch and heave motions. For example, the inclusion of a linear free surface effect changes the added mass, and adds a damping force to the motion if the 'Froude number', $\frac{b\omega^2}{g}$ (where b is the half beam, ω the circular frequency and g the acceleration of gravity), is less than about 4. For the heave and pitch motions of the destroyers described earlier, $\frac{b\omega^2}{g} \simeq 1$ and these modes and the deduced rigid body motions may be expected to be slightly in error, but for even the lowest frequency vibration mode $\frac{b\omega^2}{g} \simeq 25$ and the approximations may be expected to be very good.

Compressible effects in ship vibration have been considered by both Taylor (D2) and Kaplan (D8) and have been found negligible.

Viscous effects seem generally to have received less attention but, since with the small amplitudes involved in the vibration frequencies a full wake cannot form beneath the ship when it is moving up, only skin drag is likely to matter. For flexural vibration the Reynolds number is of order 10^7 and such forces will be small. Both compressibility and viscous effects lead principally to damping which is very small in vibrating ships. In ship vibration work damping is usually attributed largely to internal effects and structural damping rather than to the hydrodynamics. Even minor damping is important in such work since it limits the amplitudes of vibrations produced by sources operating close to one of the natural frequencies. In the explosion induced whipping application however the vibration exciter (the explosion bubble) is only effective over about two basic whipping cycles and the effect of damping is very small.

Another possible source of error in vibration work is sympathetic vibration of local structure. Even if the frequency of the bottom of the ship (distorting as a panel, or two panels, over its whole width is much higher than the ship frequency, it may be forced in and out at the ship frequency and so reduce the amount of water being moved with the ship. The effect has been investigated in (34) and shown to be important for modes higher than the 4-node, mode but below this the effect seems to be small.

Aside from the general and well known limitations, there are several approximations which are related to the interaction between the explosion and the ship and which are consequently exclusive to the whipping problem. The principal such approximation is the determination of the force distribution acting on the ship through the use of the fluid accelerations which would be induced

by the explosion at the ship axis if the ship were not present. In both the strip theory and the 3-D flow theory this approximation implicitly assumes that, in the absence of the ship, the acceleration would be uniform throughout a region around the ship position which is large compared to the ship cross-section. Under such conditions very little flow will be induced along the ship axis by the ship and it can be expected that the approximation will be good but, for fairly close charges, the spherical flow divergence around the charge will certainly lead to non-uniform conditions. The forces will be acting on a short length of ship, considerable flow along the axis will occur and the undisturbed flow at any cross-section will certainly not be uniform. This spherical divergence will impose an inner limit to the range at which the 'distant flow' approximation can be expected to apply.

A second possible limitation of the 'strip theory' type forces is that, even for distant charges where conditions are uniform, near the bow and stern of the ship flow along the axis (around the ends) can be expected. The 3-D approximation should, in principle, be capable of allowing for such flow but strip theory is not.

A third possible source of error is the neglect of Bernoulli pressures due to the bubble flow. Although such pressures can be neglected when they relate to the induced ship vibration, the direct flow due to the bubble expansion, when the explosion is close, could possibly lead to more effective pressures of this type.

These three possible sources of error are considered in the following paragraphs.

a. Spherical Flow Divergence

Because of the linearity of the assumed forces on the ship, the equations of motion derived in section E are equivalent to a

separation of the problem into two parts:-

(i) the determination of the forces acting on the ship, assumed rigid and motionless, due to the explosion bubble.

(ii) The response of the ship to these forces, calculated as though the bubble were not present.

In consequence, to investigate the effect of spherical flow divergence, etc., it is only necessary to consider the forces on a rigid target .

The most convenient idealisation for such a target is an infinite rigid circular cylinder. As before the effect of the explosion is assumed to be equivalent to a point source of varying strength e(t), e being given by

$$e(t) = \frac{V(t)}{4\pi}$$

where V is the bubble volume. The problem to be solved is then that of a point source near an infinite circular cylinder, the geometry and coordinate system being as illustrated in Figure M1.

For the geometry shown, the source induced velocity at the cylinder axis is

$$u = \frac{e}{r'^2} = \frac{e}{(b^2+x^2)}$$

Resolving this velocity perpendicularly to the axis gives

$$u_p = \frac{eb}{(b^2+x^2)^{3/2}} .$$

Since the strip theory added mass μ_w per unit length and 'buoyancy' $\bar{\mu}_w$ per unit length are both simply $\pi\rho a^2$ for the cylinder, the distribution of force per unit length, on the basis of the distant flow approximation, is given by

$$f_1(x) = (\mu_w+\bar{\mu}_w)\dot{u}_p = \frac{2\pi\rho u^2 \dot{e} b}{(b^2+x^2)^{3/2}} = 2\pi\rho\dot{e}\,\frac{\beta}{(\beta^2+\xi^2)^{3/2}} \qquad (M1)$$

in terms of the dimensionless quantities $\xi = x/a$, $\beta = b/a$.

The problem has been solved, exactly and independently, by at least two authors. Savic (M5) solved for the potential flow in order to estimate the effect of the cylinder on the bubble pulsation, and Murray (M6) solved the similar but more difficult case of the interaction between a spherical acoustic source and an infinite cylinder. The methods used were also similar. Savic's solution for the velocity potential is

$$\phi = \frac{2e}{\pi} \sum_{n=o}^{\infty} \epsilon_n \cos n\theta \int_{\lambda=o}^{\infty} \frac{K_n(b\lambda)}{K_n'(a\lambda)} [K_n'(a\lambda)I_n(r\lambda) - I_n'(a\lambda)K_n(r\lambda)]$$

$$\cos(x\lambda)d\lambda; \quad r<b \qquad \text{(M2)}$$

$$= \frac{2e}{\pi} \sum_{n=o}^{\infty} \epsilon_n \cos n\theta \int_{\lambda=o}^{\infty} \frac{K_n(r\lambda)}{K_n'(a\lambda)} [K_n'(a\lambda)I_n(b\lambda) - I_n'(a\lambda)K_n(b\lambda)]$$

$$\cos(x\lambda)d\lambda; \quad r>b$$

where $\epsilon_o = 1$, $\epsilon_n = 2$ $(n \geq 1)$ and $I_n(x)$, $K_n(x)$ are Bessel functions of the second kind. On the surface of the cylinder, r = a, the Wronskian relation

$$I_n(x)K_n'(x) - K_n(x)I'_n(x) = -1/x$$

simplifies the potential to

$$\phi = -\frac{2e}{\pi a} \sum_{\lambda=o}^{\infty} \epsilon_n \cos n\theta \; \vartheta_n(\beta,\xi) \qquad \text{(M3)}$$

where $\vartheta_n(\beta,\xi) = \int_{\lambda=o}^{\infty} \frac{K_n(\beta\lambda)}{\lambda K_n'(\lambda)} \cos(\xi\lambda)d\lambda$.

Since the pressure is given by

$$p = \rho\dot{\phi},$$

the force per unit length of the cylinder can be found by integrating round the circumference of the cylinder and is given by

$$f_2(x) = \int_0^{2\pi} (pad\upsilon)\cos\theta = 2ap \int_0^{\pi} \dot{\phi} \cos\theta d\theta = 2ap \left[-\frac{2\dot{c}}{a} I_1(\beta,\xi)\right]$$

so that the exact inertial force corresponding to (M1) is

$$f_2(x) = -4\rho\dot{c} \int_{\lambda=0}^{\infty} \frac{K_1(\beta\lambda)}{\lambda K_1'(\lambda)} \cos(\xi\lambda) d\lambda \qquad (M4)$$

Figure M2 shows the function $-K_1(\beta\lambda)/\lambda K_1'(\lambda)$ for several values of β. The curves show that most of the contribution to the integral will come from very small values of λ since the function decays very rapidly as λ increases, except for β very close to unity (the charge very close to the target). In fact

$$\frac{K_1(\beta\lambda)}{\lambda K_1'(\lambda)} \sim O\left(\frac{e^{-\alpha\lambda}}{\lambda}\right) \quad ; \quad \alpha = \beta - 1 ,$$

so that the integral converges for all (β,ξ) except $\beta = 1$, $\xi = 0$, where it has a logarithmic singularity.

For $\beta > 5$ Figure M2 shows that there will be very little contribution to the integral in (M4) from values of $\lambda > 1$. For values of λ in the range $0 < \lambda < 1$, the denominator of the integrand, $\lambda K_1'(\lambda)$, is represented quite well by the first term of its power expansion in λ. Thus, for $\beta > 5$ the denominator may be replaced by the leading terms of its power expansion and the integral can be represented approximately by

$$\int_0^{\infty} \frac{K_1(\beta\lambda)}{\lambda K_1'(\lambda)} \cos(\xi\lambda) d\lambda \sim - \int_0^{\infty} \lambda K_1(\beta\lambda) \cos(\xi\lambda) d\lambda -$$

$$\tfrac{1}{2}\int_0^\infty \lambda^3 \log\lambda\, K_1(\beta\lambda)\cos(\xi\lambda)\,d\lambda -$$

$$\frac{(\gamma+\tfrac{1}{2})-\log 2}{2}\int_0^\infty \lambda^3 K_1(\beta\lambda)\cos(\xi\lambda)\,d\lambda$$

$$-\frac{\partial H_1}{\partial\beta}+\tfrac{1}{2}\frac{\partial^2 H_2}{\partial\beta\partial\xi}-\frac{(\gamma+\tfrac{1}{2})-\log 2}{2}\frac{\partial^3 H_1}{\partial\beta\partial\xi^2}$$

where

$$H_1 = \int_0^\infty K_0(\beta\lambda)\cos(\xi\lambda)\,d\lambda = \pi/2\sigma \quad ; \sigma = (\beta^2+\xi^2)^{\frac{1}{2}}$$

$$H_2 = \int_0^\infty \lambda\log\lambda\, K_0(\beta\lambda)\sin(\xi\lambda)\,d\lambda = -\frac{\xi}{2\sigma^2}\left[\log\left(\frac{2\sigma^2}{\beta}\right)+\gamma-2\right].$$

H_1 is a well known integral given in reference [M7]. H_2 was deduced from H_1 by Fraenkel [M8] for the asymptotic evaluation of a very similar integral. Substitution of these expressions gives the asymptotic expression, valid for large β,

$$f_2(x) \sim 2\pi\rho\dot{e}\,\frac{\beta}{(\beta^2+\xi^2)^{3/2}} - 3\pi\rho\dot{e}\,\frac{\beta}{(\beta^2+\xi^2)^{5/2}}$$

$$\left(1-\frac{5\xi^2}{\beta^2+\xi^2}\right)\left[\log\left(\frac{\beta^2+\xi^2}{\beta/4}\right)-5/2\right] -$$

$$\frac{\pi\rho\dot{e}}{\beta(\beta^2+\xi^2)^{3/2}}\left(1-\frac{3\xi^2}{\beta^2+\xi^2}\right)\left(1-\frac{2\beta^2}{\beta^2+\xi^2}\right) - \qquad [M5]$$

$$10\pi\rho\dot{e}\,\frac{\beta\xi^2}{(\beta^2+\xi^2)^{7/2}} + 0(\sigma^{-6}\log\sigma)$$

The leading term in this expansion is simply the 'distant flow' approximation given in equation [M1].

The results given for $f(x)/4\rho\dot{e}$ by the 'distant flow' approximation (equation [M1]), the asymptotic expansion (equation [M5]) and direct numerical integration of the exact integral in equation [M4] are compared in Figure M3 and in the following table.

Exact and Asymptotic Force Distributions

$f(x)/4\rho\dot{e}$

β \ ξ	0.0	0.5	1.0	3.0	10.0		
1.111	1.972	0.776	0.390	0.068	0.0032	Exact (numerical)	(4)
	1.272	0.965	0.523	0.053	0.0017	Distant flow	(1)
	3.347	0.673	-0.189	0.087	0.0033	Asymptotic	(5)
1.250	1.243	0.710	0.381	0.069	0.0033	Exact	(4)
	1.005	0.805	0.479	0.057	0.0019	Distant flow	(1)
	2.187	0.761	0.003	0.081	0.0033	Asymptotic	(5)
1.667	0.600	0.488	0.318	0.070		Exact	(4)
	0.566	0.497	0.357	0.065	0.0025	Distant flow	(1)
	0.851	0.560	0.224	0.071	0.0036	Asymptotic	(5)
2.500	0.246	0.232	0.195	0.066	0.0043	Exact	(4)
	0.251	0.237	0.201	0.066	0.0036	Distant flow	(1)
	0.283	0.252	0.190	0.063	0.0044	Asymptotic	(5)
5.000	0.060	0.060	0.058	0.0396	0.0059	Exact	(4)
	0.063	0.062	0.059	0.0396	0.0056	Distant flow	(1)
	0.062	0.061	0.058	0.0386	0.0060	Asymptotic	(5)

The results show that, for $\beta = 5$ the three methods give almost identical answers. For $\beta < 5$ the asymptotic solution continues to represent the exact solution well for large ξ, even for β as small as 1.111. The distant flow approximation (just the first term of the asymptotic series) is far less satisfactory in this region and for $\beta = 1.111$, $\xi = 10.0$ is in error by a factor of almost 2. This region of large ξ however represents the part of the cylinder well away from the point source, where the flow is directed principally along the axis rather than across it, and the transverse force is very small.

For the smaller values of ξ, closer to the point source, the asyaptotic series is much less satisfactory and, surprisingly, its first term alone (the distant flow approximation)represents the integral far more accurately. This is most clearly seen in the Figure M3. Although only expected to apply for $\beta > 5$, even for β as small as 1.4 the distant flow approximation is in error by only 12% for small ξ. Since the small values of ξ correspond to points near the point source, where the transverse forces are largest, the distant flow approximation is a far better approximation for practical use than the more extended asymptotic result [M5], and can be applied down to very short ranges ($\beta \approx 1.4$).

b. The Force Distribution Near the Bow and Stern

While the strip theory force distribution can reasonably be expected to apply over most of the length of the ship, near the bow and stern it might be expected that flow around the ends could relieve the fluid pressures and so alter the force distributions in these areas. For the overall still water vibration problem, the inaccuracies found earlier (Section L) for the strip theory forces did not make much difference to the frequencies. However, for a charge close to either the bow or stern, most of the force acting on the target will be applied in this error prone region and it seems possible that small errors could lead to large differences in the forcing function. Since it can allow for such flow the 3-D approximation should not be so likely to cause error. The accuracy of both the strip theory and the 3-D approximation are investigated here.

The simplest idealisation to use in this case is an ellipsoidal target, with a point source to represent the explosion bubble. As in Section L the ellipsoidal co-ordinates (ζ, μ, ω) are used (they

are shown in Figure M4). They are related to cylindrical co-ordinates (r, θ, x) by

$$r = k(\zeta^2 - 1)^{\frac{1}{2}} (1 - \mu^2)^{\frac{1}{2}}$$

$$x = k\,\zeta\mu$$

$$\theta = \omega \qquad \text{where k is a constant.} \qquad [M6]$$

In terms of the ellipsoidal co-ordinates the general solution of Laplaces equation for the velocity potential ϕ, is of the form

$$\phi = \sum_{n=o}^{\infty} \sum_{m=o}^{n} (A_n \cos m\omega + B_n \sin m\omega)(C_n P_n^m (\zeta) + D_n Q_n^m (\zeta)) T_n^m (\mu) \qquad [M7]$$

where $T_n^m (x)$, $P_n^m (x)$, $Q_n^m (x)$ are associated Legendre functions of the first and second kinds and are defined here as

$$T_n^m (x) = (-1)^m (1 - x^2)^{\frac{1}{2}m} \frac{d^m}{dx^m} P_n(x) \qquad -1 < x < 1$$

$$P_n^m (x) = (x^2 - 1)^{\frac{1}{2}m} \frac{d^m}{dx^m} P_n (x) \qquad x^2 > 1 \qquad [M8]$$

$$Q_n^m (x) = (-1)^m (x^2 - 1)^{\frac{1}{2}m} \frac{d^m}{dx^m} Q_n (x) \qquad x^2 > 1$$

For the problem of a point source of strength e(t) at the position $(\zeta = \zeta_1, \mu = \mu_1, \omega = o)$ near the ellipsoid $\zeta = \zeta_o$, the potential can be written as

$$\phi = \phi_1 + \phi^*$$

where ϕ_1 is the potential of the point source alone and ϕ^* represents the disturbance potential due to the presence of the rigid ellipsoid. ϕ^* is the potential needed to reduce the velocity of the fluid at the

ellipsoid to zero in the direction of normals to the ellipsoid.

According to [M9] the potential ϕ_1, in the form [M7], is given by

$$\phi_1 = \frac{e}{r'} = \frac{c}{k} \sum_{n=o}^{\infty} (2n+1) \left[Q_n(\zeta)\, P_n(\zeta_1)\, P_n(\mu)\, P_n(\mu_1) + 2 \sum_{m=1}^{n} (-1)^m \left\{ \frac{(n-m)!}{(n+m)!} \right\}^2 Q_n^m(\zeta)\, P_n^m(\zeta_1)\, T_n^m(\mu)\, T_n^m(\mu_1) \cos m\omega \right]$$

for values of $\zeta > \zeta_1$ and

$$\phi_1 = \frac{e}{k} \sum_{n=o}^{\infty} (2n+1) \left[Q_n(\zeta_1)\, P_n(\zeta)\, P_n(\mu)\, P_n(\mu_1) + 2 \sum_{m=1}^{n} (-1)^m \left\{ \frac{(n-m)!}{(n+m)!} \right\}^2 Q_n^m(\zeta_1)\, P_n^m(\zeta)\, T_n^m(\mu)\, T_n^m(\mu_1) \cos m\omega \right] ; \quad \zeta < \zeta_1$$

Since ϕ^* must be continuous and finite everywhere outside the ellipse $\zeta = \zeta_o$ its expansion must be of the form

$$\phi^* = \frac{e}{k} \sum_{n=o}^{\infty} a_n \left[Q_n(\zeta)\, P_n(\mu) + \sum_{m=1}^{n} b_{nm}\, Q_n^m(\zeta)\, T_n^m(\mu) \cos m\omega \right] ; \quad \zeta > \zeta_o$$

where the coefficients a_n, b_{nm} are to be chosen to make

$$u_n = -\frac{\partial \phi}{\partial n} = 0 \qquad \text{on } \zeta = \zeta_o.$$

Since on the ellipsoid $\frac{\partial}{\partial n} \propto \frac{\partial}{\partial \zeta}$, this condition becomes

$$\left(\frac{\partial \phi^*}{\partial \zeta} \right)_{\zeta = \zeta_o} = - \left(\frac{\partial \phi_1}{\partial \zeta} \right)_{\zeta = \zeta_o}$$

so that

$$a_n Q_n'(\zeta_o) = - (2n + 1) Q_n(\zeta_1) P_n'(\zeta_o) P_n(\mu_1)$$

$$a_n b_{nm} Q_n^m{}'(\zeta_o) = - (2n + 1) \cdot 2(-1)^m \left\{\frac{(n - m)!}{(n + m)!}\right\}^2$$

$$Q_n^m(\zeta_1) P_n^m{}'(\zeta_o) T_n^m(\mu_1)$$

(from the orthogonality of the functions $\cos m\omega$ and $T_n^m(\mu)$ over the ranges $(0, 2\pi)$, $(-1, +1)$ respectively).

whence

$$\phi = \phi_1 + \phi^* = \frac{e}{k} \sum_{n=o}^{\infty} (2n + 1) \left[Q_n(\zeta_1) P_n(\mu_1) P_n(\mu) \left\langle P_n(\zeta) - Q_n(\zeta) \frac{P_n'(\zeta_o)}{Q_n'(\zeta_o)} \right\rangle + \right.$$

$$\left. 2 \sum_{m=1}^{n} (-1)^m \left\{\frac{(n - m)!}{(n + m)!}\right\}^2 Q_n^m(\zeta_1) T_n^m(\mu_1) T_n^m(\mu) \left\langle P_n^m(\zeta) - Q_n^m(\zeta) \frac{P_n^m{}'(\zeta_o)}{Q_n^m{}'(\zeta_o)} \right\rangle \cos m\omega \right] \qquad [M9]$$

With the above definitions of P_n^m and Q_n^m the Wronskian relations are

$$P_n^m(\zeta) Q_n^m{}'(\zeta) - P_n^m{}'(\zeta) Q_n^m(\zeta) = \frac{(n + m)!}{(n - m)!} \frac{1}{\zeta^2 - 1}$$

so that on the ellipsoid $\zeta = \zeta_o$ the potential reduces to

$$\phi = \frac{e}{k(\zeta_o^2 - 1)} \sum_{n=o}^{\infty} (2n + 1) \left[P_n(\mu)\, P_n(\mu_1) \frac{Q_n(\zeta_1)}{Q_n'(\zeta_o)} + \right.$$

$$\left. 2 \sum_{m=1}^{n} (-1)^m \frac{(n - m)!}{(n + m)!} T_n^m(\mu)\, T_n^m(\mu_1) \frac{Q_n^m(\zeta_1)}{Q_n^{m\prime}(\zeta_o)} \cos m\omega \right] \qquad [M10]$$

Once again, the inertial pressure in the water is simply $p = \rho\dot{\phi}$ so that, resolving in the direction away from the charge and integrating around the ellipsoid, the force distribution is given by

$$f(x) = \int_o^{2\pi} p\, r\, d\theta \cos\theta = \rho r \int_o^{2\pi} \dot{\phi} \cos\theta \; d\theta \text{ , } r \text{ being the radius}$$

of the ellipsoid at the position x. This gives

$$f(x) = -\frac{2\pi\rho\dot{e}}{k(\zeta_o^2 - 1)} \sum_{n=1}^{\infty} \frac{2n + 1}{n(n + 1)} T_n^1(\mu)\, T_n^1(\mu_1) \frac{Q_n^1(\zeta_1)}{Q_n^{1\prime}(\zeta_o)} \qquad [M11]$$

If the given ellipsoid has semi-major axis a and semi-minor axis b then

$$k = \sqrt{a^2 - b^2} \quad \text{and} \quad \zeta_o = a/k$$

so that

$$\frac{f(x)}{2\pi\rho\dot{e}} = -\sum_{n=1}^{\infty} \frac{(2n + 1)}{n(n + 1)} T_n^1(\mu_1) \left[(1 - \mu^2)^{1/2} T_n^1(\mu) \right]$$

$$\frac{Q_n^1(\zeta_1)}{(\zeta_o^2 - 1)^{1/2} Q_n^{1\prime}(\zeta_o)} \cdot \qquad [M12]$$

Here $\mu = x/a$ and ζ_1, μ_1 are given by

$$c = k (\zeta_1^2 - 1)^{1/2} (1 - \mu_1^2)^{1/2}$$

$$x_1 = k \zeta_1 \mu_1 \cdot$$

A computer routine was written to evaluate this series at a specified set of values of x along the ellipsoid for given values of a, b, c and x_1. The Legendre functions are readily generated from the usual recurrence relation except for the Q's, which have arguments greater than unity. To avoid the divergent solution in this case it is necessary to use the common technique of starting with $Q_n = 0$, $Q_{n-1} = 1$ and working back. This gives a value Q_o^* for Q_o and multiplying all the generated Q's by $\frac{Q_o(\zeta)}{Q_o^*}$ gives the corrected values. Many terms in the series are necessary as the charge approaches the ellipsoid and for a = 10, b = 1, c = 1.5, 150 terms are necessary to achieve reasonable accuracy (0.1%). For a = 10, b = 1, c = 2.5, 50 terms are sufficient.

The results given by the program are compared in Figure M5 with the results produced by both strip theory and by the 3-D flow technique. The strip theory result corresponding to [M12] is

$$\frac{f_{strip}(x)}{2\pi\rho\dot{e}} = \frac{b^2 c\,(1 - \frac{x^2}{a^2})}{\left[c^2 + (x_1 - x)^2\right]^{3/2}} \qquad [M13]$$

The 3-D flow result, in the notation of Section L (equation [L17]) is

$$\frac{\underset{\sim}{f}}{2\pi\rho\dot{e}} = \left[B^* + B\bar{A}^{-1}\right] \underset{\sim}{\dot{u}}_o \qquad [M14]$$

where B^* is the diagonal matrix (b_i^2/ℓ^2) and $\underset{\sim}{\dot{u}}_o$ is given by

$$\dot{u}_{oi} = \tfrac{1}{2} \frac{c\ell^2}{\left[c^2 + (x_i - x_1)^2\right]^{3/2}}$$

The results show that in fact there is little difference between the exact result, strip theory, and the 3-D approximation when the charge is at one end of the ellipsoid, even when it is very close (c/b = 1.5). Strip theory, although slightly less accurate than the 3-D flow approximation near the peak force region is nevertheless quite accurate. The table shows detailed values for the charge directly opposite the end of the ellipsoid. The two 3-D flow sets of values refer to the results given by equation [M14] above firstly with A in place of $\bar{A}$ and secondly direct. Although significant in the vibration case, the correction is everywhere very small for the explosion induced force distribution.

The table also includes values for the case of the charge opposite the centre of the ellipsoid (illustrated in Figure M6). Again strip theory is a very good approximation, even for the very close geometry but, surprisingly, in this case the 3-D approximation is rather less satisfactory, particularly opposite the charge. The difference cannot be attributed to the coarseness of the dipole distribution representation since doubling the number of constant dipole segments (giving forty segments over the ellipsoid length) confirmed the values shown. Considering the closeness of the charge however, even the 3-D flow results are quite reasonable.

The analysis shows that as regards the forcing function the strip theory and the 3-D flow are roughly comparable, strip theory giving better results near the target centre and 3-D flow being slightly better near the target ends. In either case both methods give very reasonable results, particularly since it is not the actual values of force per unit length which are important but integrals of this function along the target length. It is clear from the figures that the inaccuracies in such integrals will be

Values of f/2 à on an Ellipsoid

a = 10 b = 1

	x_i	-9.5	-8.5	-7.5	-6.5	-5.5	-4.5	-3.5	-2.5	-1.5	-0.5	0.5	1.5	2.5	3.5	4.5	5.5	6.5	7.5	8.5	9.5
	b_i	0.3123	0.5268	0.6614	0.7539	0.8352	0.8930	0.9368	0.9683	0.9887	0.9988	0.9988	0.9887	0.9683	0.9368	0.8930	0.8352	0.7599	0.6614	0.5268	0.3123
x_o = 10	Exact	0.0000	0.0001	0.0002	0.0003	0.0004	0.0006	0.0009	0.0011	0.0015	0.0019	0.0024	0.0030	0.0036	0.0045	0.0065	0.0089	0.0124	0.0173	0.0232	0.0261	0.0139
	Strip	0.0000	0.0001	0.0001	0.0003	0.0004	0.0006	0.0008	0.0011	0.0014	0.0019	0.0025	0.0035	0.0047	0.0064	0.0090	0.0127	0.0181	0.0247	0.0279	0.0147
c = 0	1D-1	0.0000	0.0001	0.0002	0.0003	0.0005	0.0007	0.0009	0.0012	0.0016	0.0021	0.0027	0.0037	0.0050	0.0068	0.0093	0.0128	0.0178	0.0235	0.0280	0.0145
	1D-2	0.0000	0.0001	0.0002	0.0003	0.0005	0.0007	0.0009	0.0012	0.0016	0.0021	0.0028	0.0038	0.0050	0.0068	0.0093	0.0129	0.0179	0.0235	0.0258	0.0143
x_o = 10	Exact	0.0000	0.0000	0.0001	0.0002	0.0003	0.0004	0.0005	0.0007	0.0010	0.0013	0.0018	0.0024	0.0033	0.0046	0.0066	0.0098	0.0152	0.0227	0.0356	0.0341
	Strip	0.0000	0.0000	0.0001	0.0001	0.0002	0.0003	0.0005	0.0007	0.0009	0.0012	0.0016	0.0022	0.0031	0.0044	0.0064	0.0095	0.0156	0.0254	0.0436	0.0369
c = 1.5	1D-1	0.0000	0.0001	0.0001	0.0002	0.0003	0.0004	0.0006	0.0008	0.0011	0.0014	0.0019	0.0026	0.0035	0.0049	0.0070	0.0104	0.0161	0.0260	0.0403	0.0350
	1D-2	0.0000	0.0001	0.0001	0.0002	0.0003	0.0004	0.0006	0.0008	0.0011	0.0014	0.0019	0.0026	0.0035	0.0049	0.0071	0.0105	0.0163	0.0263	0.0401	0.0347
x_o =	Exact	0.0003	0.0012	0.0026	0.0050	0.0090	0.0160	0.0285	0.0517	0.0931	0.1465	0.1465	0.0931	0.0517	0.0285	0.0160	0.0090	0.0050	0.0026	0.0012	0.0003
	Strip	0.0002	0.0009	0.0022	0.0047	0.0079	0.0146	0.0275	0.0530	0.0986	0.1504	0.1504	0.0986	0.0530	0.0275	0.0146	0.0079	0.0042	0.0022	0.0009	0.0003
c = 2.5	1D-1	0.0004	0.0013	0.0029	0.0054	0.0096	0.0173	0.0310	0.0554	0.0949	0.1362	0.1362	0.0949	0.0554	0.0310	0.0173	0.0096	0.0053	0.0026	0.0011	0.0004
	1D-2	0.0004	0.0013	0.0029	0.0052	0.0096	0.0171	0.0307	0.0551	0.0947	0.1361	0.1361	0.0947	0.0551	0.0307	0.0171	0.0096	0.0053	0.0026	0.0013	0.0004
o = 0	Exact	0.0002	0.0009	0.0022	0.0047	0.0079	0.0148	0.0285	0.0546	0.1349	0.3528	0.3528	0.1349	0.0566	0.0285	0.0148	0.0079	0.0043	0.0022	0.0009	0.0002
	Strip	0.0001	0.0006	0.0014	0.0029	0.0056	0.0112	0.0238	0.0567	0.1535	0.3785	0.3785	0.1535	0.0567	0.0238	0.0112	0.0056	0.0029	0.0014	0.0006	0.0001
c = 1.5	1D-1	0.0003	0.0011	0.0024	0.0047	0.0088	0.0167	0.0329	0.0694	0.1588	0.3300	0.3300	0.1588	0.0694	0.0329	0.0167	0.0088	0.0047	0.0024	0.0011	0.0003
	1D-2	0.0003	0.0010	0.0022	0.0046	0.0086	0.0164	0.0325	0.0688	0.1582	0.3297	0.3297	0.1582	0.0688	0.0325	0.0164	0.0086	0.0046	0.0023	0.0010	0.0003

even less than in the values of force per unit length.

It may be noticed from Figures M5 and M6, or from Figure M3, that even when the charge is very close the force distribution on the target is spread over a considerable length of the target. This means that the overall forces will only be marginally affected by local distortion of the target and also that even when the charge is very close the loading is never really equivalent to a point load. In terms of the normal modes excited, this wide load region means that the higher modes will be much less important than for a point load.

c. Bernoulli Pressures

The full equation for the pressure in a fluid in unsteady motion is

$$p = p_\infty + \rho \frac{\partial \phi}{\partial t} - \tfrac{1}{2}\rho u^2$$

where p_∞ is the ambient pressure, u the fluid velocity and ϕ the velocity potential. Throughout the theory so far it has been assumed that the inertial pressure $\rho \frac{\partial \phi}{\partial t}$ was much more important than the 'Bernoulli' pressure $\tfrac{1}{2}\rho u^2$. It has long been accepted that this is certainly a reasonable assumption so far as the still water vibration modes are concerned but it has yet to be established for the flow around the bubble. As described earlier the undisturbed flow around the bubble can be represented quite well by the source potential

$$\phi_o = \frac{\dot{V}}{4\pi r}$$

The inertial pressure is therefore

$$p_{inertial} = \rho \dot{\phi}_o = \frac{\ddot{V}}{4\pi r}$$

and the Bernoulli pressure is

$$p_{Bern} = \tfrac{1}{2}\rho u^2 = \tfrac{1}{2}\rho \left(\frac{\dot{V}}{4\pi r^2}\right)^2 = \frac{\rho \dot{V}^2}{32\pi^2 r^4}$$

The ratio of the two pressures is therefore

$$\frac{p_{Bern}}{p_{inert}} = \frac{\dot{V}^2}{8\pi r^3 \ddot{V}} \quad .$$

On using the bubble scaling factors L and T defined in Section H, equation [H5], and the corresponding non-dimensional variables x and τ, this becomes

$$\frac{p_{Bern}}{p_{inert}} = \frac{L^3}{6r^3} \frac{(\dot{x^3})^2}{\ddot{x^3}}$$

Clearly there are times during the bubble motion when $\dot{x^3}$ is almost zero and $\ddot{x^3}$ is large so that the inertial term dominates. Equally there are instants when $\ddot{x^3}$ is zero, and at these $\dot{x^3}$ is obviously a maximum so that the stagnation term dominates. What is important is the relative magnitudes of the maxima of $\dot{x^3}$ and $\ddot{x^3}$ and their durations.

From the bubble equations given in Section H, the volume acceleration will have a short duration but very high maximum at the bubble minimum, and a long duration much lower secondary 'maximum' (a suction) at the bubble maximum. The equations give

$$\ddot{x^3}_{max} = \frac{9}{2} \frac{(\gamma - 1)}{x_m^2} \left[1 - \frac{\gamma}{\gamma - 1} x_m^3\right]$$

so that, at the bubble minimum,

$$\ddot{x}^3 \sim \frac{9}{2} \frac{(\gamma - 1)}{k^2(\gamma - 1)} \sim 200 \quad \text{at moderate depths}$$

and at the bubble maximum,

$$\ddot{x}^3 \sim -\frac{9}{2}\left[1 - (\gamma - \tfrac{2}{3})k\right] \sim -4 \quad \text{at moderate depths.}$$

For $(\dot{x}^3)_{max}$, $\ddot{x}^3$ must be zero and, from equation [H12] this will occur when $x^3 \approx \frac{1}{4}$. Then, from equation [H6],

$$(\dot{x}^3)_{max} \sim 1.75 \quad \text{again at moderate depths.}$$

On using these values it is clear that

$$\left|\frac{p_{Bern}}{p_{inert}}\right| \sim \frac{L^3}{8r^3} \sim \frac{1}{7}\frac{a_m^3}{r^3} \quad \text{where } a_m \text{ is the maximum bubble radius}$$

(normally between 0.9L and 0.94L). Hence, the maximum Bernoulli stagnation pressures are much smaller than the bubble underpressures even at very short range and decrease very rapidly compared to the inertial pressures at all greater ranges. In addition, the duration of the Bernoulli pressures, being related to the period when the bubble volume expansion rate is high, will be much less than that of underpressure phase and so will be of much lesser importance. Compared to the peak bubble overpressures the stagnation pressures are completely negligible. The stagnation pressures can consequently be ignored at all ranges down at least to the range at which the bubble touches the target at its maximum.

References

1. Kline and Clough; "Dynamic Response of a Ship's Hull as Influenced by Proportions, Arrangement, Loading and Structural Stiffness", Paper read at Spring Meeting of SNAME in Montreal on 23-26 July 1967.

2. Porter; "Pressure Distributions, Added Mass and Damping Coefficients of Cylinders in a Free Surface", Univ of California Inst Eng Res, Series 82, Issue 16, July 1960.

3. Choung Mook Lee; "The Second Order Theory of Cylinders Oscillating Vertically in a Free Surface", Jn Ship Research, Vol 12, No 4, December 1968.

4. Kumai, T; "Influence of the Virtual Inertia of Vibrating Bottom Panels on the Hull Natural Frequencies", Reports of Research Inst for App Mech, Kyushu Univ, Vol XVII, No 58, 1969.

5. Savic, P; "Behaviour of an Underwater Explosion Bubble Near an Infinitely Long Rigid Circular Cylinder", Admiralty Undex Works Report No AUW/TRI.14/RP20, 1944.

6. Murray, W W; "Interaction of a Spherical Acoustic Wave with a Beam of Circular Cross Section", UERD Report 1-55 (1955).

7. Watson, G N; "A Treatise on the Theory of Bessel Functions", Cambridge Univ Press (1944).

8. Fraenkel, L E; "Incompressible Flow Past Quasi-Cylindrical Bodies and Some associated Problems", Quart Jn Mech & App Math, Vol XI, p212 (1958).

9. MacRobert, T M; "Spherical Harmonics", Methven & Co Ltd, London, 1947.

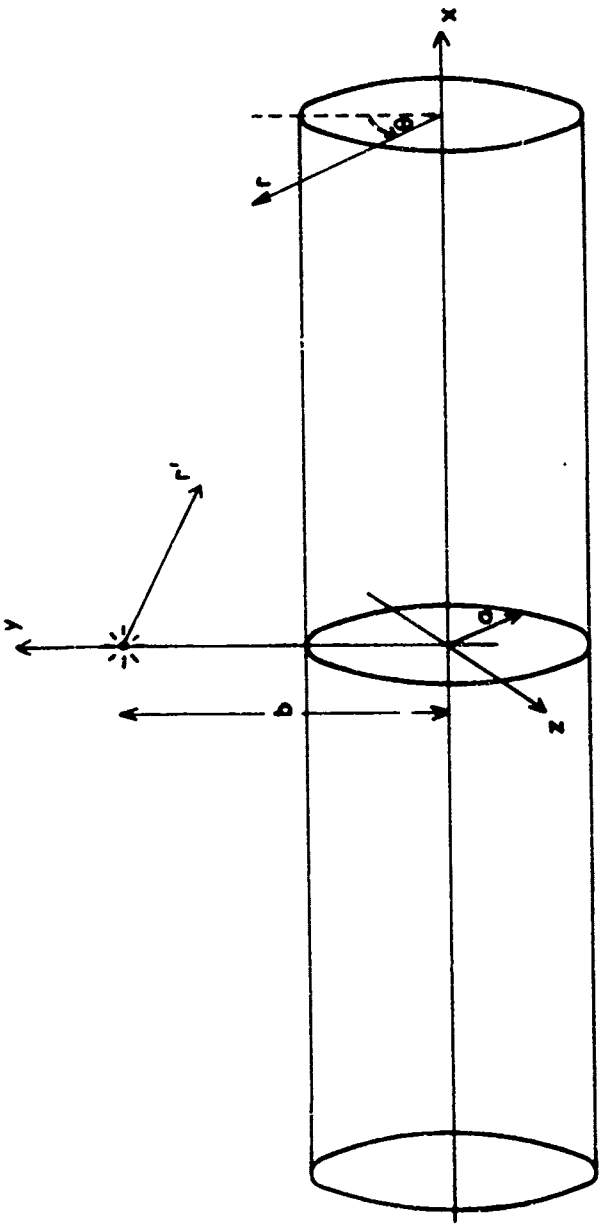

GEOMETRY FOR A POINT SOURCE NEAR A CIRCULAR CYLINDER

FIGURE M1

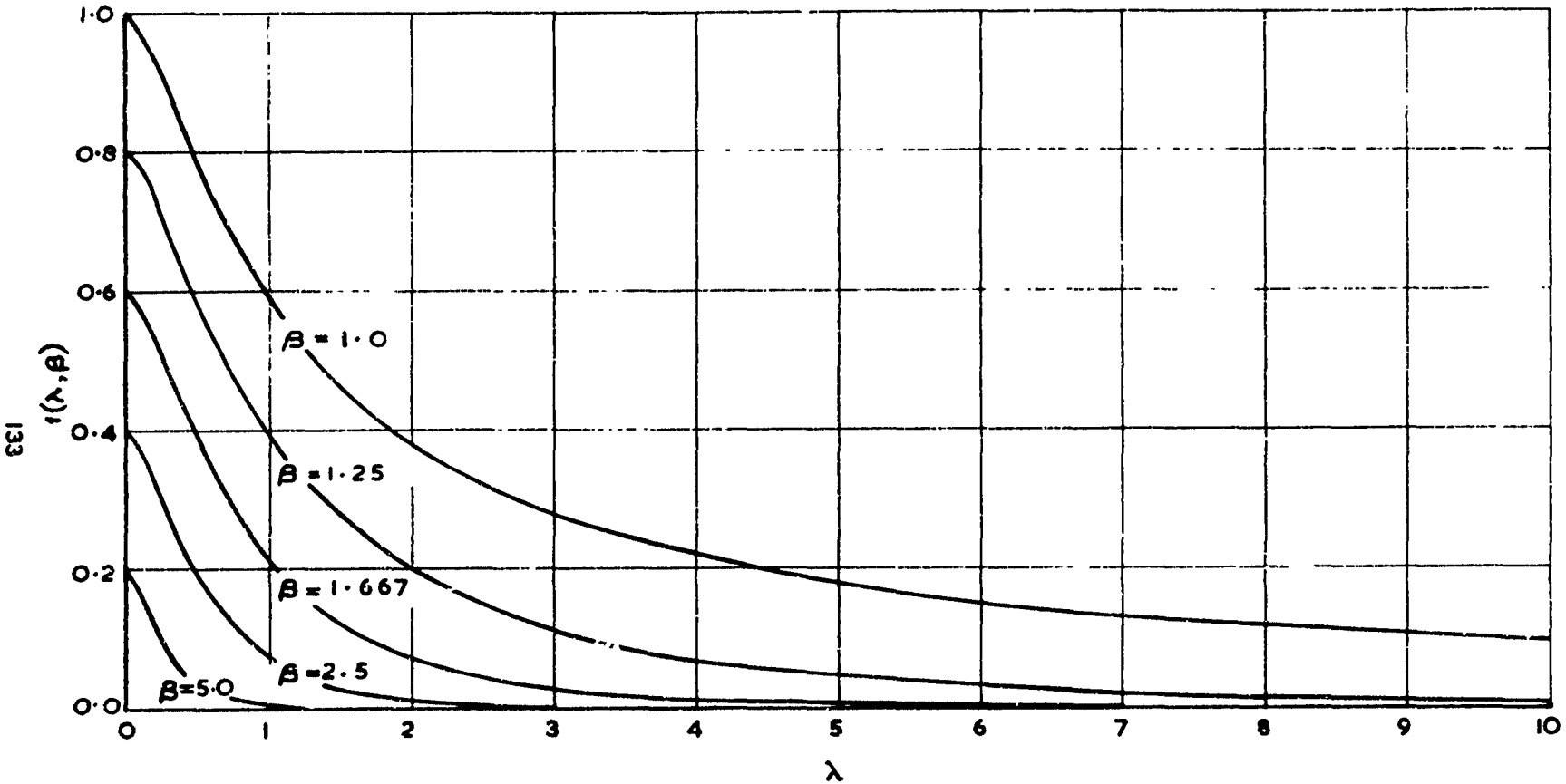

CURVES OF THE FUNCTION $f(\lambda,\beta) = -K_1(\beta\lambda)/\lambda K_1'(\lambda)$

FIGURE M2

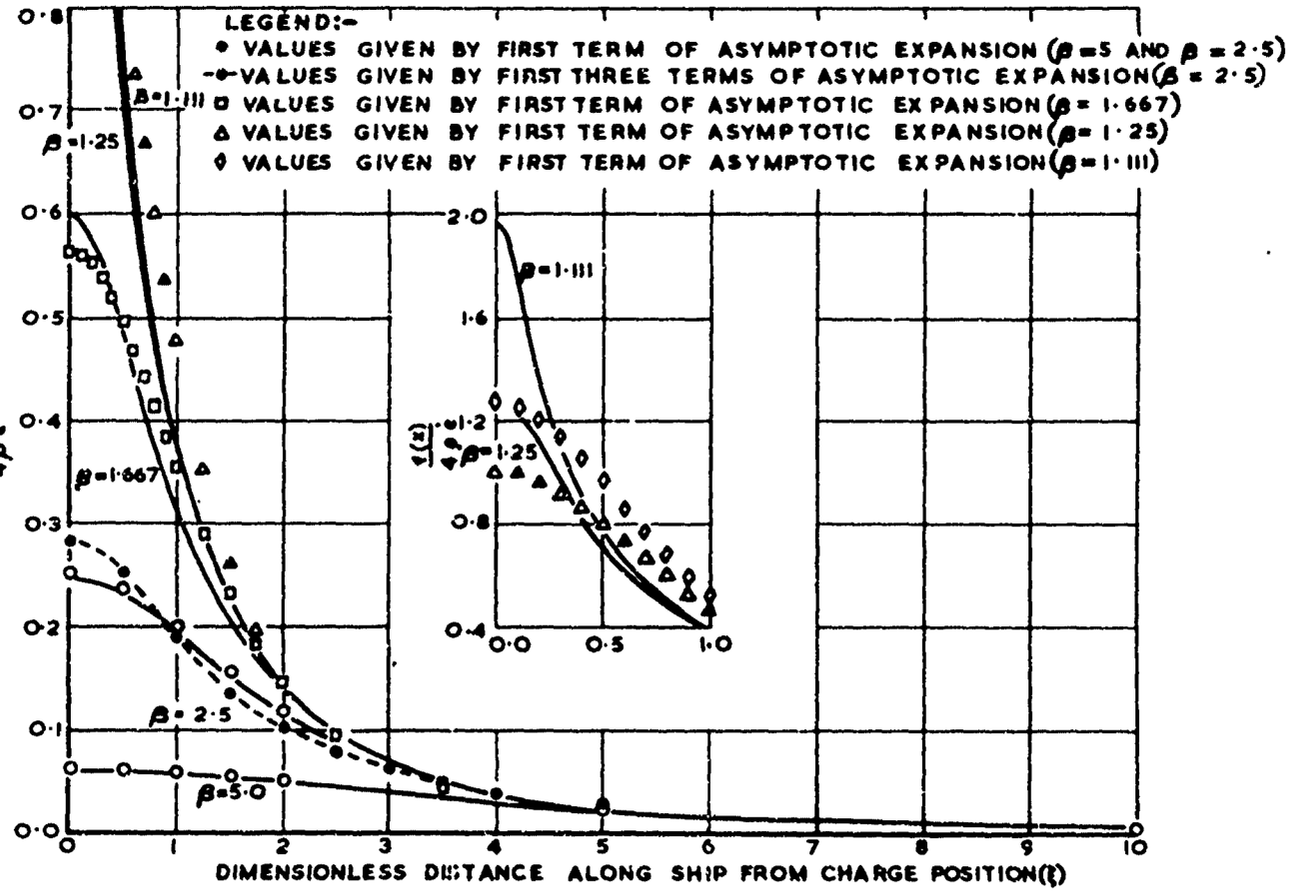

EXACT AND ASYMPTOTIC FORCE DISTRIBUTIONS ALONG THE CYLINDER

FIGURE M3

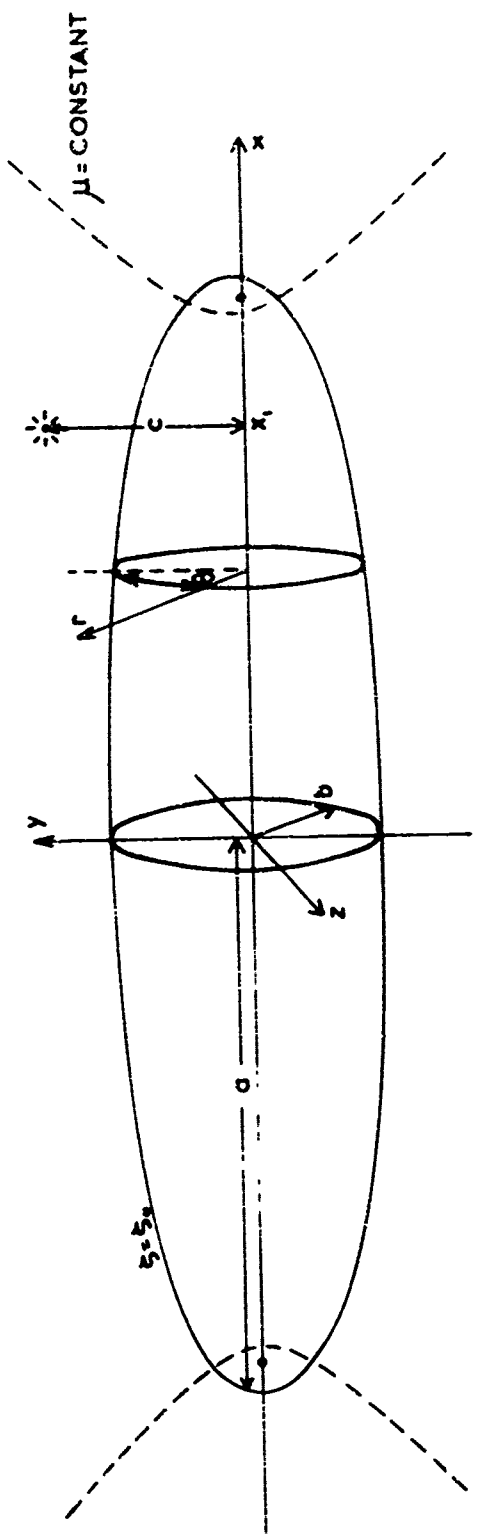

GEOMETRY FOR A POINT SOURCE NEAR AN ELLIPSOID

FIGURE M4

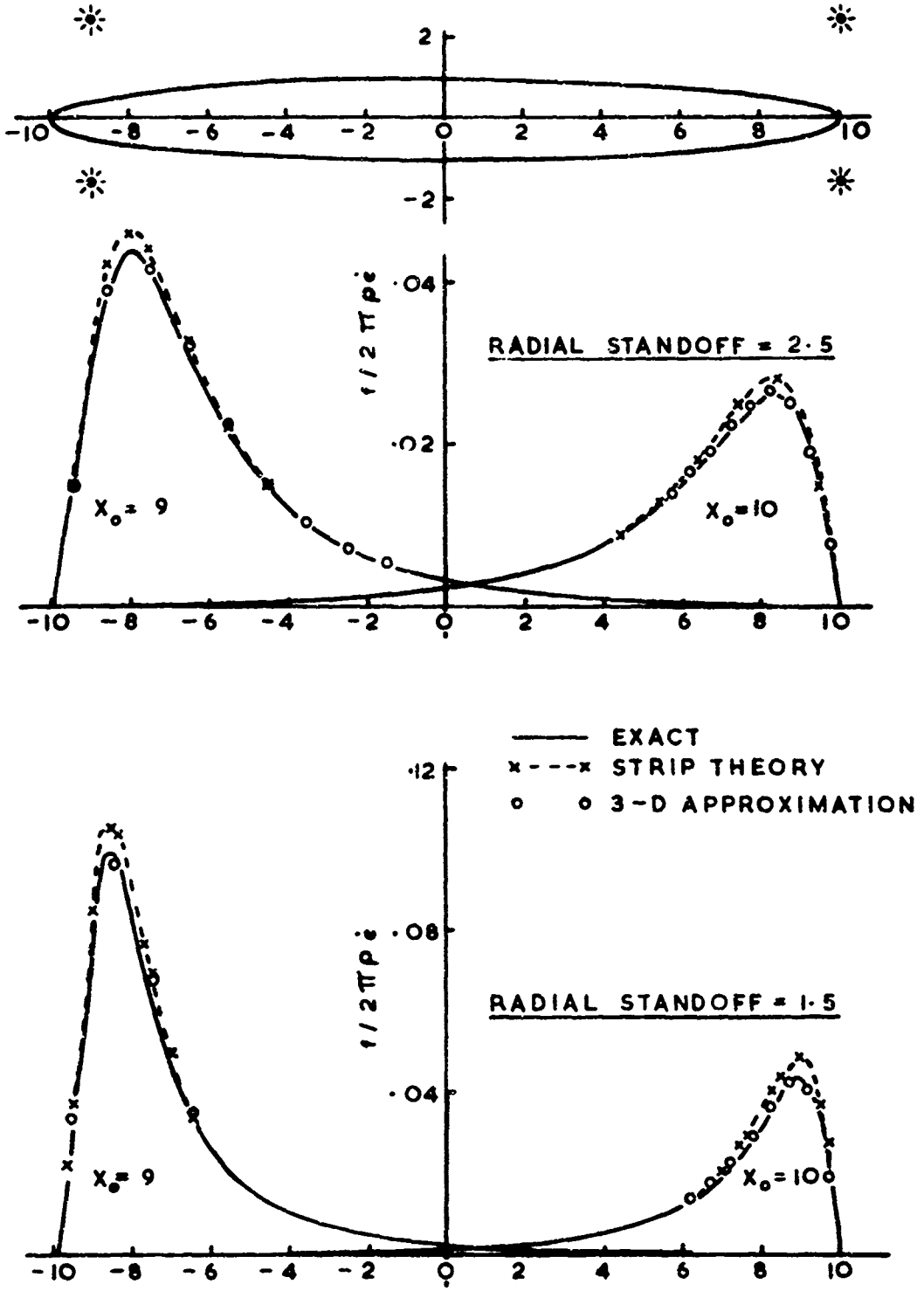

FORCE DISTRIBUTIONS ON ELLIPSOID

CHARGE NEAR ENDS

FIGURE M5

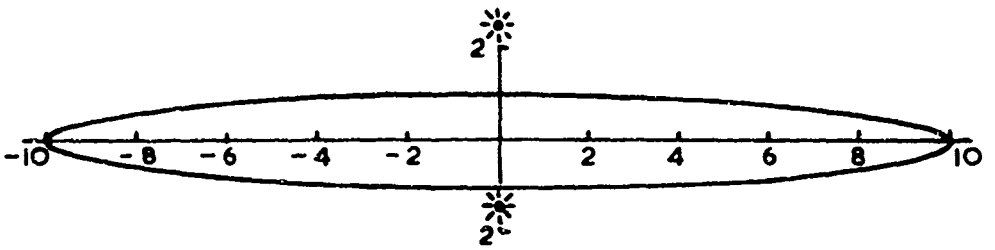

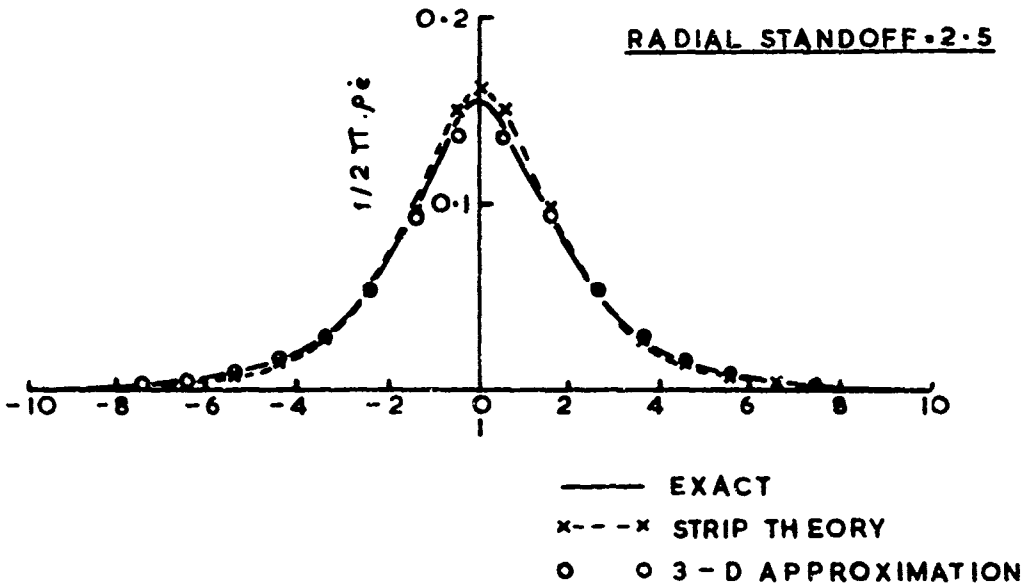

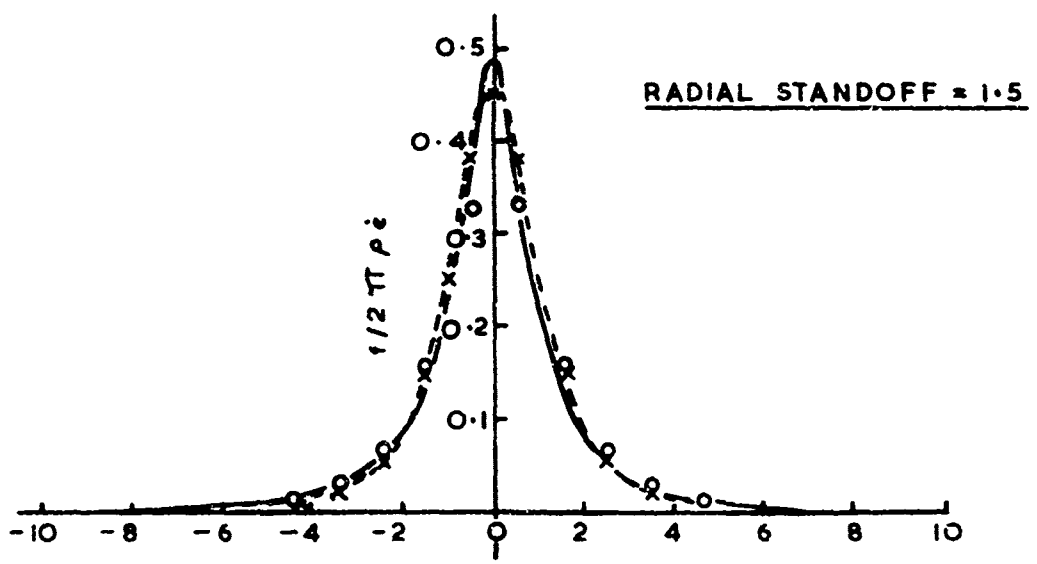

FORCE DISTRIBUTIONS ON ELLIPSOID

CHARGE AT CENTRE

FIGURE M6

N Modification of the Forcing Function Due to Local Damage

The discussion in Section M showed that the forcing functions described in Section H, based on the 'distant flow' approximation, are valid down to very short ranges. The discussions however assumed throughout that the target remained sensibly rigid. Since, particularly at short ranges, the magnitudesof possible relative displacements of the target cross-sections are small compared to the fluid particle displacements, the rigid cross-section assumption should be valid unless very severe damage occurs. The type of severe damage which would most dramatically change the fluid flow fields is hull rupture since the presence of a hole, at a constant, sensibly zero pressure, will divert part of the flow into the hole instead of out around the target.

An approximation to the local flow near such a hole is obtained by considering the flow due to a point source on the axis of a circular hole in a flat plate. This problem has been considered by Haywood [N1], using the oblate ellipsoidal coordinates (ζ,ξ,ω) shown in Figure N1. These coordinates are related to the cylindrical coordinates also shown by the equations

$$r = a(1 + \zeta^2)^{\frac{1}{2}}(1 - \xi^2)^{\frac{1}{2}}$$

$$x = a\zeta\xi$$

$$\theta = \omega$$

The surfaces ζ = const form a family of confocal oblate ellipsoids and the surfaces ξ = const form the orthogonal family of confocal hyperboloids of one sheet. The hole, of radius a, is the surface $\zeta = 0$. The plate around it is the surface $\xi = 0$. The axis through the centre of the hole is the line $\xi = 1$ (a degenerate hyperboloid).

Haywood found that the velocity potential for the flow produced by a source of strength e at a distance x_o from the centre of the hole (which is assumed to be a surface at constant zero potential) can be written

$$\phi = \frac{e}{R_1} - \frac{e}{R_2} - \frac{2e}{i\pi}\{F(\zeta, \xi) + F(\zeta, -\xi)\} \qquad (N1)$$

where R_1 and R_2 are the distances from the source and its image respectively. The function $F(\zeta, \xi)$ is given by

$$F(\zeta, \xi) = \tfrac{1}{2}\int_{i}^{-i} (\zeta - t)^{-1} \left[(\zeta_o - t\xi)^2 + (1 + t^2)(1 - \xi^2)\right]^{-\frac{1}{2}} dt \qquad (N2)$$

the source being at the point ($\zeta_o = x_o/a$, $\xi = 1$). The first two terms in equation (N1) give the usual potential for a source near a free surface. The third term represents the disturbance in the flow due to presence of the plate, which acts as a baffle.

The integral (N2) can be written

$$F(\zeta, \xi) = \frac{1}{2R_1}\left[\sinh^{-1}(\alpha_1 - i\beta_1) + \sinh^{-1}(-\alpha_1 - i\beta_1)\right]$$

$$F(\zeta, -\xi) = -\frac{1}{2R_2}\left[\sinh^{-1}(\alpha_2 - i\beta_2) + \sinh^{-1}(-\alpha_2 - i\beta_2)\right] \qquad (N3)$$

where $\alpha_1 = \dfrac{(\zeta\zeta_o + \xi)(\zeta_o - \xi\zeta)}{(1+\zeta^2)(1 + \zeta_o^2)^{\frac{1}{2}}(1 - \xi^2)^{\frac{1}{2}}}$;

$$\beta_1 = \frac{(\zeta_o - \xi\zeta)^2 + (1 + \zeta^2)(1 - \xi^2)}{(1 + \zeta^2)(1 + \zeta_o^2)^{\frac{1}{2}}(1 - \xi^2)^{\frac{1}{2}}}$$

$$\alpha_2 = \frac{(\zeta\zeta_0 - \xi)(\zeta_0 + \xi\zeta)}{(1+\zeta^2)(1+\zeta_0^2)^{\frac{1}{2}}(1-\xi^2)^{\frac{1}{2}}} \; ;$$

$$\beta_2 = \frac{(\zeta_0 + \xi\zeta)^2 + (1+\zeta^2)(1-\xi^2)}{(1+\zeta^2)(1+\zeta_0^2)^{\frac{1}{2}}(1-\xi^2)^{\frac{1}{2}}} \qquad \text{(N4)}$$

If $\sinh^{-1}(\alpha - i\beta)$ is written in the form $\gamma + i\delta$, then γ and δ are given by

$$2\sinh^2\gamma = \left[(1-\alpha^2-\beta^2)^2 + 4\alpha^2\right]^{\frac{1}{2}} - (1-\alpha^2-\beta^2)$$

$$\text{and} \quad 2\sin^2\delta = (1+\alpha^2+\beta^2)^2 - \left[(1+\alpha^2+\beta^2)^2 - 4\beta^2\right]^{\frac{1}{2}} \qquad \text{(N5)}$$

where positive values are to be taken for the square roots. Clearly both γ and δ are multi-valued; both being indeterminate in sign and δ also being indeterminate to a multiple of π. The correct values to be used must be selected to ensure that ϕ is continuous within the fluid. From (N5), γ changes sign only when $\alpha = 0$ so that the real parts of $\sinh^{-1}(\alpha - i\beta)$ and $\sinh^{-1}(-\alpha - i\beta)$ are equal and opposite and $F(\zeta, \xi)$ and $F(\zeta, -\xi)$ are both purely imaginary. The potential ϕ is therefore real as required. Similarly, δ can only change sign when $\beta = 0$ and, since β is always > 0, cannot change sign. It is therefore restricted to the range $0 < \delta < \pi$. This leaves open which of the ranges $(0, \pi/2)$ and $(\pi/2, \pi)$ δ occupies. It is clear from (N5) that δ can change from one of these ranges to the other only when $\alpha = 0$ and then only if $\beta > 1$. For $F(\zeta, \xi)$, $\alpha_1 = 0$ when $\xi = \zeta_0/\zeta$ and then $\beta_1 = \dfrac{|\zeta^2 - \zeta_0^2|^{\frac{1}{2}}}{\zeta(1+\zeta_0^2)^{\frac{1}{2}}}$ and so is always < 1. δ_1 will

therefore be confined to the range $(0, \pi/2)$. For $F(\zeta, -\xi)$, $\alpha_2 = 0$

when $\xi = \zeta\zeta_0$ and then $\beta_2 = \dfrac{(\zeta_0^2 + 1)^{\frac{1}{2}}}{(1 - \xi^2)^{\frac{1}{2}}}$ which is always > 1.

Consequently δ_2 changes from one of the ranges $(0, \pi/2)$ and $(\pi/2, \pi)$ to the other when α_2 changes sign. Since ϕ must be zero for $\zeta = 0$, the range $(0, \pi/2)$ corresponds to $\alpha < 0$.

These results may be summarised by

$$\phi = \frac{e}{R_1} - \frac{e}{R_2} - \frac{2e}{\pi}\left[\frac{\delta_1}{R_1} - \frac{\delta_2}{R_2}\right] \qquad (N6)$$

where δ_1 and δ_2 are the positive angles given by equations (N4) and (N5), with δ_1 in the range $(0, \pi/2)$ and δ_2 in the range $(0, \pi/2)$ or $(\pi/2, \pi)$ according as α_2 is less than or greater than zero. A simple verification is provided by two special cases:-

(i) $a \to \infty$ (so that there is no plate, only a source near a free surface).

Then, for moderate values of x_0, x and r

$$\alpha_1 \to \frac{\xi(x_0 - x)}{r} \; ; \quad \beta_1 \to \frac{(x_0 - x)^2 + r^2}{ar} \to 0$$

and so $\delta_1 \to 0$. Also,

$$\alpha_2 \to -\frac{\xi(x_0 + x)}{r} \; ; \; \beta_2 \to \frac{(x_0 + x)^2 + r^2}{ar} \to 0$$

so that δ_2 tends to either 0 or π. Since $\alpha_2 < 0$, $\delta_2 \to 0$

and $\phi \to \dfrac{e}{R_1} - \dfrac{e}{R_2}$

which is the usual potential for a source near a free surface.

(ii) $a \to 0$ (so that there is no hole in the plate).

Then $\alpha_1 \to \frac{x_o - x}{r}$; $\beta_1 \to 0$

$\alpha_2 \to \frac{x_o + x}{r}$; $\beta_2 \to 0$

and again $\delta_1 \to 0$. This time since $\alpha_2 > 0$, $\delta_2 \to \pi$ and the potential ϕ has the limiting value

$$\phi \to \frac{e}{R_1} - \frac{e}{R_2} - \frac{2e}{\pi}\left[0 - \frac{\pi}{R_2}\right] = \frac{e}{R_1} + \frac{e}{R_2}$$

which again is the correct potential for a source near a rigid plate.

Neglecting the Bernoulli pressures (in keeping with the previous approximations) the pressure on the plate is given by

$$p = \rho\dot{\phi}_{\xi=0} = -\frac{2\dot{e}\rho}{\pi}\left[\frac{\delta_1}{R_1} - \frac{\pi - \delta_1}{R_1}\right] = \frac{2\rho\dot{e}}{R_1}\left[1 - \frac{2\delta_1}{\pi}\right] \qquad (N7)$$

since $\alpha_2 > 0$ for $\xi = 0$.

If there were no hole in the plate, δ_1 would be zero and the pressure on the plate would be simply

$$p = \frac{2\rho\dot{e}}{R_1} .$$

The effect of the hole is consequently to reduce the pressures by the factor $(1 - \frac{2\delta_1}{\pi})$ from the value for the plate without a hole.

Figure N2 shows the values of $p(r)/2\rho\dot{e}$ for several values of x_o/a.

For large values of r, the factor $(1 - \frac{2\delta_1}{\pi})$ rapidly approaches its asymptotic value

$$R_\infty = 1 - \frac{2}{\pi} \tan^{-1} \left(\frac{a}{x_o}\right) \qquad \text{(N8)}$$

so that, except very close to the hole, the pressures everywhere are given by

$$p = p_o R_\infty$$

where p_o is the pressure ignoring the hole. This approximation provides a very reasonable method for allowing for the effect of the hole. All forces on the target are calculated as though the forcing function were reduced in strength by the factor R_∞.

The factor R_∞ has a simple physical interpretation. The amount of fluid flowing through the hole per unit time may be shown by integration across the hole to be given by $8 \epsilon p a \tan^{-1} (a/x_o)$. Since the total mass of fluid flowing from the source per unit time is $4\pi\rho\epsilon$ the fraction of this which enters the hole is

$$\frac{2}{\pi} \tan^{-1} \left(\frac{a}{x_o}\right)$$

and the remaining fraction of fluid, which avoids the hole, is simply R_∞. The source and hole together consequently appear, at a distance, as a source of reduced strength ϵR_∞. Figure N3 shows the variation of R_∞ with the ratio x_o/a.

This approximation should be quite reasonable when the charge is close to the target but as the charge standoff is increased the curvature of the cylinder will begin to affect the quantity of water which is deflected through the hole. It will become easier for the fluid to flow around the cylinder. In consequence less water will be lost through the hole and the factor R will become slightly larger than for the corresponding standoff from a flat plate. The magnitude of this effect is readily estimated. The new value of R must obviously be less than the value which would pertain if there were no plate at all to deflect flow into the hole, just a hole in the fluid. This extremely artificial case can be solved fairly easily. Bryant [N2] determined the potential due to a point source on the axis of a rigid circular disc to be

$$\phi_1(r) = \frac{e}{(r^2 + x_o^2)^{\frac{1}{2}}} \left[1 + \frac{2}{\pi} \cot^{-1} \left(\frac{x_o^2 + r^2}{a^2 - r^2} \right)^{\frac{1}{2}} \right] ; \quad r < a \qquad (N9)$$

on the surface of the disc facing the source. In the problem to be solved, the same boundary condition over the rear of the disc applies, ie $\frac{\partial \phi}{\partial n} = 0$, but over the front face the condition should now be $\phi = 0$. The potential for this problem may be found from Bryant's by adding a 'disturbance' potential ϕ_2 given by

$$\phi_2 = e \sum_{n=o}^{\infty} a_n Q_n (i\zeta) P_n (\xi) \qquad (N10)$$

where the coefficients a_n are chosen to satisfy

$\phi_2 = - \phi_1$ for the front face of the disc

and (N11)

$$\frac{\partial \phi_2}{\partial n} = 0 \quad \text{on the rear face.}$$

This mixed type of boundary condition is difficult to satisfy exactly but if the series for ϕ_2 is assumed to be convergent then the first few coefficients can be found approximately by simply satisfying the appropriate boundary conditions at an arbitrary set of collocation points. From the nature of the problem it is likely that these collocation points would be best chosen as the zero's of an appropriate Tschebyscheff polynomial. However, for simplicity a set of equally spaced points was in fact used. The condition on the front face was satisfied at n internal points and also at the rim of the hole. The condition on the rear face was satisfied at n internal points. A short computer program was used to solve for the first $(2n+1)$ coefficients in the series. The coefficients were determined for several values of n and their values were found to be rather slowly convergent but the value of the first coefficient, a_o had settled to under 0.25% variation for n = 10, ie for a 21 term approximation to the solution.

With the coefficients in (N10) known the quantity of fluid flowing into the hole is most easily found by considering the flow at very large distances from the origin. Then the ellipsoids ζ = const are very nearly spheres of radius $a\zeta$ so that the outward flow across such a surface per unit time, due to the disturbance potential ϕ_2, is approximately

$$4\pi (a\zeta)^2 u_\zeta = - 4\pi (a\zeta)^2 \cdot \frac{1}{a} \frac{\partial \phi_2}{\partial \zeta} = - 4\pi a e i \sum_{n=o}^{\infty} a_n \zeta^2 Q_n'(i\zeta) P_n(\xi).$$

Now, for large ζ, $Q_n(i\zeta) \simeq \frac{n!}{1.3.5....(2n+1)} \zeta^{-(n-1)} + O(\zeta^{-(n+3)})$

(reference N3, art 106), so that in the limit as $\zeta \to \infty$, $\zeta^2 Q_n' \to 0$

for all $n \geq 1$ and the outflow at ∞ is simply

$$4\pi a e i a_0$$

The outflow due to the original potential ϕ_1 is the source outflow $4\pi e$ so that $-4\pi a e i a_0$ represents the decrease in outflow due to the hole. The reduction coefficient in this case is then simply

$$R = 1 + iaa_0$$

This function is compared with R_∞ in Figure N3. For very small values of x_0/a the source sees only the hole, not the plate or fluid surrounding it and so R and R_∞ are identical. As x_0 increases the effect of the difference becomes apparent but is always relatively small. Since R is an upper limit for the true reduction coefficient, which would be expected to be much closer to R_∞ than to R, use of R_∞ for cylinders seems completely justified.

References

N1* Haywood, J H; "The Importance of the Surrounding Baffle on Afterflow Reloading of Target Plates", NCRE Report R359. (1956).

N2 Bryant, A R; "The Pressures Exerted by an Underwater Explosion Bubble on a Circular Target Plate in a Disc-like Baffle", Proc Phys Soc of London, Vol XI p341 (1945).

N3 Lamb, H; "Hydrodynamics", Cambridge Univ Press, 1932 (Sixth Edition).

*"This report is not necessarily available to members of the public or to commercial organisations".

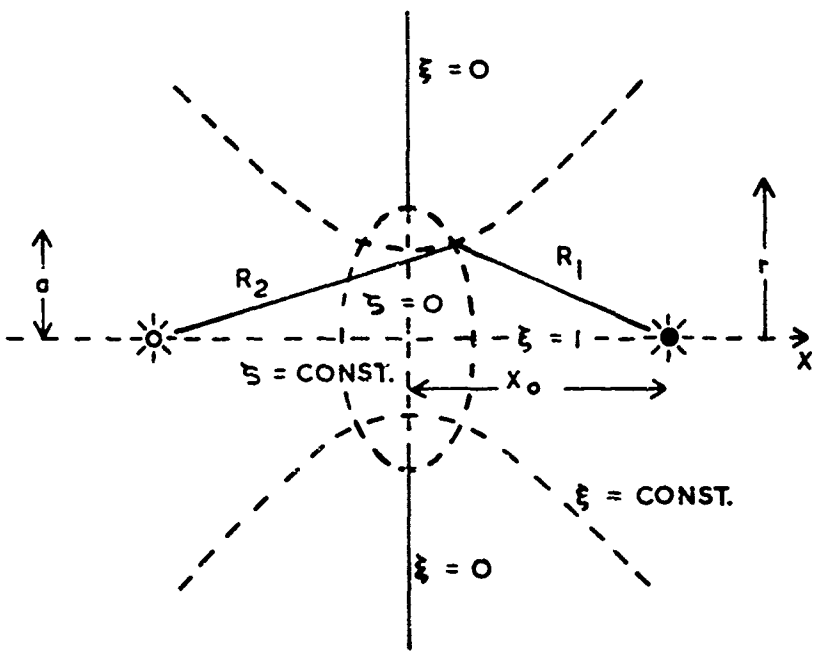

GEOMETRY FOR A SOURCE NEAR A HOLE IN A PLATE

FIGURE N1

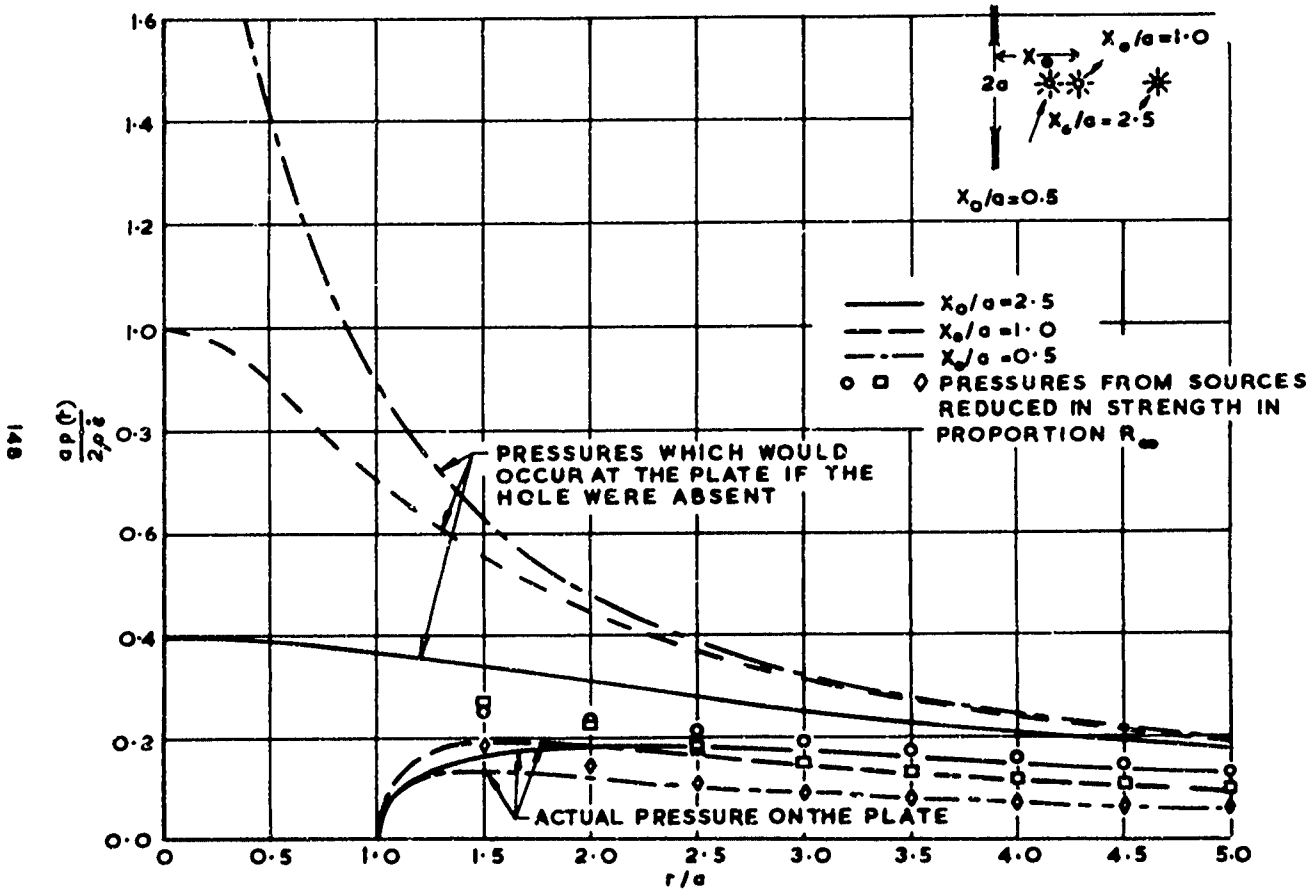

PRESSURE DISTRIBUTION FROM A POINT SOURCE NEAR AN INFINITE PLATE WITH A HOLE

FIGURE N2

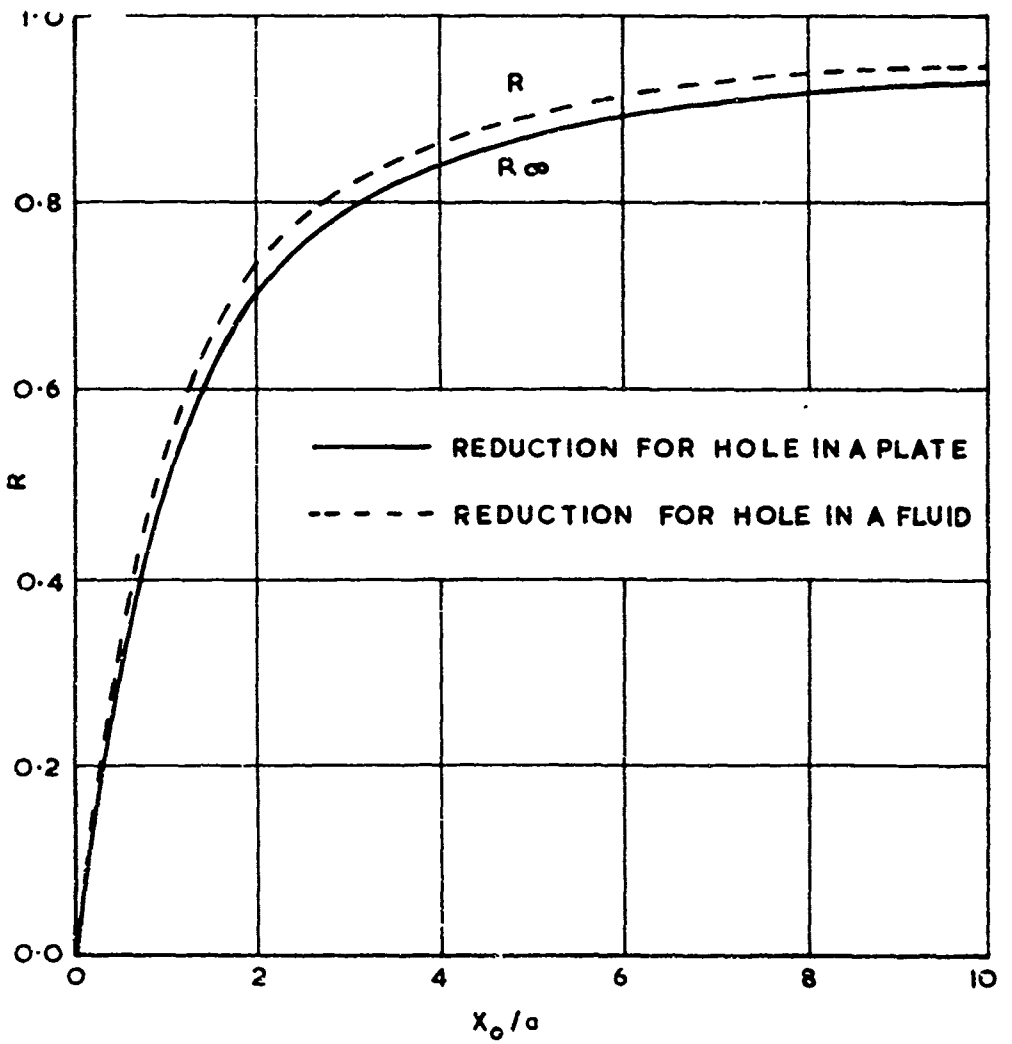

ASYMPTOTIC REDUCTION FACTOR AS A FUNCTION OF STANDOFF/HOLE RADIUS RATIO

FIGURE N3

0 The Effect of Bubble Migration

Throughout the entire discussion so far on the limitations of the theory it has been assumed that the bubble remained fixed in space throughout its pulsations. For small charges of the type used in Chertock's experiments this is a reasonable assumption since, except in special circumstances (eg an underpressure tank), the pressure difference across the bubble is small compared to the absolute hydrostatic pressure. For larger charges, of the sizes likely to affect ships, the pressure differences will be very much larger but the hydrostatic pressure will not change greatly. For example, consider the model in Chertock's experiments. It was 10 ft long and the maximum bubble radius was about 6 ins when the charge was suspended 16 ins beneath the water surface. On full scale the target might be 40 times as big so that a scaled bubble would have a 20 ft radius and its centre would be 50 ft beneath the surface. In the model case the ratio of (pressure difference between the bubble top and bottom) over (pressure at bubble centre) is

$$\left(\frac{\Delta p}{p}\right)_{\text{model}} = \frac{1.0 \text{ ft}}{33 \text{ ft} + 1.3 \text{ ft}} = 0.031$$

where atmospheric pressure is equivalent to a 33 ft head of water

On full scale the comparable ratio is

$$\left(\frac{\Delta p}{p}\right)_{\text{full scale}} = \frac{40}{33 + 50} = 0.48$$

Clearly in this case the relative buoyancy forces acting on the bubble will be sixteen times greater than on the small scale and migration will be more important.

The mechanism of bubble migration is very well understood (reference 01). During the early expansion very little migration occurs since the bubble is small and the hydrostatic force on it (its displacement) is similarly small. During its underpressure phase, when it is large, the buoyancy force is very large but so is the effective mass of the bubble; although the gas within the bubble has a negligible mass compared with the mass of water displaced by it, the added mass associated with the flow of water around the bubble is not negligible - for a spherical bubble it is half the mass of the displaced water. In consequence the bubble accelerates upwards but does not have time to achieve a significant displacement or velocity before the bubble contraction occurs. It does however have time to acquire a considerable momentum (actually contained in the water around it). During the contraction phase the mass of water displaced is reduced to a very small fraction of maximum displacement and the added mass is naturally similarly reduced. Since the momentum acquired during the underpressure phase is still associated with the bubble the reduction in added mass implies an equivalent increase in vertical velocity and the bubble shoots upwards when near its minimum. During this phase it distorts greatly, the bottom surface inverts and forms a jet which penetrates through the bubble, producing a toroidal shape. During re-expansion the bubble regains an approximately spherical shape and its velocity falls as its added mass rises. Thus the bubble is almost stationary during the phase when the vertical forces on it are large, but migrates rapidly later when the vertical forces are least. During the rapid migration phase, since the vertical force is small the momentum is almost constant so that the product of bubble volume and vertical velocity is almost constant.

The main and most obvious effect of migration is to bring the point of emission of the first bubble pulse much nearer to the surface of the water. Since this pulse, as discussed earlier, can be almost twice as effective as the initial expansion, this can considerably affect the motion of a target above the bubble. There are however other effects. The peak pressure during the bubble pulse is well known to be considerably reduced by vigorous migration (reference 01). The reduction in pressure however is accompanied by an increase in duration so that the impulse is less affected. In addition, the motion of the bubble causes a dipole pressure field around it in addition to the usual radial field. This dipole field was first investigated by Taylor [02] who showed how very intense it can be, although of course it decays much more rapidly with distance from the bubble than the radial field and is seldom observed in pressure gauge measurements.

Another effect due to gravity is distortion of the bubble from its spherical form. Such deviations have been the subject of a number of studies, eg [03] and [04], but in the main these have been based on perturbation techniques and have only applied to the early bubble deformations. Quite recently, purely numerical techniques have been used to describe the flow around pulsating bubbles, particularly around collapsing cavitation bubbles. These have shown clearly [05] the sort of distortions suffered by a bubble collapsing in an external pressure gradient, although in the case of [05] the gradient was due to the presence of a rigid wall rather than a gravity field. These distortions are related to multipole terms in the flow field of higher order than dipole. These higher order terms decay with distance even more rapidly than the dipole terms and so are neglected here. The distortions lead to drastic changes in the

motion of the bubble during the collapse phase when near the minimum and a significant redistribution of energy occurs at this time. Since such effects cannot at present be treated analytically, they are allowed for here only on an empirical basis.

With the geometry of Figure 01, assuming first that the explosion is deep so that the effect of the water surface can be neglected, the velocity potential for the migrating bubble will be approximately

$$\phi = \frac{e_1}{r_1} + \frac{e_2}{r_1^2} \cos\theta_1 \ . \qquad (01)$$

While the bubble is spherical this will represent the motion exactly but late during the bubble collapse phase, when it begins to distort, higher order terms will also be present. Since these will affect the flow only very close to the bubble surface they are neglected and equation (01) is assumed to apply throughout the motion, the bubble being assumed to remain spherical at all times. The strengths e_1 and e_2 are then readily found to be related to the bubble volume V(t) and velocity v(t) by

$$e_1 = \dot{V}/4\pi \quad \text{and} \quad e_2 = \frac{3Vv}{8\pi} \qquad (02)$$

From equation (01) the vertical velocity due to the pulsating migrating bubble is

$$u_y = -\frac{\partial\phi}{\partial y} = \frac{e_1}{r_1^3}(y + D) - \frac{e_2}{r_1^3}\left[1 - \frac{3(y + D)^2}{r_1^2}\right] \qquad (03)$$

Since the bubble is rising with velocity v, the vertical acceleration $\dot{u}_y$ is given by

$$\dot{u}_y = \frac{\partial u_y}{\partial t} - v\frac{\partial u_y}{\partial y} = \frac{\dot{e}_1 (y + D)}{r_1^3} - \frac{\dot{e}_2}{r_1^3}\left[1 - \frac{3(y + D)^2}{r_1^2}\right] -$$

$$v\left\{\frac{e_1}{r_1^3}\left[1 - \frac{3(y + D)^2}{r_1^2}\right] + \frac{3e_2}{r_1^5}(y + D)\left[3 -\right.\right.$$

$$\left.\left.\frac{5(y + D)^2}{r_1^2}\right]\right\} \qquad (04)$$

The nature of the four terms is easily seen by substituting the expressions (02) for e_1 and e_2. The first term, proportional to $\dot{e}_1$ is therefore proportional to the bubble volume acceleration, $\ddot{V}$, and so in principle is the same as for the non-migrating bubble (although the value of $\ddot{V}$ will be changed). The second term is proportional to $\frac{d}{dt}(Vv)$. Now the mass of the bubble itself is negligible compared to the added mass of the water moving around it, which for a spherical bubble is just one half the displaced water mass. The quantity Vv is therefore proportional to the momentum associated with the moving bubble and the term $\dot{e}_2$ is consequently proportional to the rate of change of bubble momentum, and so also to the force acting on the bubble. This force is simply the bucyancy force due to the gravity induced pressure gradient in the water, ie ρVg. The second term is therefore proportional to the bubble volume. It will be negligible in the early expansion and again later near the bubble minimum. It will be greatest during the long expansion phase. The third term is proportional to $e_1 v \propto \dot{V}v$ and will therefore be greatest when $\dot{V}$ and v are both

large, ie late in the collapse phase and again early in the subsequent re-expansion. It will be very small during the under-pressure phase since then both $\dot{V}$ and v are very small, and will also be small at the bubble minimum since $\dot{V}$ is zero then. The fourth term is proportional to $e_2 v \propto V v^2 \propto m^2/V$ where m is the vertical momentum of the bubble. It will consequently be largest at the bubble minimum.

On assuming that the bubble remains spherical, the kinetic energy equation given in section H, when applied to the moving bubble, becomes

$$E_c = 2\pi\rho a^3 \dot{a}^2 + \frac{4}{3}\pi\rho a^3 gZ + \frac{k_1}{\gamma - 1} \frac{V^\gamma}{\left(\frac{4\pi}{3}\right)^{\gamma-1} a^{3(\gamma-1)}} + \frac{1}{3}\pi\rho a^3 v^2 \qquad (05a)$$

Equating the buoyancy force to the rate of change of momentum gives the migration equation

$$\frac{d}{dt}\left\{\frac{2}{3}\pi\rho a^3 v\right\} = \frac{4}{3}\pi\rho a^3 g \qquad (05b)$$

In terms of the non-dimensional variables x and τ defined in section H, and with $Z/L = \zeta$, these equations become

$$\dot{x}^2 + \dot{\zeta}^2/6 + \zeta/\zeta_0 = \left[1 - k/x^{3(\gamma-1)}\right]/x^3$$

$$\frac{d}{dt}(x^3 \dot{\zeta}) = -3x^3/\zeta_0 \qquad (06)$$

and the four terms in the expression (04) for the fluid acceleration may be re-written (for the surface y = 0)

$$f_1 = \frac{\dot{e}_1 d}{r_1^3} = \frac{4}{9}\zeta_o \frac{\delta}{\rho^3} \ddot{x}^3 \; ; \; r_1/L = \rho \; , \; d/L = \delta$$

$$f_2 = \frac{\dot{e}_2}{r_1^3}\left(1 - \frac{3d^2}{r_1^2}\right) = -2\left(1 - \frac{3\delta^2}{\rho^2}\right)\frac{\dot{x}^3}{\rho^3}$$

$$f_3 = -\frac{e_1 v}{r_1^3}\left(1 - \frac{3d^2}{r_1^2}\right) = \frac{4}{9}\zeta_o\left(1 - \frac{3\delta^2}{\rho^2}\right)\frac{\dot{x}^3\dot{\zeta}}{\rho^3} \qquad (07)$$

$$f_4 = -\frac{3e_2 vd}{r_1^5}\left(3 - \frac{5d^2}{r_1^2}\right) = -2\zeta_o\left(3 - \frac{5\delta^2}{\rho^2}\right)\frac{\delta \dot{x}^3 \zeta^2}{\rho^5}$$

In each of these terms the acceleration is measured in units of g, the acceleration of gravity. The expressions (07) have all been multiplied by the factor 2 to allow for usual doubling effect of the free surface. Since, for rapid motions where surface waves can be neglected, the boundary condition to be satisfied is $\phi = 0$, the condition is satisfied by a negative image above the surface which produces the assumed enhanced acceleration.

The Free Surface Effect

The free surface is well known to affect not only the accelerations near it but also the motion of the bubble itself if it is within a few bubble maximum radii. The velocity potential in such cases is given approximately by

$$\phi = \frac{e_1}{r} + \frac{e_2}{r_1^2}\cos\theta_1 - \frac{e_1}{r_2} + \frac{e_2}{r_2^2}\cos\theta_2 \qquad (08)$$

for the geometry of Figure 01. In this case, as Taylor showed, the source and dipole strengths are, to order (a^2/d^2),

$$e_1 = a^2\dot{a} \quad ; \quad e_2 = \frac{a^3}{2}\left(v - \frac{a^2\dot{a}}{4d^2}\right)$$

The kinetic energy of the flow, to the same order, is

$$T = 2\pi\rho a^3 \dot{a}^2\left(1 - \frac{a}{2d}\right) + \frac{\pi}{3}\rho a^3 v^2 - \frac{\pi}{2}\rho a^3 \dot{a}v\left(\frac{a^2}{d^2}\right)$$

and the energy equation becomes

$$E_o = 2\pi\rho a^3 a^2\left(1 - \frac{a}{2d}\right) + \frac{\pi}{3}\rho a^3\dot{Z}^2 + \frac{\pi}{2}\rho a^3 a\ddot{Z}\frac{a^2}{d^2} + \frac{4}{3}\pi\rho a^3 gZ +$$

$$\frac{4}{3}\frac{\pi a^3 p}{\gamma - 1} \qquad (09)$$

where p is the pressure within the bubble.

The migration equation may in this case be derived from the Lagrangian form of the equations of motion, ie

$$\frac{d}{dt}\left\{\frac{\partial}{\partial\dot{Z}}(T - V)\right\} = \frac{\partial}{\partial Z}(T - V)$$

In terms of the previous non-dimensional variables the resulting equations are

$$x^3\dot{x}^2\left(1 - \frac{x}{2\delta}\right) + \frac{1}{6}x^3\dot{\zeta}^2 + \frac{1}{4}x^3\dot{x}\dot{\zeta}\left(\frac{x^2}{\delta 2}\right) + x^3\zeta/\zeta_o +$$

$$\frac{k}{x^{3(\gamma-1)}} = 0 \qquad (010)$$

$$\frac{d}{d\tau}\left[\frac{1}{3}x^3\dot{\zeta}\right] = -\frac{3}{4}\frac{x^4\dot{x}^2}{\delta^2} - \frac{x^5\ddot{x}}{4\delta^2} - \frac{x^3}{\zeta_o}$$

Since $Z = d + h$, h being the static head of water equivalent to atmospheric pressure, $\delta = \zeta - \zeta_1$ where $\zeta_1 = h/L$. For computational purposes these equations are best reduced to the equivalent set of first order equations

$$\dot{x} = \sigma$$

$$\dot{\zeta} = \lambda$$

$$\dot{\sigma} = -3\left\{\frac{\sigma^2}{x}\left(1 - \frac{2\beta x}{3\delta}\right) - \frac{\lambda^2}{6x} + \frac{\zeta}{x\zeta_0} - \frac{(\gamma - 1)k}{x^{3\gamma+1}} + \right.$$

$$\left. \frac{\beta x}{4\delta^2}\left(\frac{\sigma\lambda}{3} - \frac{x}{\zeta_0}\right)^2\right/2\left(1 - \frac{\beta x}{2\delta}\right)\right\}$$

$$\dot{\lambda} = -3\alpha\left[\frac{1}{\zeta_0} + \frac{\sigma\lambda}{3} + \frac{\beta x}{4\delta^2}\left(3\sigma^2 + x\dot{\sigma}\right)\right] \qquad (011)$$

where two parameters α and β have been introduced to enable the same equations to cover three distinct cases of idealised bubble motion. The appropriate values for α and β are

α	β	Type of Motion
0	0	Non-migrating
1	0	Migrating
1	1	Migrating near a free surface

The appropriate initial conditions are those used earlier in the non-migrating case, ie

$$x = k^{4/3}\left[1 + \frac{4k^4}{3}\right]$$

$$\zeta = \zeta_0$$

$$\sigma = 0$$

$$\lambda = 0$$

As with the earlier equations the factor $\left(1 + \frac{4k^4}{3}\right)$, although very close to unity in value, is vital to the successful integration of the equations. A computer program to integrate these equations has been written, using a standard Runge-Kutta integration routine to integrate the first order differential equations (011). Because the variables change very rapidly near the bubble minima, but are relatively static during the underpressure phase, a constant time increment in the integration routine is very inefficient and the program has been written to select its own step length.

Corresponding to the use of equations (011) for the bubble behaviour, the four component accelerations at the free surface become

$$f_1 = \frac{4}{9}\zeta_o \frac{\delta}{\rho^3}\ \ddot{x}^3$$

$$f_2 = -\frac{2a}{\rho^3}\left(1 - \frac{3\delta^2}{\rho^2}\right)\ x^3\left[1 + \frac{\beta\zeta_o \ddot{x}^3}{18\delta^2}\right]$$

$$f_3 = \frac{4}{9}\ \frac{\zeta_o}{\rho^3}\left(1 - \frac{3\delta^2}{\rho^2}\right)\dot{x}^3\,\lambda \qquad (012)$$

$$f_4 = -2\,\zeta_o \frac{\delta}{\rho^5}\ \left(3 - \frac{5\delta^2}{\rho^2}\right)\ x^3\,\lambda\left(\lambda + \frac{\beta\dot{x}^3}{12\delta^2}\right)$$

Figure 02 shows the bubble motion and the surface accelerations above the bubble for a typical large explosion bubble. The figure compares the non-migrating results with those given by equations (06) and (07) for the migrating case and with the results from (011) and (012) for the same case with surface effects included. In the figure only the results prior to the bubble minimum are given for

the migrating cases since the bubble equations break down at the minimum due to proximity to the free surface. The necessity of allowing both for migration and for the free surface is clear.

Inclusion of a Drag Term

In all the above equations the accelerations depend directly on the migration velocities of the bubble, as deduced from ideal flow around a spherical bubble. It is well known however, eg [06], that such migrations are considerably larger than the measured values and the surface acceleration deduced from them will be correspondingly in error. Since it is impractical to attempt to describe the full, distorting flow around the bubble except by very extensive numerical methods it is necessary to introduce an empirical correction to the migration equations.

The most obvious such correction would be to give the parameter α introduced into equation (011) a suitable value less than unity. Unfortunately this simple technique, through equations (012) would affect the f_2 component of the acceleration. This component is a maximum when the bubble itself is a maximum and is scarcely moving, ie when the ideal flow conditions are most nearly satisfied and it would be expected that the component f_2 should be most accurate. Also, it would affect small weakly migrating bubbles relatively as much as large strongly migrating ones since a reduction in the value of α is equivalent to a reduction in the buoyancy force acting on the bubble. What is required is an effect which is principally apparent when the bubble is migrating most rapidly. This suggests a turbulent wake type of drag force of the form

$$F = C_D \left(\tfrac{1}{2} \rho v^2 A\right)$$

where A is the bubble cross-sectional area transverse to the motion and C_D is a drag coefficient. If the bubble were a solid sphere such a drag term would certainly exist as a typical bubble from a large explosion could easily be 5 ft in radius when near its minimum and moving at up to 200 ft/sec. The Reynolds number for such a motion is of the order of 10^8. Since the actual bubble is a surface of constant pressure, the mechanism of wake formation is not so obvious as for a solid body but some such force seems likely. A correct physical picture is not however required of an empirical correction. It is sufficient that the assumed force should lead to realistic results.

Assuming the existence of a force of the above type, the motion of the bubble will be expending energy at the rate

$$-\frac{dE}{dt} = Fv = \frac{\pi}{2}\rho C_D a^2 v^3 = -\frac{\pi}{2}\rho C_D a^2 \dot{Z}^3$$

Similarly momentum is being lost to the wake at the rate F

$$\text{ie } \frac{\pi}{2}\rho C_D a^2 v^2 = \frac{\pi}{2}\rho C_D a^2 \dot{Z}^2$$

Although the Lagrangian derivation of the bubble motion equations is no longer available, the simpler type of 'derivation' due to Taylor leads to the equations

$$\frac{d}{d\tau}\left[x^3 \dot{x}^2\left(1 - \frac{\beta x}{2\delta}\right) + \frac{1}{6}x^3\zeta^2 + \frac{\beta}{4}x^3 \dot{x}\dot{\zeta}\left(\frac{x^2}{\delta^2}\right) + \right.$$

$$\left.\frac{x^3\zeta}{\zeta_o} + \frac{k}{x^{3(\gamma-1)}}\right] = \frac{C_D}{4}x^2\dot{\zeta}^3$$

$$\frac{d}{d\tau}\left(\frac{1}{3}x^3\dot{\zeta}\right) = -\alpha\left[\frac{x^3}{\zeta_o} + \beta\left(\frac{3}{4}\frac{x^4\dot{x}^2}{\delta^2} + \frac{x^5\ddot{x}}{4\delta^2}\right)\right] + \frac{C_D}{4}x^2\zeta^2$$

These equations are equivalent to the first order equations

$$\dot{x} = \sigma$$

$$\zeta = \lambda$$

$$\dot{\sigma} = -3\left[\frac{\sigma^2}{x}\left(1 - \frac{2\beta x}{3\delta}\right) - \frac{\lambda^2}{6x} + \frac{\zeta}{x\zeta_o} - \frac{(\gamma-1)k}{x^{3\gamma+1}} + \right.$$

$$\left.\frac{\beta x}{4\delta^2}\left(\frac{C_D\lambda^2}{4} + \frac{\sigma\lambda}{3} - \frac{x}{\zeta_o}\right)\right] \Big/ 2\left(1 - \frac{\beta x}{2\delta}\right)$$

$$\dot{\lambda} = -3\alpha\left[\frac{1}{\zeta_o} + \frac{\sigma\lambda}{x} - \frac{C_D}{4}\frac{\lambda^2}{x} + \frac{\beta x}{4\delta^2}(3\sigma^2 + x\dot{\sigma})\right]$$

The corresponding component accelerations at the free surface become

$$f_1 = \frac{4}{9}\zeta_o\frac{\delta}{\rho^3}\ddot{x^3}$$

$$f_2 = -\frac{2\alpha}{\rho^3}\left(1 - \frac{3\delta^2}{\rho^2}\right)\left(1 + \frac{\beta\zeta_o\ddot{x^3}}{18\delta^2} - \frac{\zeta_o C_D}{4}\frac{\lambda^2}{x}\right)x^3$$

$$f_3 = \frac{4}{9}\zeta_o\frac{1}{\rho^3}\left(1 - \frac{3\delta^2}{\rho^2}\right)\dot{x^3}\lambda \qquad (014)$$

$$f_4 = -2\zeta_o\frac{\delta}{\rho^5}\left(3 - \frac{5\delta^2}{\rho^2}\right)x^3\lambda\left(\lambda + \frac{\beta\dot{x^3}}{12\delta^2}\right)$$

The computer program for the bubble motion, which was described earlier, in fact integrates equations (013) (all the previous cases can be obtained from (013) using suitable values for α, β and C_D). A series of calculations were carried out for a 500 lb charge of TNT at a depth of 150 ft using a series of values for C_D. The results are summarised in the Table.

Migration Variables for Different Drag Coefficients for a 500 lb Charge at 150 Ft

Drag Coefficient C_D	Migration to First Pulse (ft)	$\frac{p_1}{p_1^{(o)}}$	$\frac{\text{Edissipated}}{E_o}$
0.00	16.9	0.47	0.00
0.50	15.0	0.37	0.19
1.00	13.3	0.40	0.22
1.50	12.3	0.46	0.19
2.00	11.3	0.52	0.15
2.25	10.9	0.56	0.12
Experimental Result	11.0	0.63	0.15

In the table p_1 is any pressure which would be measured at large standoff and $p_1^{(o)}$ is the pressure which would be measured at the same point if the bubble did not migrate. In the near field the pressures will be affected by the dipole field but at large distances only the radial field will be felt and the ratio $\frac{p_1}{p_1^{(o)}}$ tends quite rapidly to a limiting value. The experimental value for p_1 is subject to considerable scatter. The 'experimental' value for $p_1^{(o)}$ is estimated from the empirical formula for bubble pulse pressures. The table shows that for this particular charge

size and depth the value $C_D = 2.25$ makes both the migration and the ratio $\frac{p_1}{p_{1(o)}}$ approximately correct.

The large value of C_D precludes its direct physical identification with a normal wake-type drag coefficient since its value would normally be fairly close to unity. However, for the strongly migrating bubbles for which the value was derived the bubble would have flattened considerably near the minimum (as is observed on small scale) so that the area to which C_D is related would actually have been rather larger than assumed. Had a more realistic value for the area been used a lower more realistic value of C_D would have resulted. However, a complete physical picture is not required here, just a simple mechanism for producing the correct bubble migrations.

One of the equations from which the bubble motion equations were derived was the energy balance equation. The addition of the drag term implies that the bubble loses energy continually throughout the motion. Most of this energy loss naturally occurs at the bubble minimum when the velocity is very high. It is well known that the period of a pulsating bubble is quite a good measure of the bubble energy and this fact has long been used to measure the bubble energy. By comparing the periods of the first and second bubble pulsations estimates have been made of the total energy loss which occurs at the bubble minimum (reference [06]). The energy still retained by the bubble at its minimum was calculated for the cases given in the table and the energy dissipated up to this time, as a fraction of the original energy, has been added to the table.

The experimental value for the energy loss for this charge size and depth is 40% of the original bubble energy, of which 10% is estimated to be due to acoustic radiation (neglected in this analysis). - If it is assumed that roughly half the remaining dissipation occurs before the minimum, this gives the 15%, quoted in the table, for the experimental dissipation. The value $C_D = 2.25$ therefore gives about the right total energy dissipation. It is of interest that the value $C_D = 1.00$ corresponds to a maximum in the energy dissipated.

One significant point regarding the energy loss is that although for very weakly migrating bubbles an energy dissipation mechanism is quite clear, the same is not true of strongly migrating bubbles. For small bubbles, or very deep ones, which do not migrate significantly, the bubble surface remains fairly spherical until late in the collapse phase when the bubble pressure rises above the ambient level and starts to decelerate the bubble surface. The acceleration then being directed from the less dense fluid to the more dense one, causes the usual Taylor surface instability to occur. High speed films show that the instability occurs as a very large number of needle like jets being projected into the bubble. Due to its adiabatic compression the gas will be very hot at this time and such an intense spray of cold water will remove much energy. For strongly migrating bubbles this form of instability does not seem to occur. An overall distortion, first into an oblate spheroid, occurs instead and later the bottom inverts and penetrates through the bubble turning it into a toroid. Since intimate mixing of the gas and water no longer occurs an alternative mechanism is required to account for the observation that migrating bubbles dissipate as much energy as non-migrating ones. The 'wake' theory provides such a dissipation

mechanism. The energy is not so much dissipated as transferred to water which loses its association with the bubble. The mechanism assumes that both momentum and energy are transferred to water behind the bubble, principally when the bubble is small and its velocity great. As the bubble begins to re-expand and slow down, it has no way of stopping the narrow following wake which could penetrate it and form a vertical water jet. The large plumes which are so evident on the surface above an explosion are known to originate at the bubble pulses and are perhaps due to such jets.

One important result of the transfer of energy and momentum to the 'wake' of the bubble is that the bubble motion is no longer symmetrical about the minimum. Figure 03 shows the displacement time history calculated for the bubble centre for the 500 lb charge at 50 ft, with $C_D = 2.25$. The bubble appears to come to a rather abrupt halt shortly after the minimum. Although this sort of motion was not described in early photographic studies of bubble motion, the actual motion of the bubble 'centre' in such studies is very difficult to measure because of the drastic shape changes which are occurring. Such behaviour has however been reported in some recent studies [07].

To further confirm the usefulness of the modified migration equations, they were integrated for several other charge depths. The results are summarized in the following table.

Charge Depth (ft)	Migration (ft)		Migration / Max Bub. Radius		$\frac{p_1}{p_1(0)}$	
	Calc	Meas	Calc	Meas	Calc	Meas
50	26.9	24.2	1.15	1.06	0.18	0.15
100	15.7	15.1	0.80	0.78	0.40	0.33
150	10.9	11.0	0.62	0.63	0.56	0.63
450	3.2	4.2	0.26	0.32	0.92	0.97

Again the agreement is very reasonable. The underestimation of the migration for the deep case is to be expected since little overall bubble distortion will occur in this case and the value of C_D will accordingly be too high.

Effect of Migration on Whipping Response

As the modified equations seem to give results in reasonable accord with measured results for the migration and the far field pressures, they are adopted here to show the sort of differences in whipping response to be expected for migrating bubbles. Figure 04 shows the surface accelerations near a 500lb charge of TNT at 50 ft depth and shows a considerable change in the bubble pulse. Directly over the charge the peak acceleration at the pulse is slightly reduced but the duration of the positive phase is greatly increased. To the side the shape becomes more similar to the non-migrating pulse shape (although still of increased duration) but the peak acceleration is much reduced. Apart from the slight change in the phasing of the bubble pulse relative to the ship motion, the only significant change in the forcing function is in the bubble pulse. Since the positive phase of this is still much shorter than the basic ship period it can be considered impulsive. The bubble pulse impulse and also the initial expansion impulse for both a 100lb and the 500lb charge have

been calculated for a large selection of depths and horizontal standoffs. The resulting impulses have been normalised to an arbitrary impulse and the resulting relative impulse contours are shown in Figures 05 and 06. In comparing the initial impulses with the bubble pulse impulses it should be remembered that for a non-migrating bubble with no energy losses the latter impulse is exactly twice the former. At shallow depths the bubble equations break down and the position of the contours shown by the dashed line is conjecture only.

The figures show clearly that over a considerable depth range the bubble impulse is greatly enhanced by migration effects: for example at a depth of 45 ft the bubble pulse gives over seven times the impulse due to the initial expansion. At 50 ft the ratio drops to 3 to 1. At points not directly above the charge the enhancement is much reduced and can fall well below the factor 2 expected for a non-migrating bubble. For the more strongly migrating 500lb charge the maximum horizontal standoffs at which given impulse levels are reached during the initial expansion and during the bubble pulse are almost the same. For the 100lb charge migration effects are clearly of much less importance.

The extent to which the enhancements in the bubble pulse impulse are due to its increased duration is emphasised in Figures 07 and 08 which show the relative peak accelerations during the initial expansion and the bubble pulse. Only for a very small depth range, and only directly over the charge, are the peak accelerations increased by migration. At all other points there is a reduction in peak acceleration.

The impulses illustrated in Figures 05 and 06 are not directly related to the total impulse on the ship. At any point on the ship axis the impulse per unit length of ship will be proportional to the

impulses shown, the constant of proportionality being the sum of the displacement and added mass (again per unit length) at the point concerned. The overall effect on the ship will be an integral of these impulses along the ship. The contours do however give some idea of the importance of including migration.

Bubble Jets

As discussed earlier, much of the momentum and energy lost by a migrating bubble during the bubble pulse will simply have been transferred to a column of water which then will travel on upward, initially at a speed close to the maximum bubble vertical velocity. For charges directly beneath a ship such jets will presumably transfer much of their momentum to the ship. Unfortunately the nature of such jets, their length, diameter and transmission characteristics, is presently unknown. Only one study of any kind seems to have been made (reference 07) and that only considers the pressure pulse emitted by the jet at its moment of creation. The pressure pulse analysis is rather dubious and since it does not consider the subsequent motion of the jet through the water the work is unsuitable for quantifying the jet effect.

Since the motion of small scale bubbles in underpressure tanks is known to closely resemble that of full scale bubbles (except for the periods when internal bubble pressure is important), the nature and motion of any jets could probably be investigated quite effectively in such tanks. The problem is not pursued in this thesis.

References

01 Cole, R H; "Underwater Explosions", Princeton Univ Press, 1948

02 Taylor, G I; "Vertical Motion of a Spherical Bubble and the Pressure Surrounding It", Underwater Explosion Research, Vol II, "The Gas Globe", O N R (1950)

03 Penney, W G; and Price, A T "On the Changing Form of a Nearly Spherical Submarine Bubble", Underwater Explosion Research, Vol II, "The Gas Globe" O N R (1950)

04 Kolodner, I I; and Keller J B "Underwater Explosion Bubbles II. The Effect of Gravity and the Change of Shape", New York Univ Rep IMM-NYU 197 (1953)

05 Plesset, M S; and Chapman, R B "Collapse of an Initially Spherical Vapour Cavity in the Neighbourhood of a Solid Boundary", Cal Inst of Tech Rep No 85-49 (1970)

06 Snay, H G; "Underwater Explosion Phenomena: the Parameters of Migrating Bubbles", NAVORD Report 4185 (1962)

07 Farley, T E; and Snay, H G "A Simplified Analysis of the Bubble Jet Pulse", NOLTR 68-42 (1968)

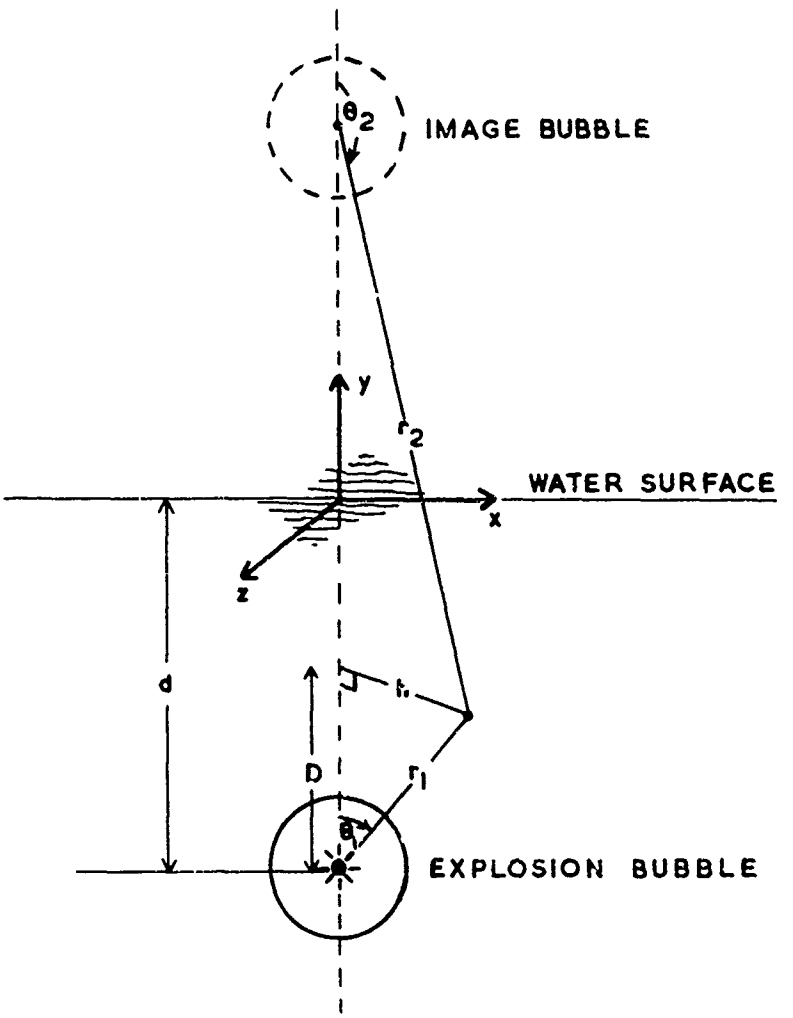

GEOMETRY FOR MIGRATING BUBBLE EQUATIONS

FIGURE 01

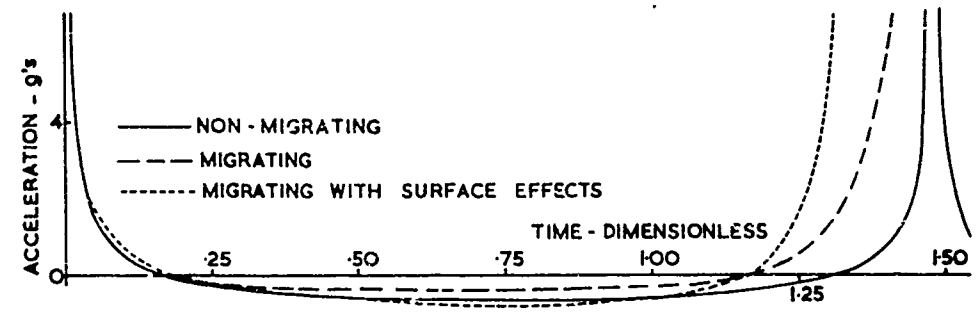

TOTAL SURFACE ACCELERATION ABOVE BUBBLE

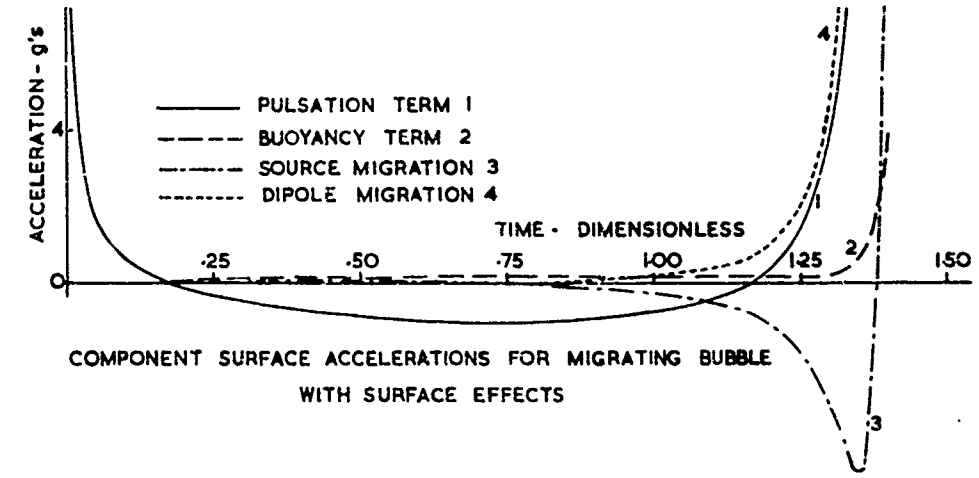

COMPONENT SURFACE ACCELERATIONS FOR MIGRATING BUBBLE WITH SURFACE EFFECTS

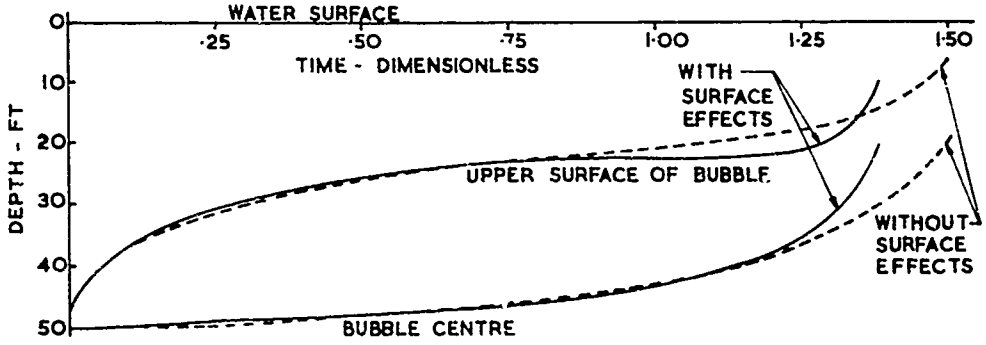

BUBBLE MOTION - MIGRATING WITH SURFACE EFFECTS INCLUDED

THE EFFECTS OF BUBBLE MIGRATION

FIGURE 02

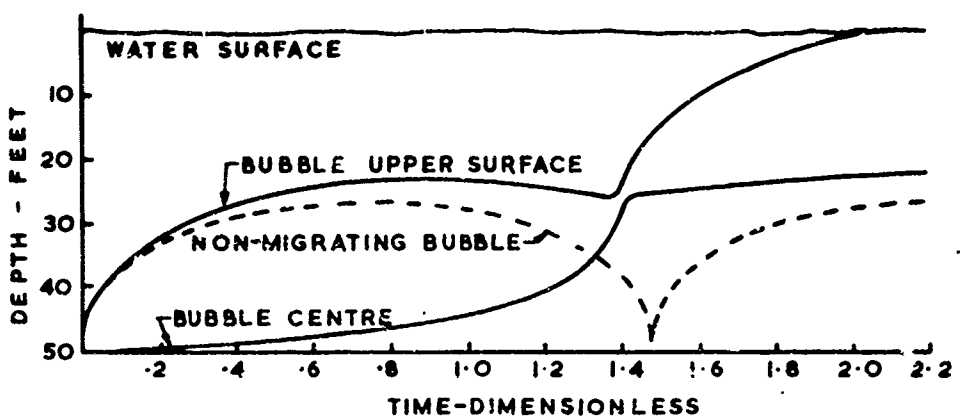

BUBBLE MIGRATION FOR A 500 LB. CHARGE AT 50 FEET DEPTH

FIGURE 03

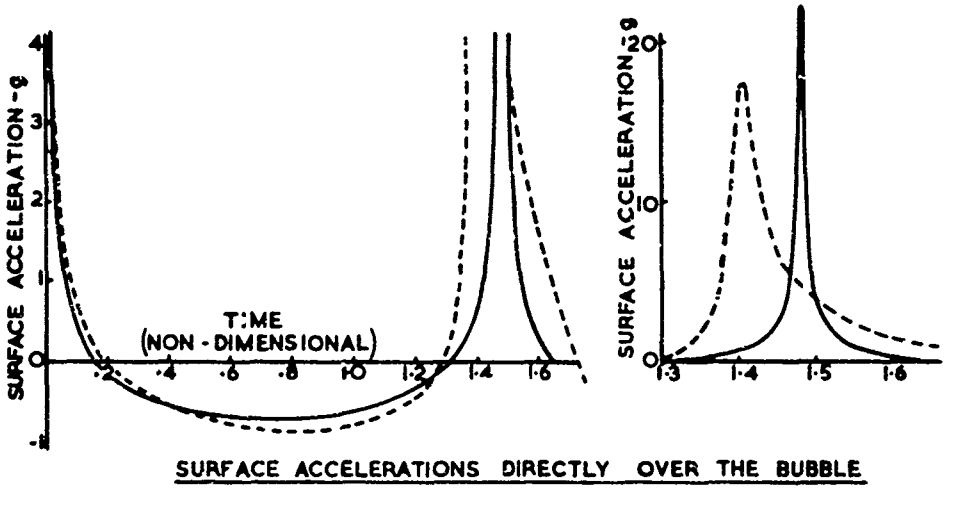

SURFACE ACCELERATIONS DIRECTLY OVER THE BUBBLE

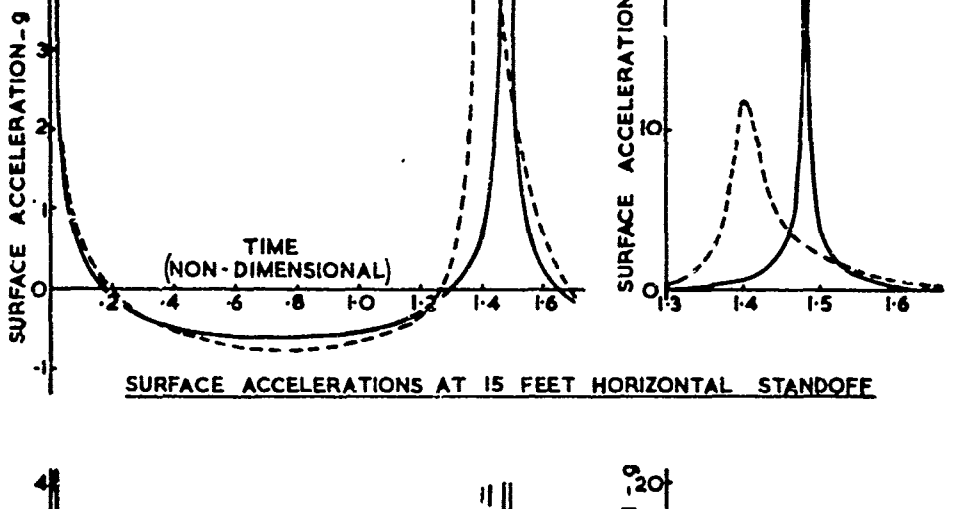

SURFACE ACCELERATIONS AT 15 FEET HORIZONTAL STANDOFF

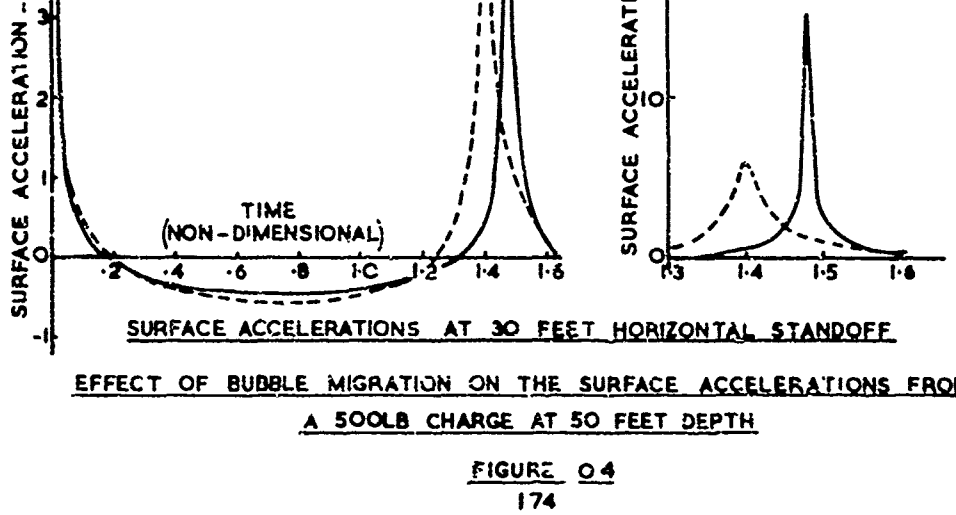

SURFACE ACCELERATIONS AT 30 FEET HORIZONTAL STANDOFF

EFFECT OF BUBBLE MIGRATION ON THE SURFACE ACCELERATIONS FROM A 500LB CHARGE AT 50 FEET DEPTH

FIGURE 04

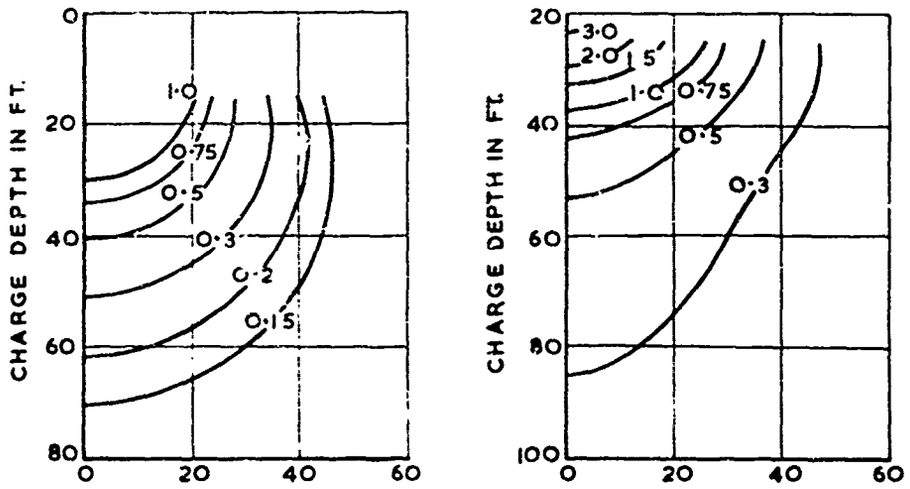

100 – POUND CHARGE OF TNT

500 – POUND CHARGE OF TNT

EFFECT OF CHARGE GEOMETRY ON THE RELATIVE INITIAL ACCELERATION IMPULSE AT A POINT ON THE WATER SURFACE

FIGURE 05

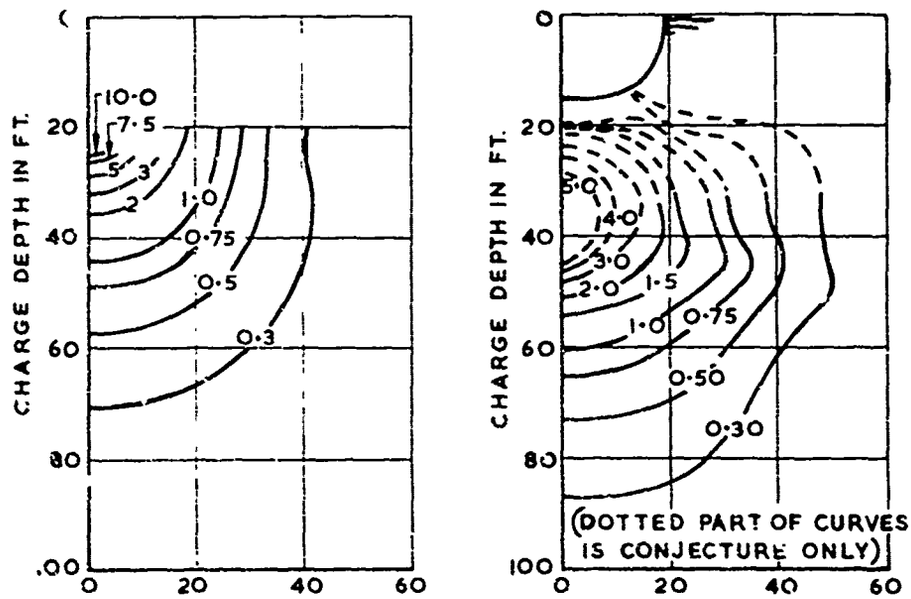

100 – POUND CHARGE OF TNT

500 – POUND CHARGE OF TNT

EFFECT OF CHARGE GEOMETRY ON THE RELATIVE BUBBLE PULSE ACCELERATION IMPULSE AT A POINT ON THE WATER SURFACE

FIGURE 06

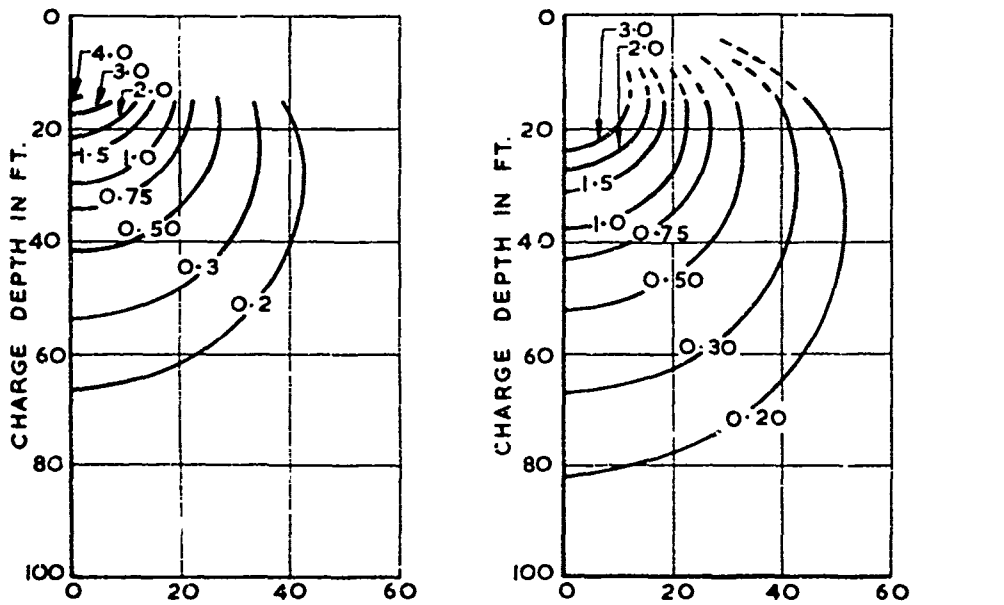

100 – POUND CHARGE OF TNT

500 – POUND CHARGE OF TNT

EFFECT OF CHARGE GEOMETRY ON THE RELATIVE PEAK INITIAL ACCELERATION AT A POINT ON THE WATER SURFACE

FIGURE 07

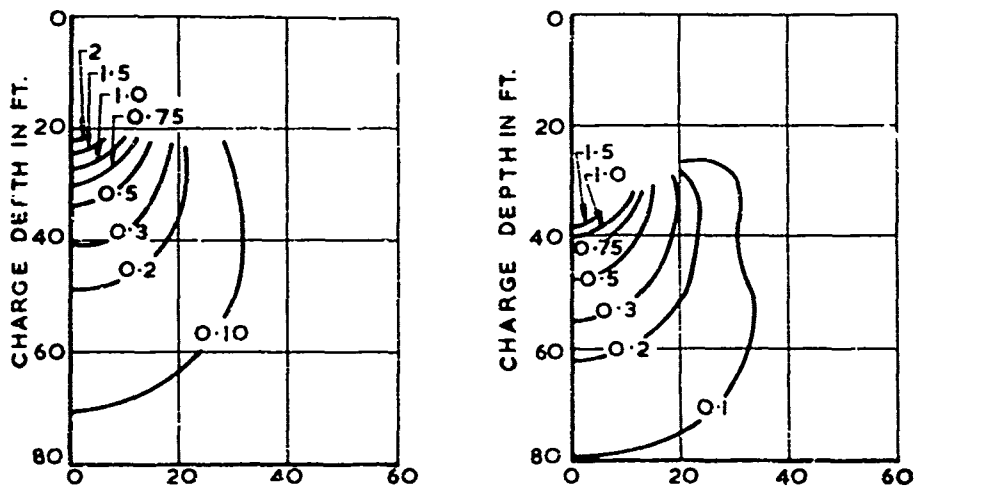

100 – POUND CHARGE OF TNT

500 – POUND CHANGE OF TNT

EFFECT OF CHARGE GEOMETRY ON THE RELATIVE BUBBLE PULSE ACCELERATION AT A POINT ON THE WATER SURFACE

FIGURE 08

P. Description of Computer Program II

The general features described in Sections L, N and O, ie. the 3-D virtual mass, the effect of a hole in the target and the effect of bubble migration, have all been incorporated into a computer program. The program is written in FORTRAN and has been implemented on both an IBM 7090 and a KDF-9 computer. As for the computer program I, the program and detailed specifications for its structure, the data format and units, and the type of output it gives are all held at the Naval Construction Research Establishment. Again as for the program I, the program has been written so that it splits naturally into two sections, the first evaluating the vertical vibration modes of the ship, and the second using these modes together with additional details on charge size and location, to determine the whipping response. The main differences from the first program are summarised below.

The elastic nature of the ship is specified in the same way as for program I but the inertial properties are given in a different form. Instead of specifying the added mass and the displaced water mass at each node the related Lewis type coefficients C and $\overline{C}$ are defined, together with the ship beam. Since rotary inertia effects appear to be generally small this program does not include them. The program uses the 3-D flow approximation equations to determine the fluid inertia matrix as described in section L. A Choleski routine is used to split the total inertia matrix into the form LL^T and an HGW eigenvalue subroutine then determines the ship frequencies and transformed mode shapes from the symmetric matrix $L^{-1}S\,L^{-T}$ where S is the elastic stiffness matrix. This part of the program produced the ship frequency results described in section L.

Using these modes the program will then calculate the positional mode coefficients $y_i(x)$, $M_i(x)$ and $S_i(x)$ described in section I for use in computing the eventual response by combining the individual modal responses. The solution of the modal equations is more complicated than for program I since the forcing function is no longer proportional to the bubble volume acceleration. Due to the use of the migrating bubble equations the forcing function is

$$\underset{\sim}{Y}_i^T \, M_2 \, \dot{\underset{\sim}{u}}(t)$$

where M_2 is the water inertia matrix defined by equations (L20), (L22) and (L23), $\underset{\sim}{Y}_i$ is the ith mode shape and $\dot{u}_j(t)$ is given by equations (013) and (014). In consequence a matrix multiplication is involved at each time step and for each mode. In computing the values of $\dot{\underset{\sim}{u}}(t)$ allowance is made (if so required) for the effect of a hole in the target, as described in Section N.

As before, the modal equations are integrated by a standard Runge-Kutta integration subroutine and the initial conditions are that the mode coefficients and their first time derivatives are all zero.

Q. Comparative Calculations

The computer program II has been used to carry out an extensive set of calculations and typical results are shown in figures Q1 to Q3. These figures compare the results of calculations carried out first with migration included and then without it. Figure Q1 shows the effect of migration on the amplitudes of the heaving mode and the basic whipping mode for a charge directly beneath the centre of the ship, and also for a similar charge at the same depth but off to one side. Figure Q2 shows the same charge and geometries but compares the vertical midship displacements and the corresponding midship longitudinal deck strains. Figure Q3 shows the vertical displacements and strains for the same charge at a slightly greater depth.

The most obvious feature of the graphs is that, despite the great enhancement of the local force above the charge which was shown in section O (Figure O6), the inclusion of migration does not markedly change the motion of the ship. At the shallower depth the deck strains are increased by 20% but to the side, and at the greater depth, the motion is little affected. This is presumably due to the considerable length of ship which is affected by the whipping forces. Section O showed that the forces on the ship, although greatly increased above the charge, were reduced at points some way off the vertical. The integrated effect of parts of the ship away from the charge evidently offsets the local intensified loading.

For deeper charges, later bubble pulses will begin to have an effect on the ship and in such cases gravity migration would be much more significant as it could bring the bubble from too far away to be important, in to potentially damaging ranges. Such later pulses are less well known than the first pulse and have been excluded from the analysis. The bubble equations will predict several oscillations for deep charges but the accuracy is not known.

Comparison of figures Q1 and Q2 shows that the basic whipping mode is the one principally responsible for the observed strains but that the higher modes still have a significant effect. The higher mode concerned in these calculations is the third whipping mode, since the longitudinal charge position is close enough to a node of the second whipping mode for it to be little excited. Only the first three whipping modes, and the two rigid body modes, are included in the calculations.

The computer program II was used to produce both the migrating curves and non-migrating ones so that minor differences in the bubble equations and the ship representation should not be included in the results. Program II has a facility for suppressing the migration terms in the bubble equations. Unfortunately, since the bubble motion is derived from direct integration of the bubble equations, when migration is suppressed the motion is that due to an undamped bubble with no energy losses. If such losses were included the bubble pulse would be slightly reduced and the amplitudes for the non-migrating case would be correspondingly reduced. A second minor deficiency in the graphs is in the displacement curves. The program automatically cuts off the bubble pulsations just after the first bubble pulse. This is because of uncertainties in the bubble forces after the pulse. In consequence an upward impulse is imparted during the pulse but the subsequent suction which, physically, should follow, has been suppressed. The ship then has only gravity restraining it and, since gravity has a much smaller effect than the bubble forces, the ship displacement grows at a steady rate over the time period concerned. This is most obvious in the heaving mode shown in figure Q1(a). Since the strains in the ship are virtually independent of the rigid body motion they are little affected.

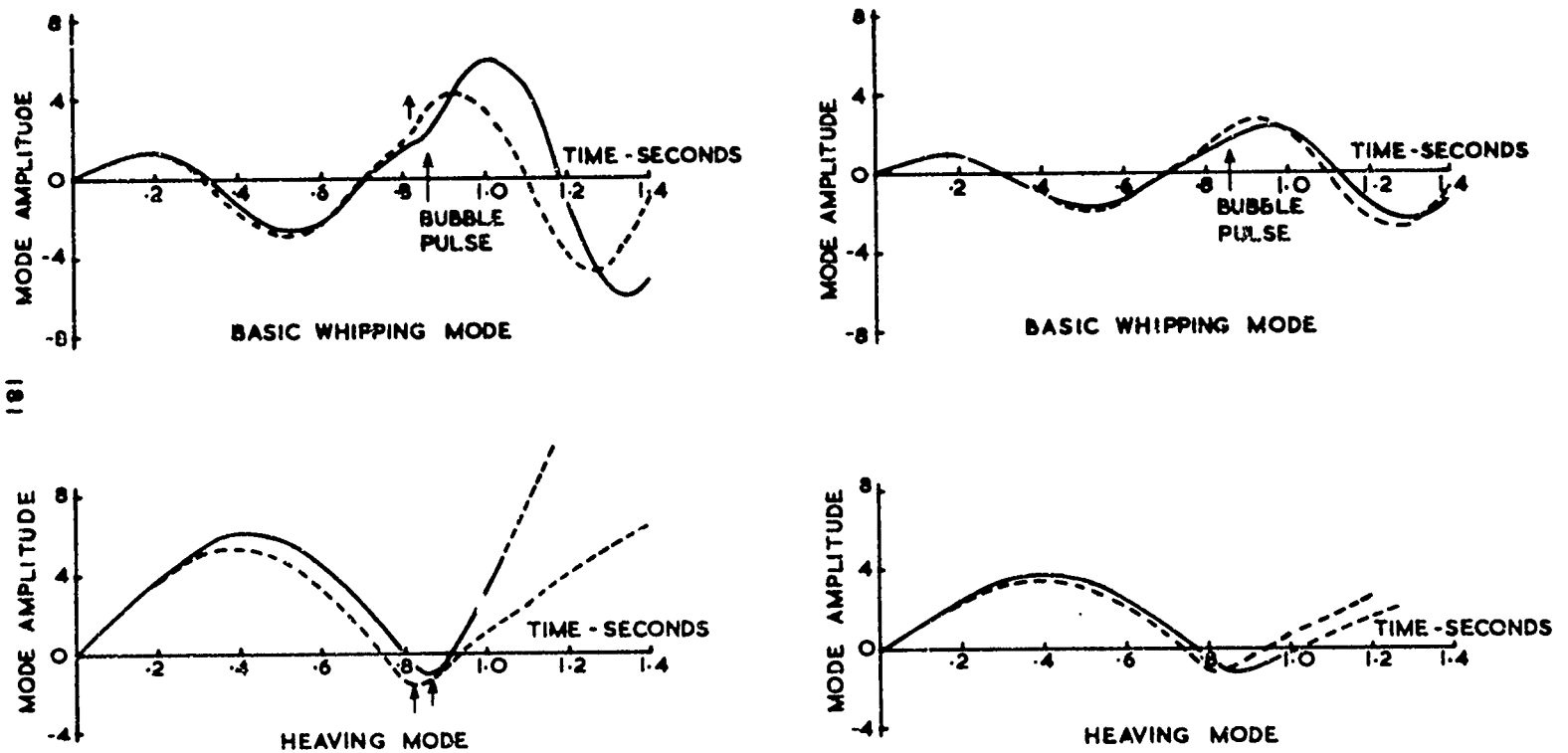

CHARGE 500 LB TNT, 45 FEET DEEP UNDER CENTRELINE

CHARGE 500LB TNT, 45 FEET DEEP 30 FEET OFF CENTRELINE

COMPARISON OF MODAL RESPONSES TO MIGRATING AND NON - MIGRATING EXPLOSION BUBBLES

FIGURE Q 1

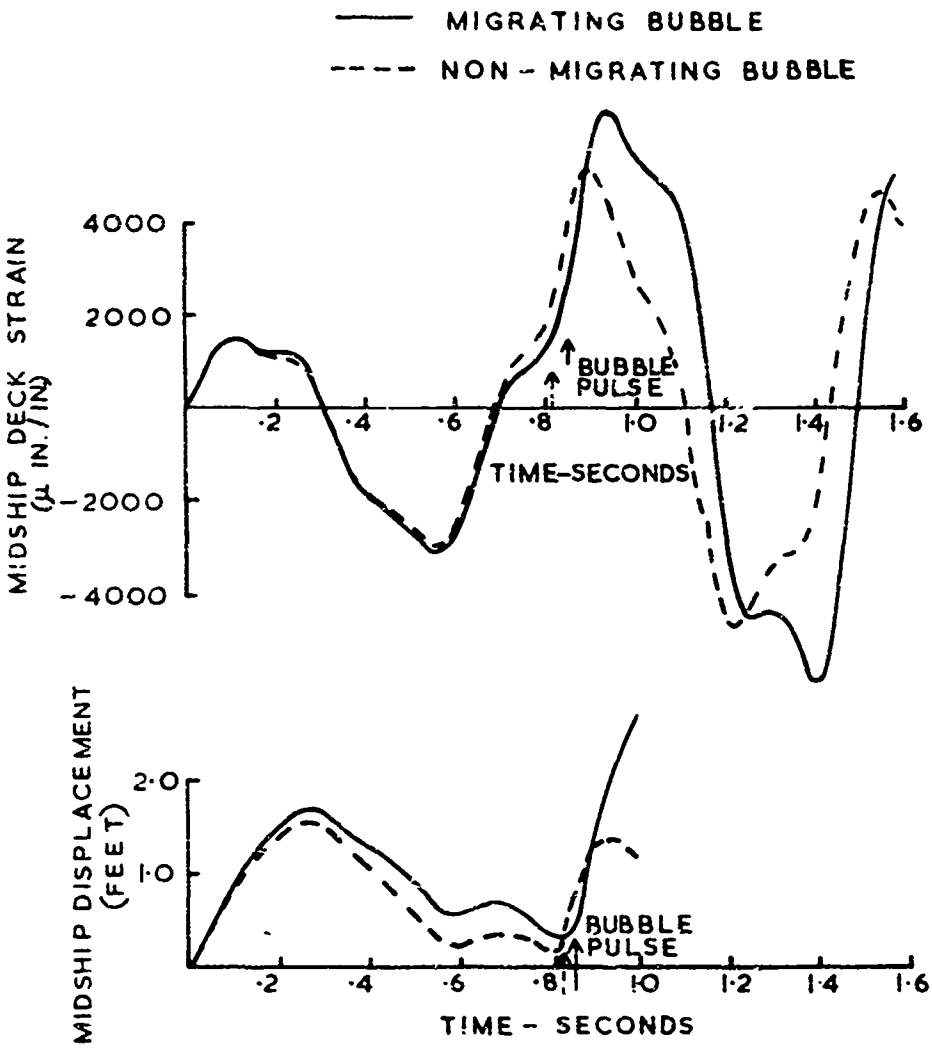

500 LB. TNT 45 FEET DEEP BELOW SHIP CENTRELINE

COMPARISON OF SHIP RESPONSES TO MIGRATING AND NON-MIGRATING EXPLOSION BUBBLES

FIGURE Q2 a

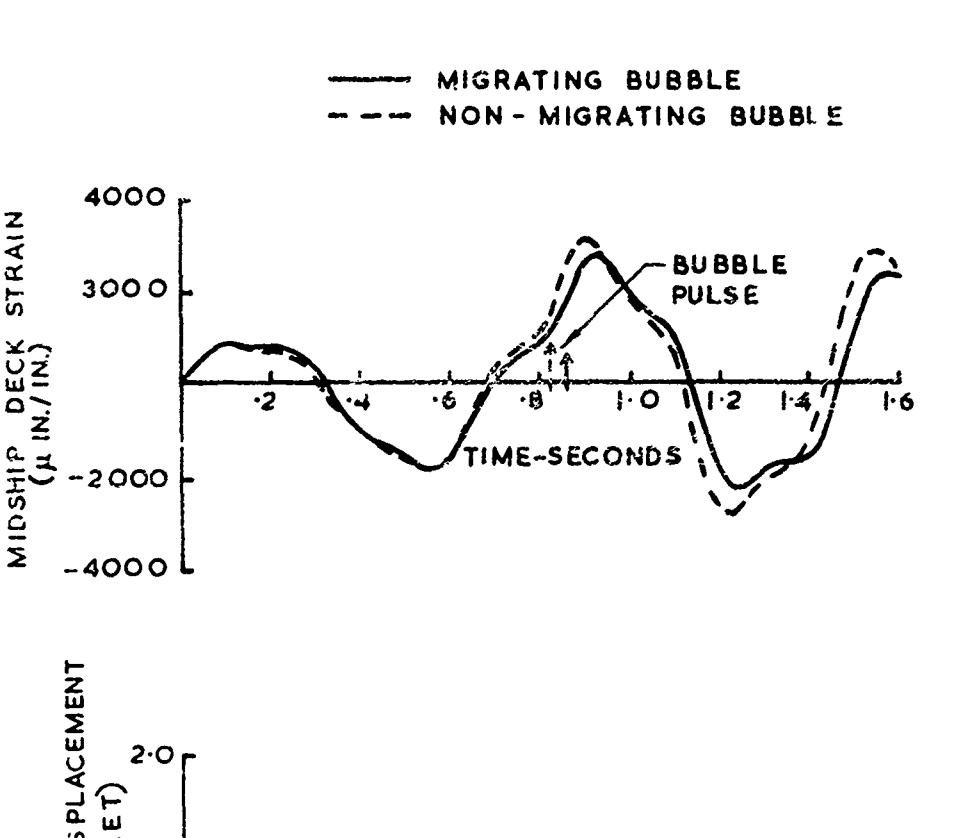

500 LB. TNT 45 FEET DEEP 30 FEET OFF CENTRELINE

COMPARISON OF SHIP RESPONSES TO MIGRATING AND NON-MIGRATING EXPLOSION BUBBLES

FIGURE Q 2b

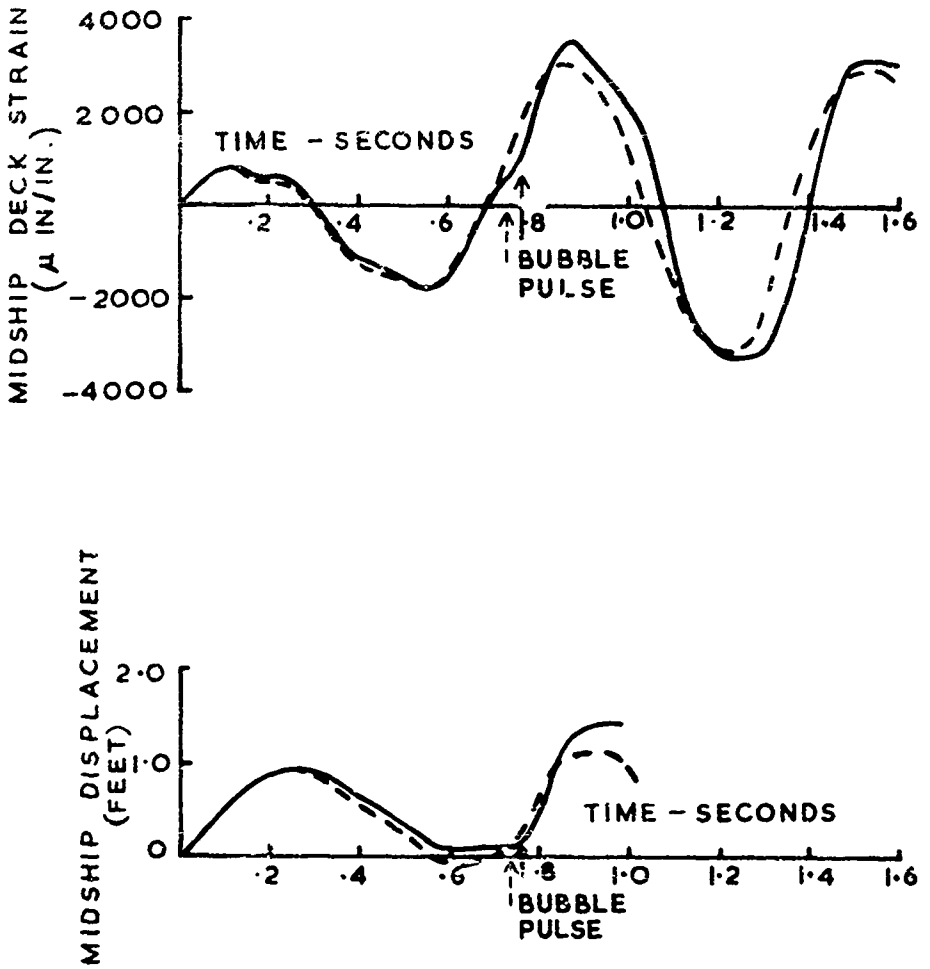

500 LB. TNT 60 FEET BELOW SHIP CENTRELINE

COMPARISON OF SHIP RESPONSES TO MIGRATING AND NON - MIGRATING EXPLOSION BUBBLES

FIGURE Q3

R. Plastic Deformation of the Target

So far the entire analysis has been based on elastic deformations of the target. If the stresses in the main girder reach yield in tension then plastic yielding will occur and the elastic equations will no longer apply. Nevertheless, so long as the total duration of such plastic yielding in each vibration cycle is short compared to the basic elastic vibration period, the motion of the ship will not differ greatly from the fully elastic motion. If however the stresses in one of the girder flanges reach either yield stress or the flange buckling stress, in compression, then the flange will buckle and the stiffness at the section will fall dramatically. Such failure has been observed in static tests on naval vessels (references [C3] and [C8]) and the buckling has been found to be very localised. The drastic reduction in stiffness at the buckled section allows the girder on either side to rotate to relieve the moments which caused the buckle. This type of failure will clearly modify greatly all subsequent target motion. To show the type of motion which results, approximate equations to describe the motion are developed here. The plastic equations described are not intended to be particularly accurate, but merely to be close enough to reality to show the type of motion which is likely to occur.

With the geometry of Figure R1, the equations of motion of the ith mass are clearly

$$\begin{aligned} m_i \ddot{y}_i &= S_{Li} - S_{R\,i-1} + P_i \\ r_i \ddot{\gamma}_i &= M_{Li} - M_{R\,i-1} + Q_i \end{aligned} \qquad \text{(R1)}$$

where P_i and Q_i are the external force and moment. P_i and Q_i are of course hydrodynamic and hydrostatic in origin and for simplicity the strip theory forces are assumed. Thus

$$P_i = m_{wi}(\dot{u}_i - \ddot{y}_i) + \bar{m}_{wi}\dot{u}_i - k_i y_i$$

$$Q_i = r_{wi}(\dot{u}'_i - \ddot{\gamma}_i) + \bar{r}_{wi}\dot{u}'_i - k_{ri}\gamma_i \qquad \text{(R2)}$$

and the equations (R1) become

$$(m_i + m_{wi})\ddot{y}_i = S_{Li} - S_{Ri} + (m_{wi} + \bar{m}_{wi})\dot{u}_i - k_i y_i$$

$$(r_i + r_{wi})\ddot{\gamma}_i = M_{Li} - M_{Ri} + (r_{wi} + \bar{r}_{wi})\dot{u}'_i - k_{ri}\gamma_i \qquad \text{(R3)}$$

When the deformations are elastic, the shear forces S and bending moments M transmitted by the beams on either side of the lumped mass are determined by the equations of Section C and the equations (R3) are identical to those already considered. The plastic nature of the problem is entirely determined by these terms.

In the theoretical model, since the beams are considered to be weightless the shear force in each is constant and the bending moment is a linear function of the distance from the end. The maximum bending moment will consequently necessarily occur at one of the ends and yielding will start at such a point. In a physical model yielding would then spread outward along the beam but, to keep the model as simple as possible, it is assumed here that the distributed 'excess' curvature near the mass is equivalent to a discrete rotation of the beam end relative to the lumped mass. The rotation is assumed to take place at a constant, plastic, bending moment. When the rotation exceeds a specified amount it is assumed that the beam will buckle. This again is assumed to be simply a rotation of the beam end relative to the lumped mass but at a much lower value of the constant plastic moment. The complete moment/plastic rotation diagram assumed is illustrated in Figure R2. The fully elastic motions already considered involve no plastic rotations

and so lie entirely on the line GOA. For the plastic case, if the lumped mass displacements and rotations are such that the moment at one end of a beam section is tending to increase, the moment will rise elastically from zero at O until it reaches the plastic moment M_{p1}. After this the plastic yielding will be equivalent to a rotation of the beam end, at constant plastic moment M_{p1} until the point B is reached, at a plastic rotation $\bar{\theta}_M$. Actually a more likely route to B is indicated by the dotted line, but OAB should be a reasonable approximation. At B it is assumed that the section buckles and the beam end instantaneously rotates to reduce the moment at the end to M_{p2}. The moment/rotation curve 'jumps' from B to B'. The rotation then increases at constant moment M_{p2} until the tendency for the moment to try to increase further stops, say at C. If the tendency then is for the moment to reduce, the beams either side of the hinge will unload elastically and normal elastic vibration could occur up and down CD. A continued tendency to unbend would lead to the plastic moment $-M_{p2}$ and plastic rotation along DE. From E', the buckled flange would start to straighten out and carry an increasing load, possibly as indicated by the dotted line, but DEF is a simple approximation for the return to full strength. Plastic rotation would then continue at the constant moment $-M_{p1}$ until the opposite flange buckled, say at H, and a jump to the point H' occurred. Along any of the horizontal branches of the curve, a reversal in the tendency of θ_p to change would lead to elastic motion along a vertical.

The whole moment/rotation relation is clearly highly over-simplified; for example the negative plastic moment would really be of different magnitude to the positive ones, the section would buckle at a lower moment the second time than the first since the plastic strain reversal between the two would not completely straighten the flange, etc. As a simple model however it probably contains most of the essential features.

For shear, since the shear force is constant along each beam, it is reasonable to assume that the beam acquires a uniform shear angle along its whole length once the shear force exceeds the full plastic shear force. A shear force/shear angle relation similar to that for the moment has been assumed although, in this case, the reduction in stiffness is probably less dramatic.

To produce an algorithm quantifying the above characteristics, the plastic rotations θ_{Li}, θ_{Ri} and θ_{si}, as defined in Figure R3, are introduced. In terms of these angles it is possible to define a deflection and rotation of the right hand end of the beam, relative to the left, in the form

$$y_R = y_{i+1} - [y_i + \ell\,(\gamma_i + \theta_{Ri} + \theta_{si})]$$

$$v_R = (\gamma_{i+1} + \theta_{Li+1}) - (\gamma_i + \theta_{Ri}) \qquad \text{(R4)}$$

These are the deflections which give rise to elastic stresses within the beams. The shear force and bending moments in a beam with these relative deflections are:-

$$M_L = \alpha\ell\,[3y_R + (\epsilon - 1)\,\ell v_R]$$

$$M_R = M_L - \ell S_L = \alpha\ell\,[-3y_R + (\epsilon + 2)\,\ell v_R] \qquad \text{(R5)}$$

$$S_R = S_L = 6\alpha[y_R - \tfrac{1}{2}\,\ell v_R]$$

where, as in Section C,

$$\alpha = \frac{EI}{\ell^3(\epsilon + \frac{1}{2})} \quad ; \quad \epsilon = \frac{12(1 + \nu)I}{A_s \ell^2}$$

In the $(y_R, \ell v_R)$ plane curves of constant M_L, M_R and S_R are straight lines of slopes $-3/(\epsilon - 1)$, $3/(\epsilon + 2)$ and 2 respectively, so that the elastic region in the $(y_R, \ell v_R)$ plane has boundaries of the form shown in Figure R4. Initially, y_R and v_R will be zero and the bending moments and shear force will all be zero. When the explosion occurs the y_i and γ_i will start to change and, for each beam section the values of y_R and ℓv_R calculated from (R4) will describe a curve in the $(y_R, \ell v_R)$ plane. The motion of the ship will be entirely elastic until one of these curves meets a boundary. After this the value of the appropriate plastic rotation $(\theta_{Ri}, \theta_{Li+1}, \theta_{si})$ will begin to vary in such a way that the appropriate force or moment remains constant. The point in the $(y_R, \ell v_R)$ plane will either remain fixed at the boundary or will slide along the boundary. In any practical computing scheme the integration of the equations of motion will proceed in a series of time steps and at each step the corresponding point in the $(y_R, \ell v_R)$ plane will jump to a new neighbouring position. Consequently instead of sliding along the boundary the point may jump just outside it. It may then be brought back to the boundary by adjustment of the appropriate plastic rotation. Changes in the different rotations move the point in the directions:

θ_{Ri} ; at 45^{o} to the y_R axis

θ_{Li+1} ; parallel to the δv_R axis

θ_{si} ; parallel to the y_R axis

In any of the regions marked I, only one of the plastic conditions is violated and there is one way to bring the point back to the elastic boundary so that its position is uniquely defined. In any of the regions marked II, two conditions are violated and the eventual position of the point on the boundary depends on the order in which the two adjustments are made. The non-uniqueness is not normally a problem however since the point will always end up close to the corner, which is where it would have been had its motion been continuous rather than in discrete steps. The only time when non-uniqueness is really a difficulty is when buckling occurs and one pair of boundary lines suddenly moves in to the new plastic moment position and leaves the point far outside. In this case it is clear which rotation should be amended first and if the movement of the boundaries is considered as a continuous process, the eventual location of the point is obvious. If the amended position of the point takes it outside one of the other boundaries it should be left at the intersection of the two boundaries which is where it would have ended had the transition been continuous. This particular problem is principally a computer programming one. In the regions marked III, all the plastic conditions are violated. In general such regions cannot be reached with a reasonable time step length, except for very exceptional boundaries.

Unlike solid beams, a ship's hull girder is usually designed, in order to give an efficient structure, to have most of the cross-

sectional material as far as possible from the neutral axis. In a small ship (eg a destroyer) most of the strength (cross-sectional inertia) is provided by the main deck and the bottom near the keel, with the neutral axis about halfway between. In consequence, instead of having a moment/curvature relation which changes slowly from fully elastic to fully plastic, as for a solid beam, the ship behaves fully plastically almost as soon as it starts yielding at the outermost fibres. It has been found convenient in the computer program to define the plastic moments M_{p1} and M_{p2} in the form

$$M_{p1} = f_1 M_y$$

$$M_{p2} = f_2 M_y \qquad \text{(R6)}$$

with

$M_y = \frac{I\sigma_y}{\bar{y}}$, the moment at which yielding first starts, $I/\bar{y}$ being the section modulus. Similarly, for shear failure

$$S_{p1} = f_3 S_y$$

$$S_{p2} = f_4 S_y \qquad \text{(R7)}$$

with $S_y = A_s \sigma_y$

The factors f_1 to f_4 can be specified as part of the data for the program.

One further detail regarding the plastic moments is that, since the initial yielding at the moment M_{p1} really represents plastic curvature in the region around the lumped mass instead of a rotation at it as assumed by the program, the changeover to M_{p2} in the program has been arranged to occur when the total rotation $(\theta_{Ri}-\theta_{Li})$

at a mass exceeds a given critical rotation $\bar{\theta}_M$. In this way the program ensures that both sides of a lumped mass reduce in plastic moment together.

Because the rotations of the masses in the plastic case form a vital part of the analysis and can no longer be readily related to displacements elsewhere, as in the fully elastic case, it is not possible to halve the number of equations by dropping all rotary terms. In consequence, instead of having say five second order equations to solve, as in the normal mode elastic analysis, each plastic integration involves two second order equations for each lumped mass, ie forty equations for a 20 mass model. This means that the time step must be very small, being restricted to a small fraction of the shortest period present (rotary oscillations of a single lumped mass with a consequent very short period). The combination of a large number of equations coupled with a very short time step leads to excessive computing times and a simple damping technique was introduced to control the instability of the integration routine and enable the normal step length stability criterion to be violated safely. Linear velocity damping was introduced between each mass and its two adjacent masses. Such damping affects principally the independent motions of each mass while leaving the overall low frequency modes largely unaltered. The final equations solved were

$$(m_i + m_{wi})\,\ddot{y}_i = S_{Ri} - S_{Li} + (m_{wi} + \bar{m}_{wi})\,\dot{u}_i - k_i y_i + (m_i + m_{wi})\,\alpha_d\,(\dot{y}_{i-1} + \dot{y}_{i+1} - 2\dot{y}_i)$$

$$(r_i + r_{wi})\,\ddot{\gamma}_i = M_{Ri} - M_{Li} + (r_{wi} + \bar{r}_{wi})\,\dot{u}_i' - k_{ri}\gamma_i + (r_i + r_{wi})\,\alpha_{rd}\,(\dot{\gamma}_{i-1} + \dot{\gamma}_{i+1} - 2\dot{\gamma}_i) \qquad \text{(R8)}$$

With this technique it cannot be expected that motion equivalent to vibrations of higher modes will be reproduced but the features of interest in whipping should be preserved. The damping constants were chosen so that the predicted strains for elastic cases were similar to those predicted by the computer program II. Even with the damping included the largest incremental time consistent with stability was found to be considerably smaller than for the corresponding normal mode case and the computing times were found to be about 20 times as great.

Since the method of solution of the basic equations for the plastic hinging program is very different from that for the elastic programs I and II, it is of interest to compare the results given by the two types of analysis for a case where plastic deformation does not occur. The results of such calculations are shown in figure R5. The agreement is very good for the early motion but falls off considerably later in the motion due to the damping included in the plastic program. The damping is actually a little too severe but the calculation shows the general agreement expected. It also shows that, as expected, the high modes are more heavily damped than the low ones. As for the earlier programs the bubble effects have been suppressed shortly after the first pulse.

Figure R6 shows a similar pair of calculations for a larger charge, where the elastic limit has been exceeded. The strains are those at the middle of the ship, very close to where buckling occurs in the plastic calculation so that, after buckling, very little bending moment is present and the longitudinal strains are small. This would not be true at other parts of the ship. The displacement curve shows that the motion of the centre of the ship is altered drastically by the plastic hinging. This is even clearer in figure R7 where the ship profiles for the same example are shown. It is of interest that in this case the charge geometry is such that the hinge occurs during the suction phase

of the bubble and bends towards the explosion rather than away as might be expected. The later impulse from the bubble pulse is also very evident. It occurs very close to the ship and the loading is fairly local. The high shear stresses indicated at this time lead to heavy local plastic shearing deformations. Although the figures do not show it, the stresses were high throughout most of the length of the ship and minor yielding, both in shear and bending, occurred at numerous points. The plastic rotation needed to allow buckling was reached first at the centre and then the deformation there partially relieved the stresses elsewhere.

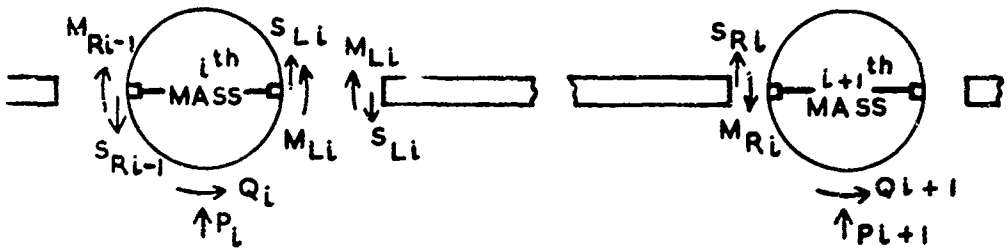

NOMENCLATURE AND SIGN CONVENTION FOR THE PLASTIC ANALYSIS IDEALISATION

FIGURE R1

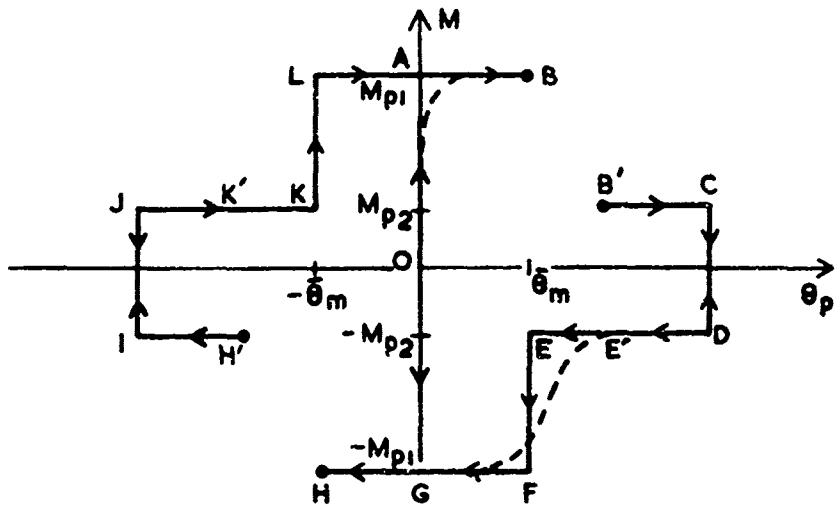

IDEALISED MOMENT/PLASTIC ROTATION RELATION

FIGURE R2

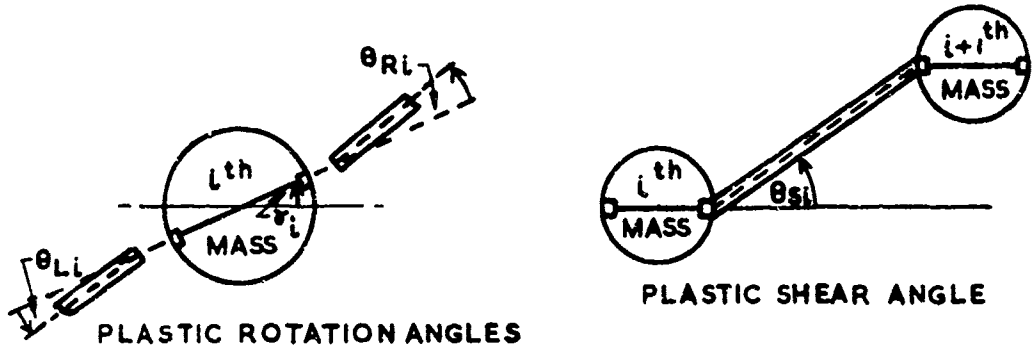

DEFINITION OF PLASTIC ANGLES

FIGURE R3

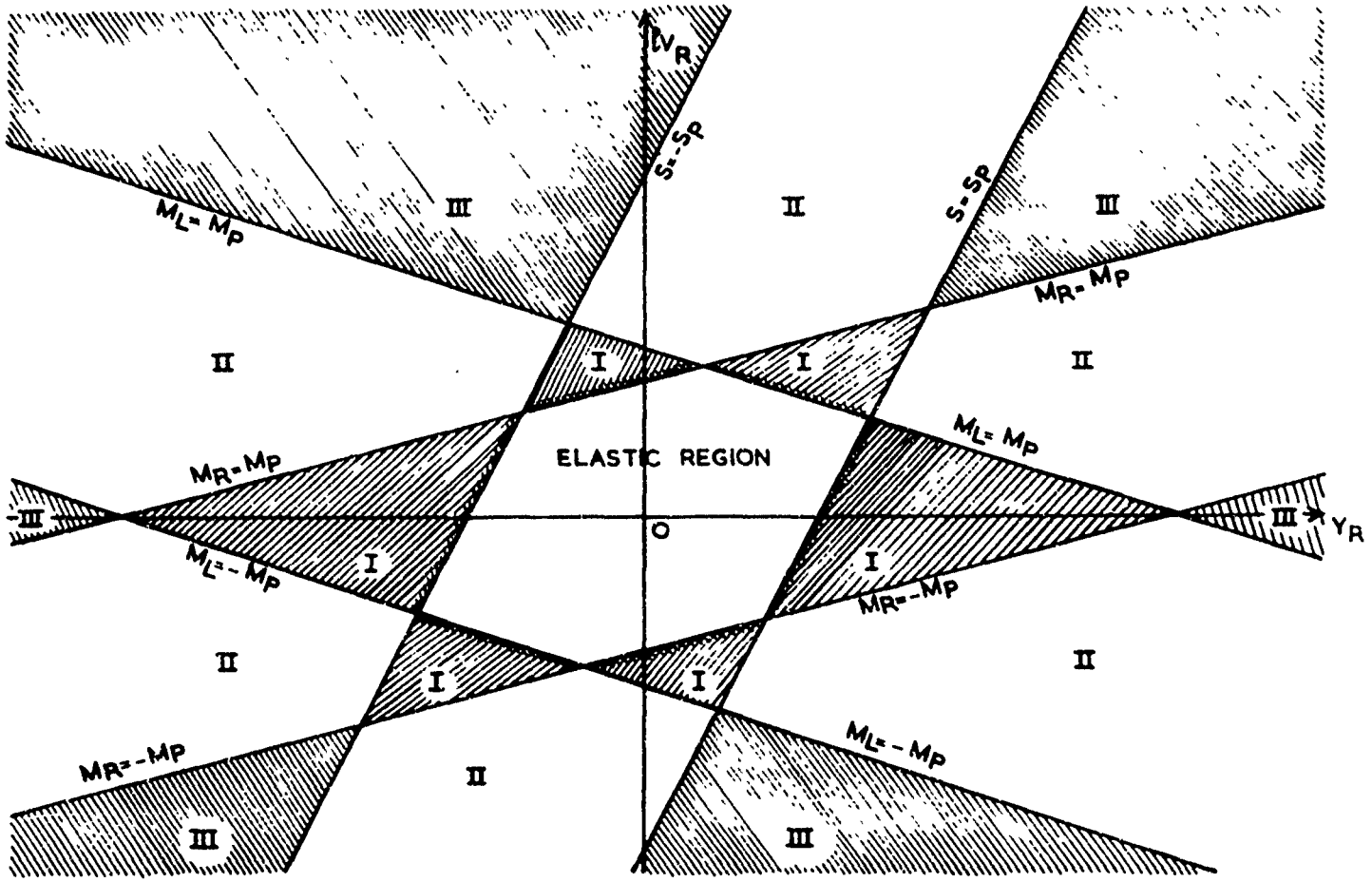

ELASTIC BOUNDARIES IN $Y_R - \ell V_R$ PLANE

FIGURE R4

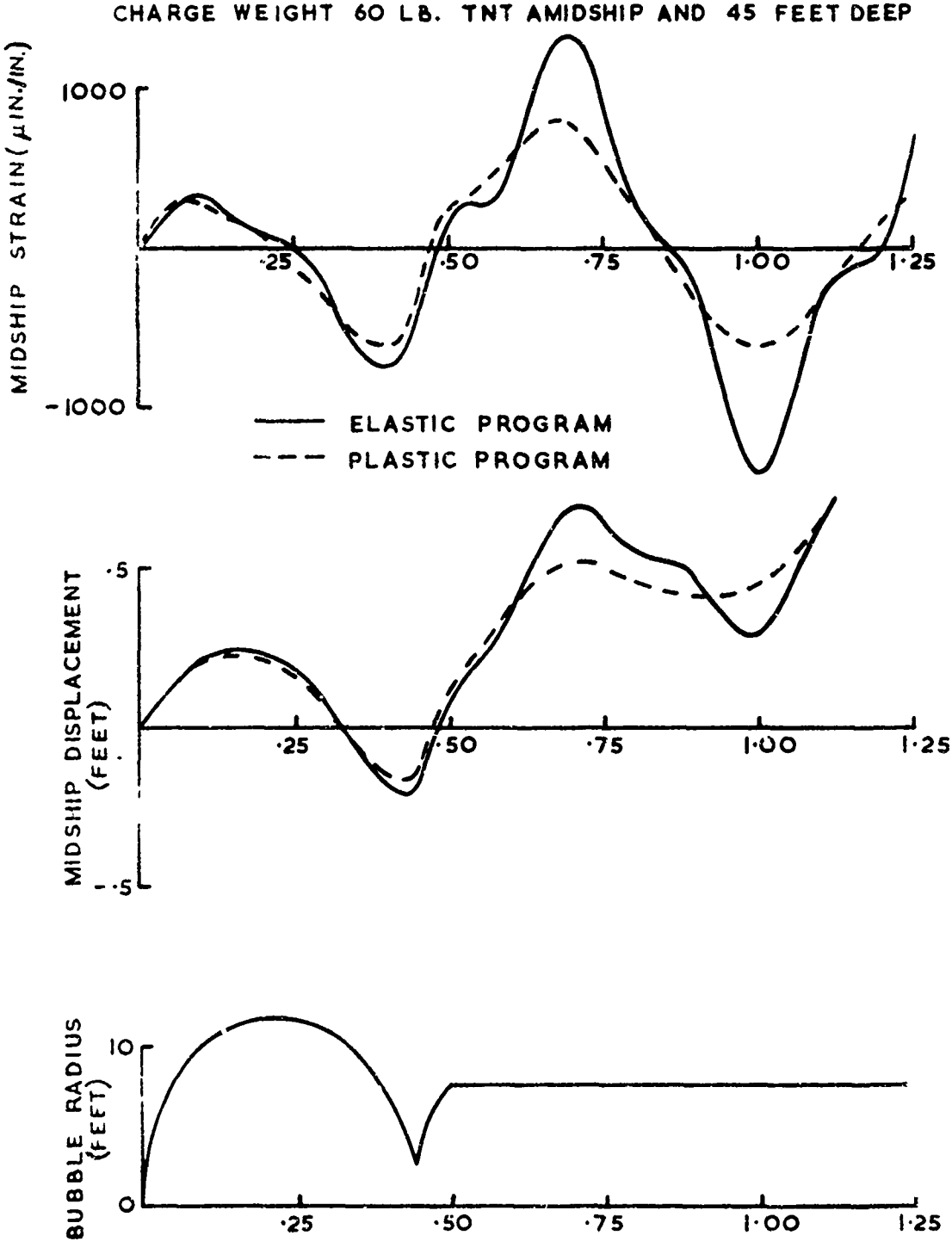

COMPARISON OF RESULTS FROM PLASTIC AND ELASTIC WHIPPING PROGRAMS: ELASTIC MOTION ONLY

FIGURE R5

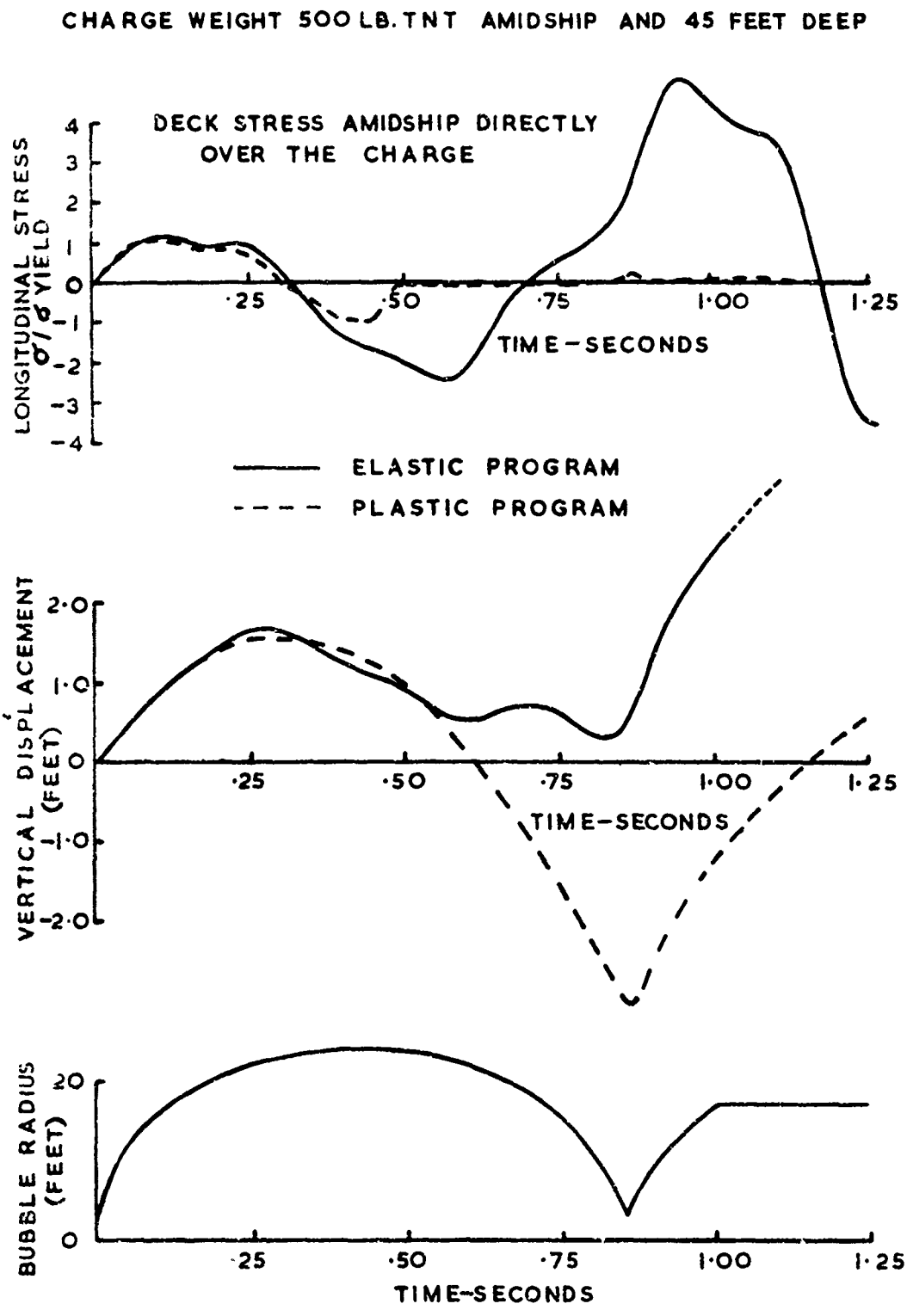

COMPARISON OF RESULTS FROM PLASTIC AND ELASTIC WHIPPING PROGRAMS: PLASTIC MOTION

FIGURE R6

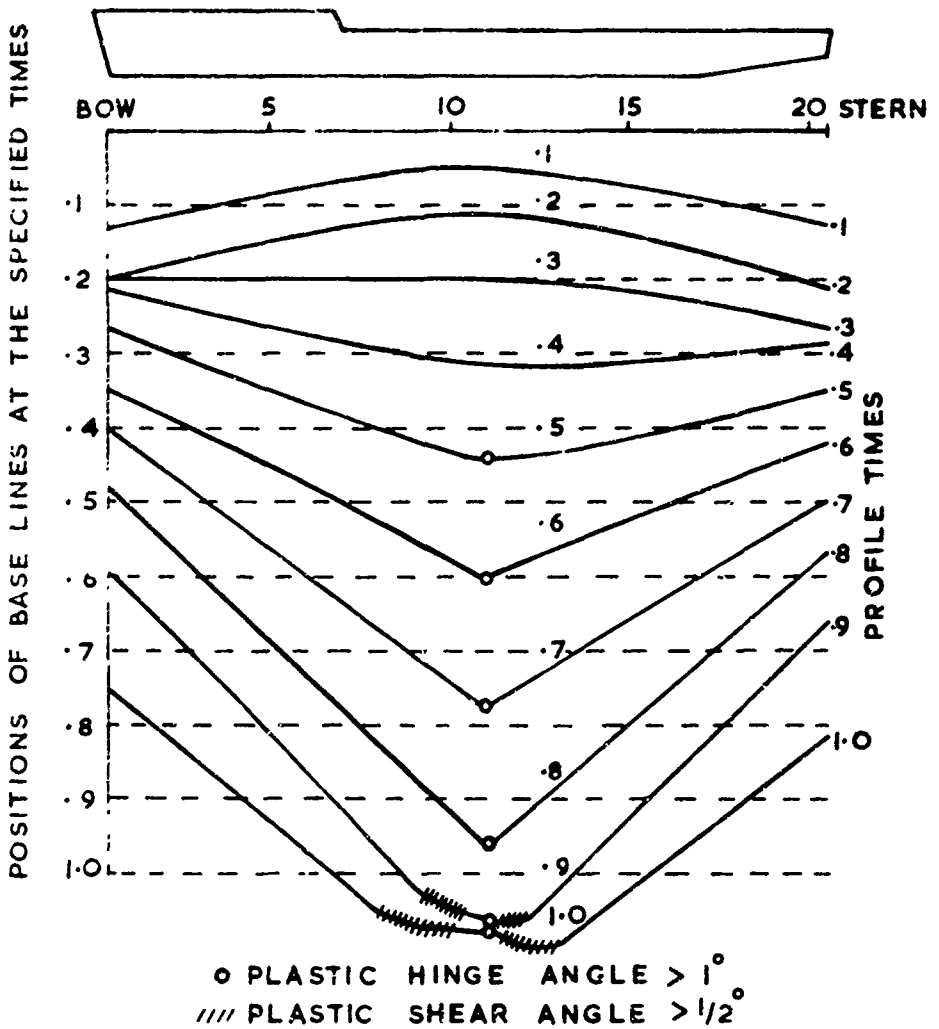

SHIP PROFILES DURING PLASTIC HINGING

500 LB. TNT CHARGE 45 FEET DEEP BELOW SHIP CENTRELINE

COMPARATIVE PROFILES FOR PLASTIC AND ELASTIC WHIPPING

FIGURE R7a

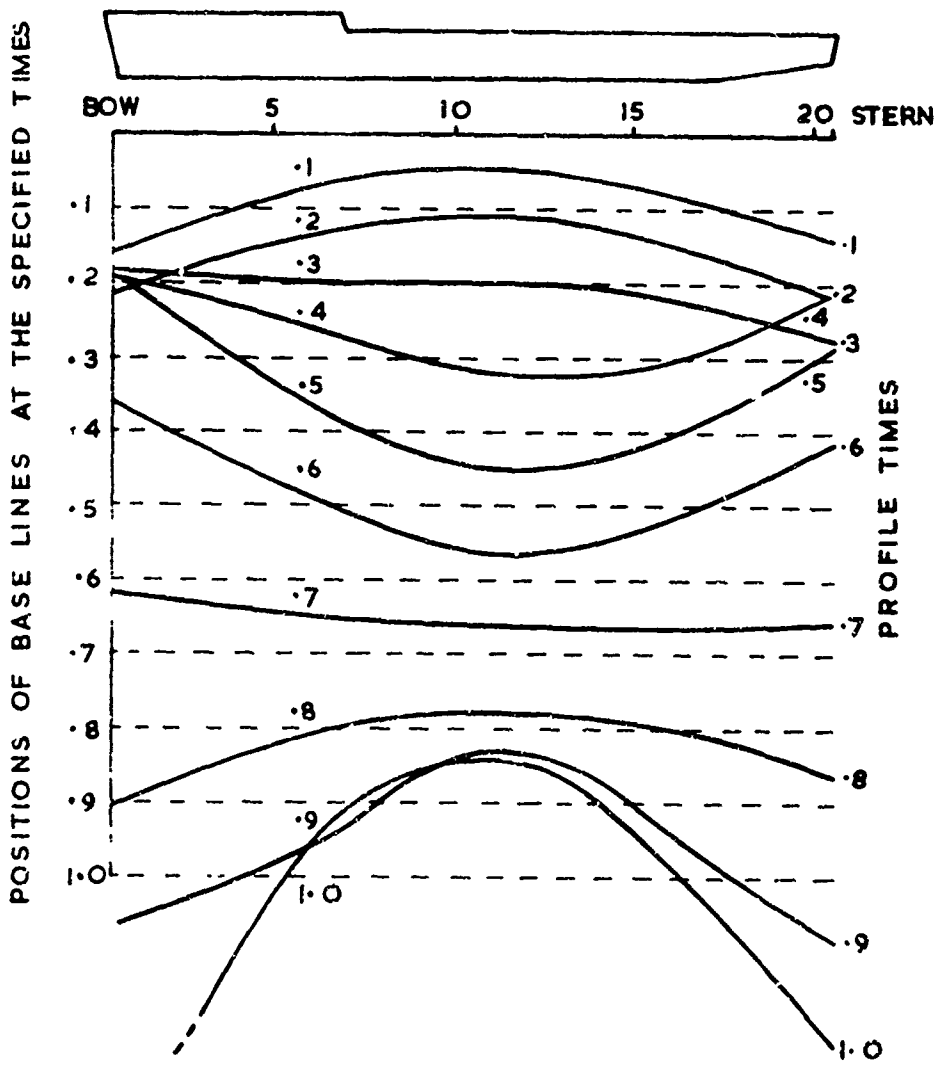

SHIP PROFILES DURING ELASTIC MOTION

500 LB. TNT CHARGE 45 FEET BELOW SHIP CENTRELINE

COMPARATIVE PROFILES FOR PLASTIC AND ELASTIC WHIPPING

FIGURE R7b

Appendix

Approximate Analysis for Bilge Keel Effect

Consider a ship section as shown in Figure 1. The free surface can be allowed for in the usual way (for whipping frequencies) by considering the flow around the underwater section and its image (the dotted curve) in the free surface. Suppose that the potential ϕ_o is known for the flow around the section without the bilge keels. If the length d of the bilge keel is very small compared to the dimensions of the section then its presence will not greatly alter the main flow and the new potential will be $\phi = \phi_o + \phi_b$ where ϕ_b is only significant close to the keel and is the disturbance potential necessary to adjust the original flow to the flow around the keel.

In the original flow, without the keel, the fluid at the bilge keel position nad the velocity

$$u_n = -\frac{\partial \phi_o}{\partial n} = -U \cos \theta_o$$

away from the plating and the velocity

$$u_s = -\frac{\partial \phi_o}{\partial s} = -\alpha U$$

tangential to it. The factor α (positive) can be found from the known potential ϕ_o.

If the length of the bilge keel is small compared to the local radius of curvature of the section, the flow local to the bilge keel attachment point will be almost like the flow past a flat plate as in Figure 2. The motion of both water and plate normal to the plate is ignored. It is clear that the relative velocity of the plate and water is

$$V = U(\alpha + \sin \theta_o) \ .$$

The necessary form of the disturbance potential ϕ_b is then that for the flow along a wall with a projecting plate as in Figure 3. This flow is identical to the flow normal to a flat plate of twice the width and is a well known flow. The added mass of a plate of width 2d is $\pi\rho d^2$ per unit length, so on the half pertinent to our problem the normal force on the bilge keel will be approximately

$$\tfrac{1}{2}\pi\rho d^2 (\alpha + \sin\theta_o)\dot{U}$$

This force is perpendicular to the keel so that, resolving vertically, the downward force on the section will be

$$\tfrac{1}{2}\pi\rho d^2 (\alpha + \sin\theta_o)\sin\theta_o \dot{U} .$$

In the flow normal to a plate there is also a pressure distribution induced along the centre line of the flow. In the problem of flow past a plate on a wall, along the plate this pressure distribution will act on the wall (ship bottom) and a component of this pressure distribution will be vertical. However, neglecting Bernoulli pressures, as is customary in added mass calculations, the positive pressures in front of the plate will be compensated by negative pressures behind and there will be no nett force, only a couple, on the ship bottom. Even the couple is balanced overall by that from the other bilge keel. The plate normal force component can therefore be ignored.

The total downward force on the whole section (image included) due to the bilge keels will be four times that given above, so, if C is the added mass coefficient for the section without keels and C′ the coefficient with the keels, it follows from the force equation

$$\dot{P}' = m'\dot{U} = m_w\dot{U} + 2\pi\rho d^2(\alpha + \sin\theta_o)\sin\theta_o\dot{U}$$

that

$$\pi\rho\left(\frac{B}{2}\right)^2 C' = \pi\rho\left(\frac{B}{2}\right)^2 C + 2\pi\rho d^2(\alpha + \sin\theta_o)\sin\theta_o$$

and the increase in the added mass coefficient, δC is

$$\delta C = C' - C = 2\left(\frac{2d}{B}\right)^2(\alpha + \sin\theta_o)\sin\theta_o$$

Unfortunately, although this analysis is quite appealing physically, it gives an order of magnitude rather than a close approximation to the true value and some judgement is necessary to apply it. This is because for two dimensional flows the pressure near a source (to which the bilge keel is equivalent) decays so slowly that the integral over the neighbouring curved wall may have some effect. This can be shown by considering the flow about a circular cylinder of diameter B with small fins of length d at either end of the diameter transverse to the motion. The method used in section D for rectangles would give a modified added mass of approximately

$$\rho\left[\frac{B}{2} + d\right]^2$$

so that the increase over the usual value is, to the lowest order in d/B,

$$\frac{\delta C}{C} \simeq \frac{4d}{B}$$

By the method proposed here, when the cylinder moves upward with velocity U the water moves downward with velocity U at the positions of the fins. The relative velocity of the fin and water is therefore 2U and the total additional mass is double that of a plate of width 2d, ie

$$2\pi\rho d^2$$

so that $\frac{\delta C}{C} \simeq 8\frac{d^2}{B^2}$, which is of lower order in d/B than before.

The exact solution to this problem has been given by Taylor (D2) and the result is actually

$$\frac{\delta C}{C} = 16\frac{d^2}{B^2},$$

double the previous result. Direct examination of Taylor's solution shows that the force on the plate itself is in fact equivalent to $\delta c^2, \delta^2$, the additional effect being due to increased pressure around the curvature of the cylinder.

This problem shows that the order of magnitude given by the above method is correct and that the force on the keel itself is likely to be very close to the value calculated by the approximate method, but that there may be some additional effect of a similar magnitude, depending on the geometry of the hull near the keel.

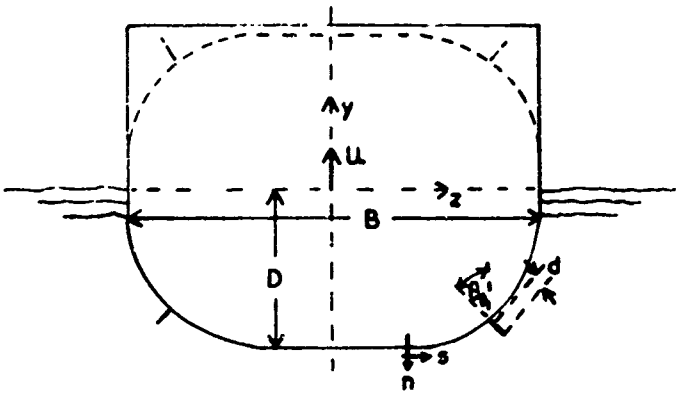

FIGURE 1

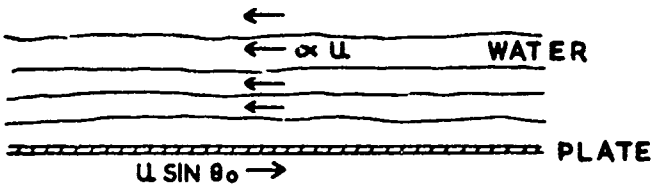

FIGURE 2

FIGURE 3

APPENDIX